2019-09-04

Optically Stimulated Luminescence Dosimetry in Permanent Breast Seed Implant Brachytherapy: a Monte Carlo Approach

Nich, Steven

UNIVERSITY OF CALGARY

Optically Stimulated Luminescence Dosimetry in Permanent Breast Seed Implant Brachytherapy: a Monte Carlo Approach

by

Steven Nich

A THESIS
SUBMITTED TO THE FACULTY OF GRADUATE STUDIES
IN PARTIAL FULFILLMENT OF THE REQUIREMENTS FOR THE
DEGREE OF MASTER OF SCIENCE

GRADUATE PROGRAM IN PHYSICS AND ASTRONOMY

CALGARY, ALBERTA
SEPTEMBER, 2019

Abstract

Permanent breast seed implant (PBSI) brachytherapy, typically performed with low energy radioactive Pd-103 x-ray sources, is a convenient treatment option for many low risk breast cancer patients. Skin is a primary organ at risk (OAR) in PBSI and is susceptible to painful toxicities when exposed to large doses of radiation. The TG-43 formalism used to calculate clinical dose distributions relies on simple assumptions that often lead to inaccurate assessments of skin dose. In this thesis, sophisticated Monte Carlo dose calculations were performed using egs_brachy to determine conversion factors relating skin doses to doses accumulated in optically stimulated luminescence dosimeters (OSLDs). These were supplemented by a procedure to calibrate OSLDs to a Pd-103 source and experimentally derived OSLD calibration factors. These results enable in-vivo dosimetry of a PBSI patient's skin dose following treatment via OSLDs placed on the surface of the skin providing valuable measurements of the actual dose delivered.

Preface

Chapter 3 of this thesis has been published as:

Steven Nich, Charles Kirkby, and J Eduardo Villarreal-Barajas. Monte Carlo study of the relationship between skin dose and optically stimulated luminescence dosimeter dose in Pd-103 permanent breast seed implant brachytherapy. *Brachytherapy*, 18(3), 387-395 (2019)

Chapter 4 of this thesis is an unpublished collaboration titled:

Steven Nich, Charles Kirkby, Thomas Mann, Tyler Meyer, J Eduardo Villarreal-Barajas. Optically stimulated luminescence dosimeter calibration procedure for Pd-103 brachytherapy source. Unpublished manuscript.

Acknowledgements

Firstly, I would like to thank my supervisors Dr. Charles Kirkby and Dr. Wendy Smith. Charlie, your advice and insights throughout this project along with your incredible patience were essential to the completion of this work and I would not have been able to do it without your support. Wendy, thank you for always asking the tough questions and making sure that I didn't lose sight of important details along the way. A special thanks goes out to Dr. Jose Eduardo Villarreal-Barajas, who despite being far away in England, was always a source of encouragement and thoughtful feedback.

I would like to thank my committee members Dr. Siraj Husain and Dr. Michael Wieser for offering their unique perspectives on the project and their continuing support as it evolved over the years. I would like to thank my internal examiner Dr. Michael Roumeliotis for his thorough responses to this work and Dr. Jeroen Stil for taking the time to preside over the examination. This project has also benefited significantly from the financial support from the Queen Elizabeth II scholarship and scholarships from the University of Calgary and the Government of Alberta.

I have had the pleasure of working with a great number of graduate students in the Medical Physics program at the University of Calgary in the last three years. To Alex Guebert, Amy Frederick, Dr. Brandon Koger, Devin Van Elburg, Dr. Elizabeth Watt, Emily Hubley, Kailyn Stenhouse, Dr. Leigh Conroy, Lingyue Sun, Pedro Martinez, Rebecca Frederick, Sarah Weppler, Svetlana Kuznetsova, and Thomas Mann, it was a joy to get to know all of you and to have the opportunity to share this journey with you. Elizabeth, as

my first contact in the program and my mentor, I thank you for all of the advice you have given me through my time at the Tom Baker Cancer Centre. Thomas, this thesis would not have been possible without your valuable contributions. To Hali Morisson, your insights played an important role in shaping this project as a whole.

I would not be where I am today without the incredible support of my family and friends. To my parents, I owe a great deal of gratitude for always being there for me no matter what challenges I face in my life. To my sisters, I am grateful to you for always having my back and for being there to talk to about anything and everything. To my friends, Chris, Colton, and Anar, you are like brothers to me and I am very lucky to have had the chance to grow into adults with you.

Last but certainly not least I would like to express my gratitude to my partner Amanda. Without your continuing love and support I would not have survived the challenges of graduate school. You always have my best interest in mind and I am forever grateful to you for building me up when life gets to be overwhelming. Thank you for pushing me to do my best and believing in me no matter what.

Table of Contents

List of Figures and Illustrations

List of Tables

List of Symbols, Abbreviations and Nomenclature

(μ_{en}/ρ)	Mass-energy absorption coefficient
$(S_K)_{\max}$	Initial air kerma strength of a source
β	Angle subtended by a source of active length L at position $P(r,\theta)$
$\dot{D}(r,\theta)$	Dose rate at position $P(r,\theta)$
$\dot{K}_\delta$	Air kerma rate due to photons with energy greater than δ *in vacuo*
Λ	Dose rate constant
λ	Decay constant of a radionuclide
$\overline{D}_j$	Average dose to voxel j
τ	Mean lifetime of a radionuclide
CAL_FACTOR	OSLD reader calibration factor
PMT_COUNTS	Raw output measurement from an OSLD reader photomultiplier tube
SENSITIVITY	OSLD specific sensitivity factor
θ	Polar angle
θ_0	TG-43 reference polar angle, $\theta_0 = 90^\circ$
d	Air kerma rate reference distance
D^j	Dose per history in voxel j
D^j_{tot}	Cumulative dose to voxel j
$D^{MC}_{skin/OSLD}$	MC calculated ratio of skin dose to OSLD dose
D_V	Maximum dose to a volume V of tissue
$D_{\max}$	Maximum point dose
$D_{0.2\,\text{cm}^3}$	Maximum dose to a $0.2\,\text{cm}^3$ volume of tissue
D_{OSLD}	Dose to OSLD
D_{skin}	Dose to skin
$D_{x,y}$	Dose to medium x with radiation transported in medium y
E	Photon energy
F	Anisotropy function
$f_{OSLD\rightarrow skin}$	OSLD to skin dose conversion factor
G_L	Geometry function using line source approximation
g_L	Radial dose function using line source approximation
h_{material}	Factor relating doses calculated in different materials adjusted for mass-energy absorption coefficients
K^j_{col}	Collision kerma per history in voxel j
k_{r^2}	Inverse square law correction factor

L	Active length
$P(r,\theta)$	Point of measurement in polar coordinates
r	Radial distance in polar coordinates, distance from source axis in rz coordinates
r_0	TG-43 reference radial position, $r_0 = 1\,\text{cm}$
S_K^{hist}	Air kerma strength per history
S_K	Air kerma strength
s_K	Air kerma strength per history (TG-43 notation)
t_i	Pathlength of photon i
t_{end}	Total decay time
t_{OSLD}	Total OSLD irradiation time
$V_{\%}$	Volume receiving a given % of the prescription dose
V_j	Volume of voxel j
z	Distance from source transverse plane in rz coordinates
3DDOSE	egs_brachy dose output file
AAPM	American Association of Physicists in Medicine
APBI	Accelerated partial breast irradiation
BCT	Breast conservation therapy
BNL	Brookhaven National Laboratory
CC	Collapsed-cone convolution/superposition
CD	Combinatorial Dimension
CPE	Charged particle equilibrium
CRPL	Carleton Radiotherapy Physics Laboratory
CSDA	Continuously slowing down approximation
CT	Computed tomography
CTV	Clinical target volume
EBRT	External beam radiation therapy
EGS	Electron gamma shower
EGS++	EGSnrc C++ class library
egsinp	egs_brachy input file
GBBS	Grid-based Boltzmann equation solver
HDR	High dose rate
ISA	Interseed attenuation
IVD	*in vivo* dosimetry
LBTE	Linear Boltzmann transport equation
LDR	Low dose rate
Linac	Linear accelerator
MBDCA	Model-based dose calculation algorithm
MC	Monte Carlo
NIST	National Institute of Standards and Technology
NNDC	National Nuclear Data Center
NRC	National Research Council
NuDat	Nuclear Structure and Decay Data
OAR	Organ at risk
OSL	Optically stimulated luminescence

OSLD	Optically stimulated luminescence dosimeter
PBI	Partial breast irradiation
PBSI	Permanent breast seed implant
PMMA	Polymethyl methacrylate
PMT	Photomultiplier tube
PTV	Planning target volume
RT	Radiation therapy
RTOG	Radiation Therapy Oncology Group
TG-186	Task Group 186
TG-43	Task Group 43
TH	Tissue heterogeneity
TLD	Thermoluminescent dosimeter
US	Ultrasound
WAFAC	Wide angle free air chamber
WBI	Whole breast irradiation
XCOM	Photon Cross Sections
Z	Atomic number

Chapter 1

Introduction

This thesis aims to facilitate *in vivo* dosimetry (IVD) using optically stimulated luminescence dosimeters (OSLD) for patients receiving permanent breast seed implant (PBSI) brachytherapy as treatment of early stage breast cancer. Monte Carlo methods were utilized throughout this work to perform dose calculations simulating doses to skin and OSLDs from implantation of radioactive Pd-103 brachytherapy seeds in breast tissue. An experimental OSLD calibration procedure for Pd-103 was implemented to establish a work-flow to apply these results clinically and to address some of the challenges of using OSLDs for IVD in brachytherapy. The techniques developed in this thesis are intended to improve skin dose monitoring in PBSI and to enable more informed decisions to be made regarding potential radiation induced skin toxicities and the appropriate treatment of these toxicities. An understanding of PBSI brachytherapy, skin toxicities due to PBSI, Monte Carlo methods and model-based dose calculation algorithms (MBDCA), radiation transport in heterogeneous media, and optically stimulated luminescence (OSL) dosimetry is essential to proceed and, in this chapter, these topics will be introduced.

1.1 Breast Brachytherapy

Brachytherapy is a form of radiation therapy (RT) used to treat a variety of cancers including breast, prostate, skin, and gynaecological malignancies. In brachytherapy, radiation is administered directly to the cancerous tissue using sealed radioactive sources inserted into or placed on the patient's body. This is in contrast to external beam radiation therapy (EBRT) which is most often delivered using a linear accelerator (linac) to produce high energy beams of photons or electrons directed at the treatment site from outside the body. In many cases, brachytherapy is a desirable treatment option either in combination with EBRT or as monotherapy due to the highly conformal dose distributions that can be achieved, which allow significant normal tissue sparing while delivering large doses to tumours [11]. Brachytherapy treatments also offer a convenient option for patients as some treatments can be completed in under one week, and even as a single outpatient procedure in the case of permanent seed implants, which is much shorter than most EBRT treatments which can take up to 5–7 weeks [11].

There are many different brachytherapy treatment techniques available, which are most often classified as either low dose rate (LDR, 0.4–2 $\mathrm{Gy\,h^{-1}}$) or high dose rate (HDR, $>12\,\mathrm{Gy\,h^{-1}}$) brachytherapy according to the rate at which dose is administered in each fraction [49]. Commonly used sources include Pd-103 and I-125 for LDR and Ir-192 for HDR treatments. The choice of treatment technique and source depends on the site, stage and the resources available amongst other considerations [78]. The variety and customizability of brachytherapy treatments has grown tremendously over more than 100 years of clinical use and it is well-established as an effective form of RT [88]. This thesis focuses on a comparatively new LDR treatment technique known as permanent breast seed implant (PBSI) brachytherapy using Pd-103 sources and directly addresses some of the dosimetric challenges related to this procedure.

1.1.1 Permanent Breast Seed Implant Brachytherapy

Breast cancer is the most commonly diagnosed type of cancer for women in Canada, representing 25 % of new cancer cases and 13 % of cancer deaths in 2017 [89]. That vast majority of these cases are diagnosed at an early stage (46.6 % at stage I and 35.1 % at stage II) [90] giving patients numerous treatment options to choose from. The standard of care for these patients consists of breast conservation therapy (BCT) where a lumpectomy is performed to remove the tumour followed by 3.5–6 weeks of whole breast irradiation (WBI) delivering a dose of between 4256 cGy in 16 treatments to 6000 cGy in 30 treatments [63] to eliminate any residual cancer cells. WBI involves irradiation of not only breast tissue but can also include organs at risks (OAR) such as skin, ribs and even the heart and lungs which can lead to radiation toxicities. Studies suggesting that the majority of recurrences occur in close proximity to the tumor bed [22] have led to the proposal of various partial breast irradiation (PBI) treatments, including brachytherapy, to minimize the amount of normal tissue irradiated [63].

PBSI is a brachytherapy procedure for early stage breast cancer patients that was first performed in 2004 at the Sunnybrook Health Sciences Centre in Toronto [66]. In it, radioactive Pd-103 brachytherapy seeds are implanted in and around the seroma following lumpectomy. Eligible patients are those aged 50 or older with ductal carcinoma in situ or low-risk (stage I) invasive carcinoma, a maximum seroma diameter of less than 3 cm that can be delineated on ultrasound (US) and computed tomography (CT), and a planning target volume (PTV) less than 125 cm^3 [65]. Patients opting for PBSI undergo US and CT imaging to determine the shape, size and position of the seroma and the clinical target volume (CTV) consisting of the seroma and surrounding fibrosis is contoured on the CT [66] (See Figure 1.1). A margin of 1.0–1.5 cm excluding the chest wall and a 5 mm thickness of skin are added to define the PTV [57,102]. The location, depth and angle of insertion of a fiducial needle is determined from the CT so that it passes through the centre of the CTV, tangential to the chest wall, and a treatment plan is created on the CT images resliced perpendicular

to the fiducial needle [65]. The fiducial needle relates the planning and delivery coordinate systems and is used a reference point for other needles.

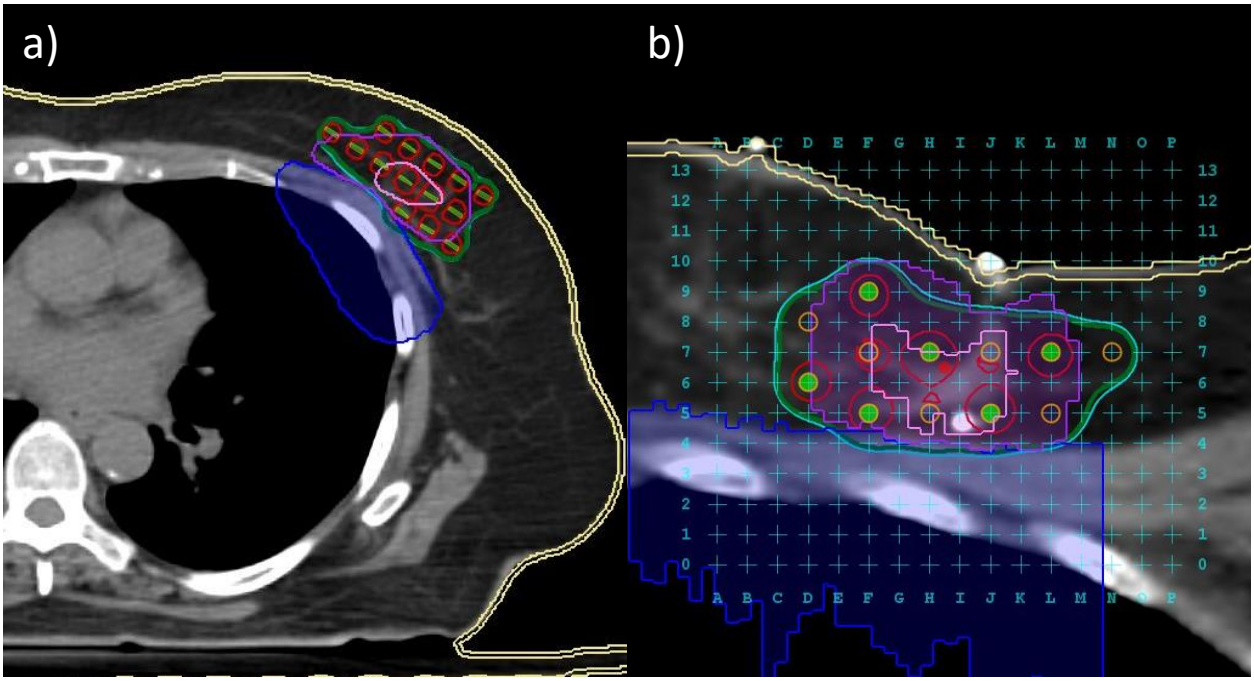

Figure 1.1: CT images showing a typical PBSI brachytherapy plan on a) an axial slice and b) an image re-sliced perpendicular to the fiducial needle (red dot in the centre of the overlaid template). The CTV, outlined in pink, is expanded to a PTV outlined in purple. A 2 mm thick skin rind is outlined in yellow and the chest wall is represented as a shaded blue region. Needle locations are shown as orange circles with seeds shown in light green as dashes in a) and solid circles in b). Isodose lines for 90 % (light blue), 100 % (dark green), and 200 % (red) of the prescription dose (90 Gy) are included. Image credit: Dr. Elizabeth Watt. For permission to reproduce figure see Appendix A.3

Treatment plans in PBSI aim to deliver a prescribed dose of 90 Gy to 100 % of the CTV with at least 98 % of the PTV receiving 90 % or more of the prescribed dose [57]. Skin dose should be minimized with no 1 cm^2 area receiving more than 90 % of the prescription [27]. To achieve these objectives, needle locations are planned on a grid centred on the fiducial needle with a needle spacing of 1 cm and seeds separated longitudinally by spacers in order to reduce hotspots (Figure 1.1) [23, 36]. On the day of treatment, the fiducial needle is inserted through the template and into the seroma under US guidance and needles loaded with stranded Pd-103 seeds are inserted in planned positions using the template to the

depth of the fiducial needle tip. Treatments are typically completed in under two hours and additional CT images are acquired immediately after treatment once the patient has recovered from the anaesthetic to analyse the quality of the implant and assess PTV coverage and OAR dose [57].

The PBSI treatment technique was developed based on experience with well-established prostate brachytherapy performed using I-125 seeds [66]. Different planning strategies have been shown to significantly influence dosimetric outcomes in prostate brachytherapy including the use of pre-planning or intraoperative planning, stranded or loose seeds, and the spacing of seeds within an implant. Decreases in OAR doses have been observed in when intraoperative planning is used [46, 108]. Differences between planned and delivered doses have been demonstrated to be higher with loose seeds compared to stranded seed in prostate brachytherapy implants [26] and urethral doses are reported to be higher with uniform seed loading compared to peripheral loading [8]. These observations emphasize the importance of dosimetry in evaluating planning strategies and identifying potential adverse treatment outcomes.

Breast treatments pose unique challenges that are less pronounced in prostate treatments due to the mobility of breast tissue and the potential for increased seed migration compared to prostate implants [25]. The use of a fiducial needle, template, US guidance, stranded seeds, and a large prescription dose are intended to address these potential difficulties while achieving the desired post-implant dosimetry [36, 57, 66]. Deviations of seed positions from their planned positions is to be expected and this has influenced the development of PBSI treatment plans to ensure that adequate dose is delivered to the PTV while minimizing hot spots and doses to skin. The PBSI procedure has been shown to be able to meet dosimetric goals and as more experience is gained using this technique, further refinements are likely to be introduced to improve patient outcomes [36,57,65]. Skin dose measurements would assist in this goal by providing valuable information regarding actual dose delivered which could be used to compare with planned doses.

PBSI is a desirable treatment option for many women diagnosed with early stage breast cancers. The implant is completed in a single day, which can greatly diminish the burden on the patient compared to daily EBRT treatments and other non-permanent brachytherapy implants such as multi-catheter interstitial, balloon-based (MammoSite), and strut-based (Savi) implants that require the patient to receive treatments over the course of a week [21, 37, 82]. In many cases, PBSI can reduce the amount of time a patient is away from work, travel time to and from the cancer centre particularly for rural patients who may also face a significant economic burden from travel and accommodation during treatment, and additional stress that accompanies daily treatments [50, 63]. This can be a deciding factor for patients who are unable to allocate the time and resources required for treatment and may otherwise refuse RT due to the inconvenience. These benefits along with the potential to reduce OAR toxicities by limiting normal tissue dose have established PBSI as a valuable alternative to other forms of treatment for suitable patients [67, 69].

1.1.2 Radiation Induced Skin Toxicities

Skin is typically the most important OAR in PBSI brachytherapy due to its close proximity to seed implant positions in many patients. As the PTV is irradiated from within the breast tissue, PBSI has the potential to reduce dose to the skin compared to EBRT by limiting the number of seeds implanted close to the skin and taking advantage of steep dose gradients around seeds to generate highly conformal treatment plans. Despite this, skin toxicities do occur in a subset of patients treated with PBSI. These toxicities arise when cells in the basal layer of skin are damaged at a rate faster than they can be replaced and adverse reactions generally appear within 10–14 days of radiation exposure, roughly the time required for new skin cells to migrate to the surface to replace old ones [71]. This occurs because DNA in skin cells is particularly vulnerable to damage from radiation during mitosis which leads to an increase in mitotic activity in the basal layer in an attempt to counteract this damage. The increased demand on the production of new skin cells cannot be sustained and adverse

reactions develop as cells die without being replaced.

The severity of skin reactions is graded on a scale from 0 (no reaction) to 4 (ulceration, bleeding and necrosis) by the Radiation Therapy Oncology Group (RTOG), which provides recommendations on how to assess skin toxicities and how to address them when they occur [17]. Most skin toxicities reported in PBSI are low grade (RTOG 2 or less) [69] with the most common reactions including reddening of the skin (erythema), flaking and peeling of the skin (dry desquamation), the appearance of red lines on the skin (telangiectasia), and thickening and hardening of the skin (induration) [47,69]. Moist desquamation, corresponding to RTOG grade 2–3, occurs very rarely and involves the loss of integrity of outer skin layers, leaving the dermis exposed [87]. All of these reactions can cause pain and discomfort for the patient ranging from relatively mild irritation to severe pain as the RTOG grade increases. Management of skin toxicities typically involves applying medicated creams to the affected areas and prescribing analgesics as needed for low grade toxicities and applying dressings to avoid infection in the most severe cases where moist desquamation is present [61,71].

A plethora of skin dose metrics are reported in breast brachytherapy literature including volumes receiving a given percentage of the prescription dose ($V_{\%}$), maximum dose to small volumes of tissue (D_{V}), and the maximum point dose to skin ($D_{\max}$) [24,31,85]. In addition, skin structure contours vary significantly across institutions, but usually skin is assumed to occupy a uniform thickness rind extending just inside the patient's body contour. The most commonly used skin dose metric related to skin toxicities is $D_{\max}$ which can be problematic as calculations of this metric are dependent on the specific discretization of the patient anatomy and it is highly susceptible to the effects of large dose gradients inherent in brachytherapy [27]. Hilts et al. have proposed $D_{0.2\,\mathrm{cm}^3}$ (maximum dose to a $0.2\,\mathrm{cm}^3$ volume for a skin rind 2 mm interior to the body contour) as a surrogate for a $1\,\mathrm{cm}^2$ area of skin based on observations of an area effect in response to radiation exposure [27]. $D_{0.2\,\mathrm{cm}^3}$ does not suffer from the disadvantages of $D_{\max}$ and strong correlations with other common metrics are cited by the authors as evidence of the robustness of this metric as a predictor of skin toxicity.

It is worth mentioning that skin is not the only OAR to be aware of in the context of PBSI brachytherapy treatments. The heart and lungs are also located in the vicinity of irradiated breast tissue and the dose to these OARs should be minimized to reduce the risk of late effects, particularly increased mortality from heart disease and secondary lung cancers [18]. There is little information available regarding doses to OARs other than skin, but Pignol et al. have emphasised sparing internal OARs given that patients receiving PBSI brachytherapy are expected to survive long after treatment [67]. However, their study found that doses to internal OARs from PBSI are generally low when compared to other breast radiotherapy techniques due to the short range of Pd-103 photons [67].

1.1.3 General Toxicities in Breast Radiation Therapy

Toxicities resulting from breast radiation therapy vary considerably depending on the techniques used as normal tissue volumes are irradiated to different levels. EBRT treatments tend to deliver more homogeneous doses than brachytherapy but irradiate much larger volumes of normal tissue. These techniques have been observed to have higher rates of moist desquamation than PBSI for intensity modulated radiation therapy (IMRT) and WBI (31.2 % and 47.8 %, respectively) [68]. Doses to the heart are generally predicted to be higher for EBRT than for PBSI with an increased risk of late cardiac toxicity associated with increasing heart dose, particularly for less-advanced EBRT techniques [7, 18, 67]. There is also potential for secondary cancers of the lungs and contralateral breast which has been reported to increase following radiation therapy. The risk of ipsilateral lung cancer is roughly twice as high after a latency period of 10 years and for contralateral breast cancers there is a 1 % increased risk for patients treated with radiation therapy compared to those who are not [7]. It should be noted that given the long latency period for secondary cancers, existing data is largely based on older treatment techniques and little is known regarding what these risks would be for PBSI.

HDR brachytherapy treatments deliver a smaller prescription dose than PBSI usually de-

livered with higher energy Ir-192 sources. These treatments have been reported to have lower rates of moist desquamation than PBSI (7 % [76]). Similarly to PBSI, HDR brachytherapy has a limited follow-up period for long term effects such as secondary cancers but it has been estimated that the excess risk for developing secondary lung cancer using HDR is 1.1 % compared to 4.1 % for WBI [28]. Doses to the heart, ipsilateral lung, and contralateral breast have been predicted to be higher for HDR brachytherapy than for PSBI due to the higher energy photons emitted by Ir-192 with potentially greater risk or late toxicities in these OARs [67]. With these details in mind, OARs other than skin will not be considered further in this thesis.

1.2 Brachytherapy Dose Calculations

Accurate dose calculations are essential to determine the optimal dose distribution to deliver the prescribed dose to the treatment volume while simultaneously sparing normal healthy tissue as much as possible. For a RT treatment to be successful, the dose delivered needs to be high enough to eliminate all cancer cells. This curative dose is constrained by the desire to limit the dose to OARs that are unavoidably irradiated during treatment. As discussed in the previous section, severe toxicities can occur when normal tissue is exposed to large quantities of radiation which can greatly affect the patient's quality of life both during and following treatment. This represents a fundamental trade-off in RT so accurate dose calculations are necessary to ensure the best possible outcome.

1.2.1 Radiological Physics Concepts

In radiological physics, absorbed dose (D) is one of the most important quantities and is defined as the expectation value of the energy imparted by ionizing radiation in a volume of matter per unit mass [4] measured in units of Gray ($1\,\mathrm{Gy} = 1\,\mathrm{J\,kg^{-1}}$). Energy from ionizing radiation is imparted to matter either directly by charged particles (electrons, protons, etc.)

or indirectly by uncharged particles (photons, neutrons, etc.) which interact with charged particles in the material. High energy photons such as x-rays and gamma rays are called indirectly ionizing radiation because they must transfer energy to charged particles (typically electrons) in order to contribute to the absorbed dose. The kinetic energy of charged particles produced in these interactions is lost to collision interactions with other charged particles by the Coulomb force or radiative interactions in which photons are produced. For electrons, kinetic energy is typically deposited near the interaction site in collision interactions but bremsstrahlung photons produced by radiative interactions can travel large distances without interacting and often do not contribute to the dose near where they are produced.

Kerma (short for "kinetic energy released per unit mass" and denoted by K) is a quantity defined for indirectly ionizing radiation as the energy per unit mass transferred to charged particles as kinetic energy in a volume of matter [4]. Unlike dose, kerma includes all kinetic energy released by indirectly ionizing radiation regardless of whether that energy is dissipated locally or away from the interaction site. As such, kerma can be expressed in terms of "collision" (K_c) and "radiative" (K_r) components which correspond to the portions of the kinetic energy dissipated in their respective interactions:

$$K = K_c + K_r \tag{1.1}$$

In general, it is difficult to calculate dose directly but under certain conditions it can be approximated by the collision kerma which is often much easier to determine. This method of approximating dose to a material is common in low energy ($< 50\,\text{keV}$) brachytherapy applications where radiative losses are effectively negligible and charged particle ranges are relatively short compared to the size of the material [5].

1.2.2 TG-43 Formalism

Clinical brachytherapy dose calculations are typically performed using the American Association of Physicists in Medicine's (AAPM) TG-43 formalism. Introduced in 1995 [58], the TG-43 formalism has been updated numerous times over the years [77, 79, 80] and provides a general framework that is meant to establish consistency in clinical brachytherapy dose calculations across institutions. This protocol standardizes procedures for calculating dosimetric quantities for brachytherapy sources including a simple method for determining the dose to water in an infinitely large, homogeneous phantom, and advocates for the use of air kerma strength (S_K) to characterize source strength over a variety of historic quantities. In general, doses are calculated for a given source and treatment geometry by looking up predetermined, tabulated dose parameters and interpolating to all representative points in a 3-dimensional grid of small volume elements called voxels. These parameters are based on a combination of consensus thermoluminescent dosimeter (TLD) measurements and Monte Carlo calculations and have been expanded to include a large number of commonly used brachytherapy sources with each iteration of the formalism.

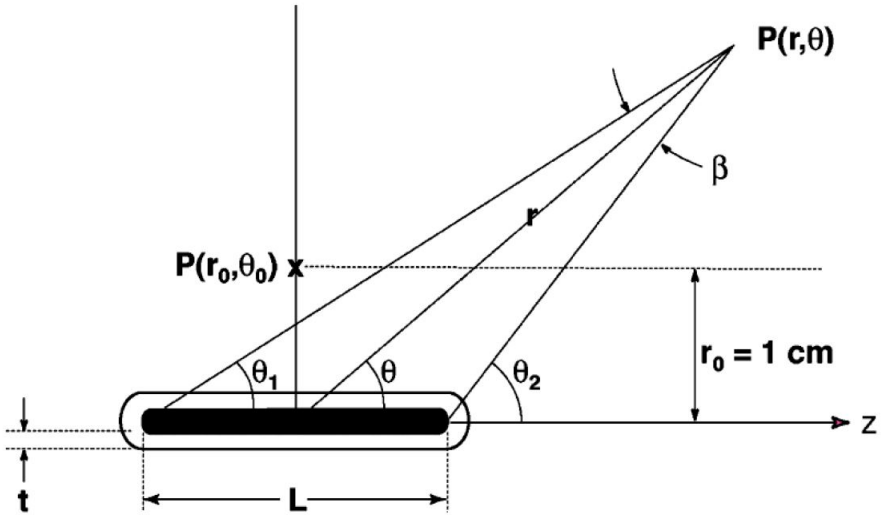

Figure 1.2: Coordinate system used in TG-43 formalism [80]. For permission to reproduce figure see Appendix A.3.

The AAPM provides two methods for calculating dose using the TG-43 formalism; a

1-dimensional point source model and a 2-dimensional line source model. The latter is the recommended approach and will be described in detail here while the former is not used in this thesis. The line source model assigns a dose-rate to water at a measurement point $P(r, \theta)$ based on its position relative to a source with active length L according to the equation below [58, 80] (see Figure 1.2):

$$\dot{D}(r, \theta) = S_K \cdot \Lambda \cdot \frac{G_L(r, \theta)}{G_L(r_0, \theta_0)} \cdot g_L(r) \cdot F(r, \theta) \tag{1.2}$$

Each of the terms in Equation (1.2) is defined as follows. Air kerma strength, S_K, is measured in units of $1\,\mathrm{cGy\,cm^2\,h^{-1}} = 1\,\mathrm{\mu Gy\,m^2\,h^{-1}}$, typically expressed as $1\,\mathrm{U}$, and is given by:

$$S_K = \dot{K}_\delta(d) d^2 \tag{1.3}$$

$\dot{K}_\delta(d)$ is the air kerma rate at a reference distance d, usually $100\,\mathrm{cm}$, from photons with energy greater than δ measured in vacuo. The source strength is represented by S_K which varies between individual seeds and needs to be determined for a subset of a batch of seeds prior to treatment.

The dose rate constant, Λ, is a constant that characterizes a given source in terms of its dose rate per unit air kerma strength at the reference position, $r_0 = 1\,\mathrm{cm}$ and $\theta_0 = 90°$ in units of $\mathrm{cGy\,h^{-1}\,U^{-1}}$:

$$\Lambda = \frac{\dot{D}(r_0, \theta_0)}{S_K} \tag{1.4}$$

The geometry function, G_L (subscript L is used to indicate that the line source model is being applied), acts as an effective inverse square law correction that accounts for the source geometry but neglects attenuation and scattering. This function is meant to improve the

accuracy of interpolated dose-rates between tabulated data points:

$$G_L(r,\theta) = \begin{cases} \frac{\beta}{Lr\sin\theta} & \text{if } \theta \neq 0^\circ \\ (r^2 - L^2/4)^{-1} & \text{if } \theta = 0^\circ \end{cases} \tag{1.5}$$

The terms in this equation are defined using the coordinate system in Figure1.2 where β is the angle subtended by the source's active length at the point of interest P.

The geometry function is combined with dose-rate measurements to define two additional functions on the same grid that these measurements were obtained on. The first of these is the radial dose function which accounts for attenuation and scattering on the transverse plane of the source as a function of the radial distance:

$$g_L(r) = \frac{\dot{D}(r,\theta_0)}{\dot{D}(r_0,\theta_0)} \frac{G_L(r_0,\theta_0)}{G_L(r,\theta_0)} \tag{1.6}$$

The anisotropy function is defined as a function of r and θ and is meant to account for the angular dependence of the dose distribution produced by the source relative to the transverse plane:

$$F(r,\theta) = \frac{\dot{D}(r,\theta)}{\dot{D}(r,\theta_0)} \frac{G_L(r,\theta_0)}{G_L(r,\theta)} \tag{1.7}$$

Each iteration of the TG-43 is published with tabulated values for the dose-rate constant, the radial dose function, and the anisotropy function up to at least 5 cm from the source for a variety of common brachytherapy sources. Dose calculations for implants involving multiple sources are determined using a superposition of single source dose distributions given by Equation (1.2).

1.2.3 Limitations of the TG-43 Formalism

Despite its widespread clinical use, the TG-43 formalism suffers from a number of major drawbacks that limit the accuracy of the dose calculations it produces. These limitations

stem from differences between realistic clinical scenarios and the simplified geometry and media scenario in which TG-43 parameters are derived. Firstly, the TG-43 formalism applies to homogeneous water geometries when in general, human tissue is a heterogeneous mixture of tissues with radiological properties different from water (tissue heterogeneity - TH). Secondly, TG-43 parameters are determined in phantoms that are large enough to achieve full backscatter conditions when this is often not the case clinically, especially for shallow implants. Lastly, TG-43 calculations are based on a superposition of single source dose distributions, ignoring attenuation and scatter due to the presence of multiple sources in the treatment volume which typically contain high atomic number (high-Z) materials (interseed attenuation - ISA).

The issues described above affect different sources and treatment sites to varying degrees and a single effect may contribute to a substantial error in dose calculations. For low energy sources ($< 50\,\text{keV}$) such as Pd-103 and I-125, TH is generally the dominant factor leading to inaccurate dose calculations followed by ISA [1, 48]. This is due to increasing importance of the photoelectric effect as a mechanism for energy deposition with decreasing photon energy compared to the Compton effect which dominates at higher energies. The interaction cross-section for photoelectric absorption is proportional to Z^3/E^3 [4] so even small differences in Z are exacerbated in dose calculations when heterogeneous tissue is modelled as pure water. The effect of backscatter (or the lack thereof) on dose distributions varies depending on the energy and depth of sources used during treatment and plays a more significant role for high energy sources (i.e. Ir-192, Co-60, etc.) and shallow treatments (i.e. breast, skin, etc.).

1.3 Model-Based Dose Calculation Algorithms

Model-based dose calculation algorithms (MBDCA) such as Monte Carlo (MC), grid-based Boltzmann equation solvers (GBBS) and collapsed-cone convolution/superposition (CC) have been proposed to address the limitations of the TG-43 formalism and improve the

accuracy of brachytherapy dose calculations [9, 16, 111]. These algorithms attempt to account for heterogeneous transport media either by finding analytical solutions to primary dose components and approximating scatter components, or generating approximate solutions to the linear Boltzmann transport equation (LBTE) numerically or deterministically on a discrete grid. It is well-known in the brachytherapy community that TG-43 based dose calculations are error-prone, but a suitable replacement in the form of an MBDCA has yet to achieve the ubiquity and consistent implementation in clinical applications of TG-43 due to the increased complexity of these algorithms. The AAPM's TG-186 report [5] intends to provide guidance for early adopters of MBDCAs and to establish a framework for the clinical implementation of these algorithms that is consistent across institutions. Discrepancies between TG-43 and MBDCA dose calculations reported in the literature [1,13,41,45,48,54,103] highlight the potential impact inaccurate calculations can have on successfully meeting treatment objectives and motivates the need for drastic changes to procedures as outlined in the TG-186 report.

Despite the potential to improve the accuracy of brachytherapy dose calculations using MBDCAs, the TG-186 report identifies three major challenges that continue to be hurdles to its clinical implementation [5]. The first of these issues comes down to the choice of whether doses should be specified in terms of the dose to the medium present in a voxel or as a dose to water, the former being a natural candidate for MBDCAs and the latter being consistent with clinical experience and arguably simpler to adopt in general. Conversions between these quantities are not straight-forward and both have their advantages and disadvantages which make it difficult to achieve a consensus on which should be used. The second issue involves identifying and assigning cross-sections on a voxel-by-voxel basis in CT scans, which is essential for MBDCAs to calculate doses accurately, but difficult to achieve in practice as tissues with similar electron densities often cannot be reliably distinguished using conventional CTs. The last issue relates to commissioning MBDCAs for clinical use and stresses the need for validation of these algorithms by reproducing TG-43 dose distributions in the

same conditions and performing additional validations against measurements in phantoms to assess the algorithm's performance.

1.3.1 Monte Carlo Methods

Monte Carlo methods are used extensively to model radiation transport and have a well-established reputation as the most accurate dose calculation algorithms [15]. These methods make use of pseudo-random number generators to sample from probability distributions associated with stochastic processes such as radioactive decay and interactions between photons and matter [3]. Through repeated sampling, useful statistics regarding the phenomenon being simulated can be obtained if the problem is modelled appropriately. In the context of radiation transport, these statistics are generated by simulating large numbers of particle "histories" which represent the time between the generation of a particle and its subsequent interactions up to the point when the initial particle and any secondary particles are terminated. This approach allows very accurate dose calculations to be performed for virtually any combination of radiation sources and transport media at the expense of increased complexity in creating specific models and greater computational resource requirements.

Brachytherapy dose calculations using MC algorithms are typically performed using more or less the same approach. A history is initiated with the production of a particle (usually a photon, but electrons are often available if desired), consistent with a source model that describes in a statistical sense the initial type, position, direction, and energy of particles emerging from the source. A set of pseudo-random numbers is used to draw specific properties of an individual source particle based on these statistical descriptions. In a brachytherapy context, the source is distributed spatially within the radioactive components of a seed model and energies are selected based on a known spectrum of decay energies with associated probabilities. Interaction cross-sections are used to determine the distance that the particle will travel before an interaction occurs, the type of interaction, the energy lost, and the state of the particle and any secondary particles following the interaction. This process is

repeated until all particles involved are terminated when their energy falls below a specified threshold through subsequent interactions, or they leave the geometry and information about the energy deposited in the transport media is scored before initializing the next history.

There is considerable flexibility in how MC algorithms are applied to brachytherapy dose calculations in terms of defining geometries, materials, and various parameters affecting the simulations. Geometries are divided into voxels where the medium and any physical properties relevant to the dose calculation need to be specified including elemental composition, mass density, and radiological characteristics. Online databases such as the National Institute of Standards and Technology (NIST) Photon Cross Sections (XCOM) Database [6] are often used to provide input data for MC algorithms in the form of tabulated data which can be retrieved by the algorithm as needed. The user typically has control over transport parameters including photon and electron cut-off energies, which interactions to model, explicit modelling of atomic relaxations, and many more details which dictate the amount of input data required, the accuracy, and length of the simulation. The specific parameters used depend on the nature of the situation being simulated and careful selection of the appropriate parameters can significantly reduce simulation time with a minimal effect on the accuracy.

1.3.2 egs_brachy

egs_brachy is a MC code developed at the Carleton Radiotherapy Physics Laboratory (CRPL) in Ottawa that serves as an extension of the prominent EGSnrc MC code with an emphasis on brachytherapy applications [12]. EGSnrc was originally developed at the Stanford Linear Accelerator Center in the 1980's as EGS and is currently maintained by the National Research Council of Canada (NRC). EGSnrc is a general purpose, open source MC package designed to simulate coupled photon-electron transport in arbitrary media while accounting for complex relativistic and quantum mechanical effects present in these interactions [34]. The code is well-known for its speed and accuracy [60] in a variety of radiation transport

applications, but it is particularly useful for medical physics research. EGSnrc is distributed with a number of user codes intended to streamline the process of modelling clinically relevant geometries for EBRT and medical imaging applications. The release of egs_brachy in 2017 greatly simplified the development of brachytherapy geometries.

egs_brachy implements the same radiation transport algorithm as EGSnrc and makes extensive use of the highly versatile egs++ geometry package. Input is provided to egs_brachy through egsinp files, which define the number of histories to simulate, run mode, media compositions, geometries, source properties, scoring properties, and additional transport parameters. Most of this information is stored in separate data files and the egsinp file merely specifies the path to these files so that commonly used data can be reused in different simulations. During simulations, egs_brachy extracts interaction cross-section data on the fly from a material data file based on the current photon's energy and materials present in the voxels of interest, and mass-energy absorption coefficients (μ_{en}/ρ) are retrieved to calculate collision kerma along the photon's path (tracklength estimator) or at the site of the interaction (interaction scoring) depending on the scoring setting. A variety of output files containing detailed information about simulations can be requested in the egsinp file, but the primary output is stored in a 3DDOSE file which lists the voxel boundaries, dose values for every scoring voxel and the statistical uncertainty of each calculated dose.

Every egs_brachy simulation requires three geometries to be defined either in the egsinp file or via references to external geom files: a source geometry, a phantom geometry, and a simulation geometry. The source geometry defines the shape, size, and material of all components that make up the radiation source in a geom file. The phantom geometry is the volume where dose is to be scored during simulations and specifies the boundaries of voxels in either Cartesian coordinates (XYZ), cylindrical coordinates (RZ), or spherical coordinates (R). The simulation geometry defines the boundaries of the simulation so that particles can be terminated if they escape. Source and phantom geometries are inserted into the simulation geometry using what is referred to as an envelope which establishes the hierarchy of the

geometries so that regions of the simulation geometry containing the phantom geometry are replaced by the phantom materials and similarly the source materials replace phantom materials wherever necessary.

In addition to appearing in the geometry definition, another required section of the egsinp file is dedicated entirely to the source(s). The source geom is referenced in this section along with a shape file that specifies the distribution of radioactivity within the source and a boundary shape file that defines a volume enclosing the source (see Figure 1.3). A transformation is required to specify the location of the source, but also can be used to indicate multiple transformations which generate copies of the original source and place them at the desired locations. The source type also needs to be defined (usually isotropic for radioactive sources) and at least one photon (or electron/positron) energy needs to be specified but a spectrum of energies and probabilities is commonly used by referencing a spectrum file containing this data.

Volume corrections are necessary to properly score dose in voxels that contain portions of the source geometry. Dose is not scored in the source geometry so if a voxel is occupied by phantom and source geometries, the volume containing only the phantom geometry needs to be calculated. The boundary shape file specifies a shape (typically a cylinder) that, ideally, is just large enough to completely surround the source. A MC calculation is performed within the boundary by randomly drawing a large number (1×10^6–1×10^8) of points to approximate the corrected volume for the affected voxels (Figure 1.3). The volume occupied by the source is subtracted from these voxels to properly calculate dose using a tracklength estimator (see Equation(1.8)).

Mass-energy absorption coefficients (μ_{en}/ρ) are required for any phantom material where dose (technically collision kerma) is to be scored. Collision kerma is calculated using a tracklength estimator by default according to the following formula:

$$D^j = K^j_{\text{col}} = \frac{\sum_i E_i t_i (\frac{\mu_{\text{en}}}{\rho})_i}{V_j} \tag{1.8}$$

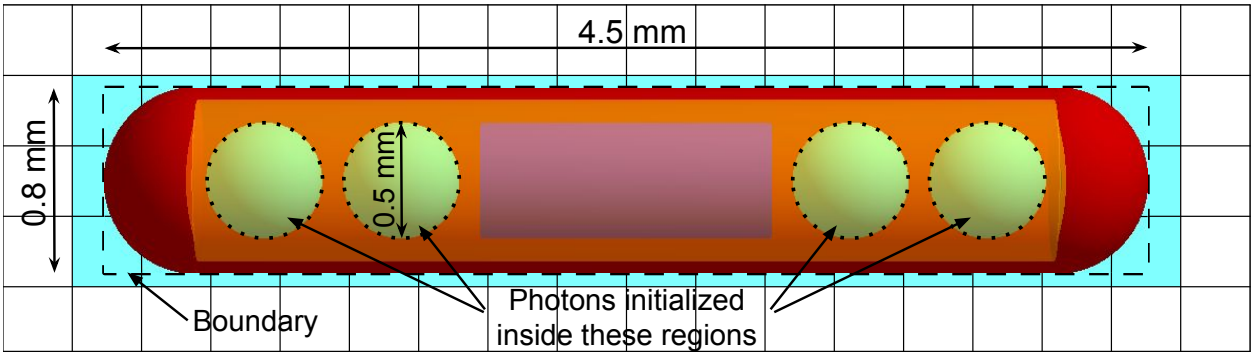

Figure 1.3: Illustration of the use of "shape" files in egs_brachy source geometry definition for a brachytherapy source inside a voxelized phantom geometry. One shape file (indicated by the regions inside the dotted lines) is used to specify the distribution of radioactivity within the source where particle histories are randomly initialized. The boundary shape file (shown as dashed lines) defines the extent of the source within the phantom geometry and voxels affected by the volume correction calculation (light blue shaded region).

In this equation, j means the $j-th$ voxel and the sum is taken over all histories i. D^j and $K^j_{\rm col}$ are the dose and collision kerma per history in voxel j, E_i is the photon energy when it enters the voxel, t_i is the pathlength within the voxel, and V_j is the volume of the voxel. The tracklength estimator is considerably faster than the more realistic interaction scoring technique and in most cases, particularly for low energy photons ($< 50\,$keV), it is an accurate approximation as the mean electron ranges are sufficiently short ($< 0.02\,$mm in water) compared to voxel dimensions to not affect the result of the calculation within experimental uncertainty [1]. All doses scored with egs_brachy are in units of Gy/history and so an appropriate scaling factor needs to be applied to the outputs to convert to absolute doses for calculations with real sources using the equation below:

$$D^j_{tot} = (S_K)_{\rm max} \frac{\overline{D}_j}{S^{hist}_K} \tau (1 - e^{\lambda t_{end}}) \tag{1.9}$$

D^j_{tot} is the cumulative dose to voxel j, $(S_K)_{\rm max}$ is the initial air kerma strength of the source, $\overline{D}_j$ is the average dose per history over all histories simulated, S^{hist}_K is the air kerma strength per history (a quantity that needs to be calculated separately), τ and λ are the mean lifetime and the decay constant of the radionuclide in the source, and t_{end} is the total decay time.

While the tracklength estimator is the default dose scoring method utilized in egs_brachy, it also possible to calculate energy deposition (and therefore absorbed dose) by enabling interaction scoring. Strictly speaking, the former approach is only valid under the condition of charged particle equilibrium (CPE) which if not satisfied can produce inaccurate results (for example, within close range of high energy brachytherapy sources such as Ir-192 [94]). However, in the case of Pd-103, an average energy photon ($\sim 20\,\text{keV}$) produces secondary electrons which generally have very short ranges (continuously slowing down approximation (CSDA) range of less than $0.02\,\text{mm}$ in water [5]) and a negligible amount of energy lost to bremsstrahlung (less than $0.02\,\%$ in water) so the assumption of CPE is justified. The motivation behind using a tracklength estimator stems from the equivalence of fluence and total tracklength per unit volume [10] which allows collision kerma to be approximated using Equation (1.8). Using this method, any photon that passes through a voxel contributes to the dose in that voxel which improves the efficiency of a dose calculation compared to interaction scoring where energy is only deposited when an interaction occurs [3, 104].

MC transport parameters can be adjusted in egs_brachy and many have default values, but global photon and electron cut-off energies must to be set for histories to be terminated properly within the simulation geometry. The egs_brachy distribution comes with files that set these parameters to commonly used defaults in MC simulations with low energy sources which include transporting photons to energies of $1\,\text{keV}$, neglecting electron transport, and modelling Rayleigh scattering. These parameters are consistent with recommendations in the literature for MC brachytherapy studies [1,12,14,42,54,93] and are intended to accurately model important aspects of radiation transport while neglecting those that reduce efficiency without making worthwhile improvements to the results. Calculation efficiency can also be increased using traditional variance reduction techniques and new techniques developed specifically by the creators of egs_brachy. Although these techniques can greatly increase the efficiency of dose calculations [12] and, therefore, address one of the primary limitations of clinical MC algorithms, they have not been implemented for the simulations performed in

this thesis for the sake of simplicity.

1.4 Optically Stimulated Luminescence Dosimetry

Optically stimulated luminescence (OSL) is a physical phenomenon where a material emits light in response to an external light source following exposure to ionizing radiation [109]. Because there is a quantitative relationship between the absorbed dose and luminescence output, OSL materials can make convenient dosimeters. These materials consist of "traps" in the form of defects in their crystalline structure that are used to store an OSL signal. These traps exist between the valence band and the conduction band of the underlying material. When the material is irradiated with ionizing radiation, electron-hole pairs are created which can become trapped in electron traps and hole traps in the band gap of the material, respectively. Optical stimulation is used excite electrons out of these traps allowing them to recombine with holes in luminescence centres producing photons in the process which constitute the measurable OSL signal.

The OSL phenomenon is observed in many materials but Al_2O_3:C (aluminum oxide doped with carbon) is the most commonly used material for radiation dosimetry applications [51, 109]. Landauer Inc. (Glenwood, USA) is a major manufacturer of Al_2O_3:C based OSL dosimeters (OSLD) and equipment to read dose measurements obtained using their OSLDs. A popular type of OSLD for medical radiation dosimetry is the nanoDot™. These are produced by melting Al_2O_3 at high temperatures and introducing carbon dopant before allowing the mixture to cool and form crystals [73, 109]. The crystals are crushed into a powder, mixed with a polyester binder and sealed between two strips of polyester tape from which small circular films are cut and encapsulated in plastic, forming the nanoDot™. The finished product is a plastic chip containing the Al_2O_3:C film that is labelled with a serial number and a bar code that identify the individual OSLDs along with their relative sensitivity.

nanoDot™OSLDs are designed to be read using Landauer's microStar® dosimetry system which consists of a bar code scanner to read the OSLD's serial number and sensitivity, a plastic plate to hold the OSLD during measurement, the microStar® reader itself, and a laptop with software to perform display and store measurements [39]. Following irradiation, a measurement is obtained by placing the OSLD in the holder which is then positioned in a drawer in the reader. A knob on the reader is turned which stimulates the OSL film with a green light (centred at 532 nm) first as a short pulse to sample the signal and determine an appropriate calibration to apply to the measurement and then a longer pulse stimulates the measured signal [39, 73]. The OSL film emits blue light (centred at 420 nm) which is filtered and fed into a photomultiplier tube (PMT) and counting electronics. The readout process takes approximately 10 s and outputs a raw PMT count and an estimate of the dose measurement.

For nanoDot™OSLD measurements to be meaningful, PMT counts need to be converted to a dose by correcting for the individual sensitivity of each OSLD, and applying a calibration factor:

$$D = \frac{\text{PMT\_COUNTS}}{\text{SENSITIVITY} \cdot \text{CAL\_FACTOR}} \tag{1.10}$$

Calibrations need to be performed to generate a minimum of two CAL_FACTOR values (in units of Counts/cGy) corresponding to low dose and high dose regimes, typically defined as $<$20 cGy and $>$20 cGy, respectively. This is done by irradiating a set of OSLDs to known doses over a range of values, measuring the PMT counts for each dose level, and obtaining linear fits for each energy regime to determine the relevant CAL_FACTORs. OSLD response is dependent on the photon energy used to irradiate them so individual calibrations need to be performed for all source energies that they are intended to be used in order properly convert from PMT count to dose. The general calibration procedure is the same for each application and specific calibrations can be selected prior to readout from a list stored in the microStar® software.

In clinical RT scenarios, OSLDs can be placed in regions of interest on or near the patient

during irradiation and used to approximate doses to the patient's anatomy with an accuracy of at least $\pm 10\,\%$ for general purpose nanoDots™or $\pm 5\,\%$ for screened nanoDots™($k = 2$) [40, 73, 75]. General purpose nanoDots™are labelled with the average sensitivity of the roll from which they were produced. Screened nanoDots™are assigned sensitivities based on individual comparisons with reference nanoDots™which have sensitivities that are known to be highly accurate and precise. In order to achieve the described accuracies, nanoDots™clinical geometries and photon energies should match calibration conditions. With proper annealing, nanoDots™can measure doses as small as $50\,\mu Gy$, far lower than typical clinical doses on the order of at least $1\,cGy$ [2].

In vivo dosimetry measurements obtained during treatment provide valuable information which can influence decisions regarding the patient's treatment. In the past, thermoluminescent dosimeters (TLD) were the standard tool used for *in vivo* dosimetry, but OSLDs have experienced a significant growth in popularity and have largely replaced TLDs in these applications [99]. This can be attributed to advantages that OSLDs have over TLDs in terms of the complexity of readout (TLDs need carefully heated to produce a signal), re-readability (measurement of TLD signal destroys the signal), and resource requirements including equipment and time costs [38, 52]. The overall simplicity of performing *in vivo* dosimetry measurements with OSLDs makes them an incredibly valuable tool with the potential to continually improve the quality of RT treatments.

It should be noted in the context of this thesis that an attempt was made in the past to use radiochromic film to measure skin doses in PBSI brachytherapy. This work was performed at the Tom Baker Cancer Centre (where the current work was conducted) and has not been published, nor has any other work utilizing radiochromic film in PBSI. The primary motivation for using radiochromic film is the ability to measure dose distributions over a 2-dimensional area and its near equivalence to tissue [64]. However, film also presents a number of challenges including the need to cut it to an appropriate size which can introduce artifacts, its cost, sensitivity of dose measurements to film orientation, a 24 hour waiting period is

required between exposure and measurement, susceptibility of low dose measurements to noise, and greater care required when handling and storing film to preserve measurements [64]. In light of these potential drawbacks, OSLDs present a desirable alternative to measure skin doses due to their simplicity as well as the advantages previously described.

1.5 Thesis Work

Monte Carlo methods have an abundance of practical applications in the field of medical physics which is evidenced by their continued use to solve challenging computational problems which may otherwise be unsolvable. Although routine clinical implementation of these algorithms for brachytherapy dose calculations has not yet been achieved, their versatility allows them to remain a valuable research tool for obtaining meaningful results. This thesis is motivated by the desire to find reasonable ways to improve the practice of treating early stage breast cancer patients with PBSI brachytherapy through better dosimetry using a combination of MC algorithms and OSLDs. Ideally, this would make it possible to optimize PTV doses for these patients in a safe manner by addressing the potential for radiation induced skin reactions. In the long term, it is hoped that this work will lead to more appropriate skin dose limits, translating into better treatments plans and patient outcomes.

The goal of this thesis is to introduce procedures for performing *in vivo* skin dosimetry using OSLDs in the context of PBSI brachytherapy. To achieve this, MC methods have been implemented using the egs_brachy code to model a Pd-103 source implanted in breast tissue as well as in a polymethyl methacrylate (PMMA) phantom. Chapter 2 covers simulations that were performed to validate the egs_brachy code for the IsoAid Advantage Pd-103 (IAPd-103A) brachytherapy seed in accordance with TG-186 recommendations and other preliminary work that was necessary to link experimental measurements to these simulations in later chapters. Chapter 3 contains the results of work relating skin dose to OSLD dose in a breast phantom representing a simplified PBSI implant to enable skin dose assess-

ments to be made based on measured OSLD doses. Chapter 4 is intended to fill the gaps of the previous chapter by providing an OSLD calibration procedure for the IAPd-103A seed that combines experimental measurements in PMMA with egs_brachy calculations. The project as a whole is summarized in Chapter 5 and directions for future work are identified.

Chapter 2

Preliminary Monte Carlo Simulations

egs_brachy is a relatively new MC code and although it uses the EGSnrc algorithms, which have been extensively benchmarked, it is necessary to perform validations to ensure the code can reproduce known dose distributions. The IsoAid Advantage™Pd-103 (IAPd-103A, IsoAid, LLC, Port Richey, Fl) brachytherapy seed was selected as a source to use in egs_brachy simulations as this was the source used to perform PBSI at the Tom Baker Cancer Centre at the time of this work. A geometry model for the source was developed from scratch using the EGS++ geometry package based on measurements available in the literature [53, 91, 95]. Validation against TG-43 dose distributions for the IAPd-103A seed as per the TG-186 recommendations [5] was performed first followed by comparisons with work by Luxton regarding dosimetry for brachytherapy sources in solid phantoms [44]. Additional simulations using the EGSnrc user code g were also conducted to generate μ_{en}/ρ coefficients for Al_2O_3:C that were required to model the nanoDot™OSLD.

2.1 Development of IAPd-103A Seed Model for egs_brachy

The IAPd-103A seed was modelled using the "combinatorial dimension" (CD) geometry from the EGSnrc C++ class library [35] (also known as egs++ for short) using the dimensions described on the CLRP Seed Database [53, 91, 95]. The CD geometry works by defining a

set of "cutting" planes that define the boundaries of the regions where separately defined geometries, corresponding to different sections of the source, exist in the overall geometry. This technique is useful for creating highly customizable geometries as only the intersection of the region contained between a pair of cutting planes and any geometry assigned to that region is modelled. For an IAPd-103A source, the seed was cut into seven regions along the z-axis (see Figure 1.2): one cap on each end of the seed composed of overlapping spheres of titanium and air, one section containing a cylindrical silver marker surrounded by an air cylinder and a titanium cylinder, and four identical sections each containing a radioactive Pd-103/polystyrene sphere surrounded by air and titanium cylinders. The final geometry essentially cuts off unnecessary portions of the individual sections (end caps cut into hemispheres, and all cylinders cut down to appropriate length as they are infinitely long by default) and joins them together along the z-axis to form an accurate model of the seed (Figure 3.1).

The egs++ library contains a variety of particle source class which specify how the initital positions and directions of particles are chosen. In the source definition section of an egsinp file, the particle source object is specified along with a shape file and the charge of the particles to simulate (0 for photons, -1 for electrons, and 1 for positrons). The IAPd-103A source was modelled using the EGS_IsotropicSource class (an isotropic source), a shape file consisting of four 0.5 mm spheres coinciding with the Pd-103/polystyrene pellets in the source (see Figure 1.3), and a charge of 0. The Pd-103 photon spectrum chosen for all simulations was from the Brookhaven National Laboratory's (BNL) National Nuclear Data Center (NNDC) Nuclear Structure and Decay Data (NuDat 2.7) [19, 59] which specifies the possible initial photon energies with their respective probabilities. Based on these specifications, source photons were initialized in egs_brachy by randomly selecting a position within one of the four spheres with a random direction cosine (both uniformly distributed for an isotropic source), and randomly sampling the initial photon energy from the probability distribution associated with the spectrum.

The source is central to all egs_brachy simulations so it is crucial that all aspects of the model are defined as accurately as possible. egs_view is an EGSnrc application that can be used to view geometries in 3-dimensional space and was a valuable first check during the development of the source model to ensure that obvious mistakes were not being made and later, to verify that the radiation distribution within the source was correct. All materials contained in the IAPd-103A source were predefined in egs_brachy's default material.dat file and the properties of these materials (mass density and composition) were compared with published values which identified a small error in the composition of the Pd-103/polystyrene material in the seed (mass fractions for N and Cl were 0.03 and 0.07 instead of 0.003 and 0.007, respectively [53]). The NNDC Pd-103 photon spectrum was compared with the spectrum included in egs_brachy which also revealed a very minor input error (the 317.72 keV energy was missing from the spectrum). These two errors were corrected in their respective files and the developers were notified, prompting two corrections to be submitted to the egs_brachy distribution on GitHub.

2.2 TG-43 Validation

Validation of the egs_brachy Monte Carlo code against consensus TG-43 dosimetric parameters for the IAPd-103A brachytherapy source was carried out as a two step process. The first of these steps involved the calculation of the source's air kerma strength per history. This value serves as a normalization factor that converts Monte Carlo doses which are generally expressed as a dose per history to a more clinically relevant dose per unit time. The second step involved simulations with all water geometries to determine the dose to water around the seed. The combination of these two steps was used to determine the dose rate constant, the radial dose function, and the anisotropy function for the IAPd-103A source for comparison against literature values [53, 77, 81, 91, 93].

2.2.1 Air Kerma Strength Simulations

To determine the air kerma strength per history for the IAPd-103A source, the source was modelled in a vacuum with dose scored in a voxel composed of air 10 cm from the source, approximating the air kerma rate *in vacuo*. This geometry is provided with egs_brachy and consists of a single voxel 2.66 cm in width and height, and 0.05 cm thick centred on the transverse plane of the seed with the front face located 10 cm from the seed's axis. The dimensions of this phantom are meant to approximate the solid angle subtended by the wide angle free air chamber (WAFAC) used by NIST to calibrate brachytherapy sources in terms of air kerma strength. In reality, the WAFAC chamber would be positioned 100 cm from the source, but the approximation is essentially equivalent with more manageable dimensions [91, 96]. 4×10^9 histories were simulated with characteristic x-rays from the seed's titanium encapsulation suppressed (photon cut-off energy of 5 keV) as is recommended for simulations of this type [80].

The simulated air kerma rate for the IAPd-103A seed was converted to a value for the air kerma strength per history using the following equations from Taylor et al. [96]:

$$s_K = \dot{k}_\delta(d) \times d^2 \times k_{r^2}, \tag{2.1}$$

where

$$k_{r^2} = \frac{1}{d^2 \cdot w^2 \cdot t} \int_d^{d+t} \int_{-w/2}^{w/2} \int_{-w/2}^{w/2} (x^2 + y^2 + z^2)\, dx\, dy\, dz \tag{2.2}$$

Here $\dot{k}_\delta(d)$ is the simulated air kerma rate at $d = 10$ cm, and k_{r^2} is a correction factor that accounts for the effect of volume averaging over the large scoring volume. w represents the width and height of the voxel and t is the thickness. s_K refers to the air kerma strength per history which is labelled with a lower-case "s" to distinguish this normalized value from the air kerma strength S_K which is a common convention [80]. Using this procedure, a value of $s_K = 8.221 \times 10^{-14}$ U/history $\pm 0.01\,\%$ was obtained.

2.2.2 Dose Calculations in Homogeneous Water Geometries

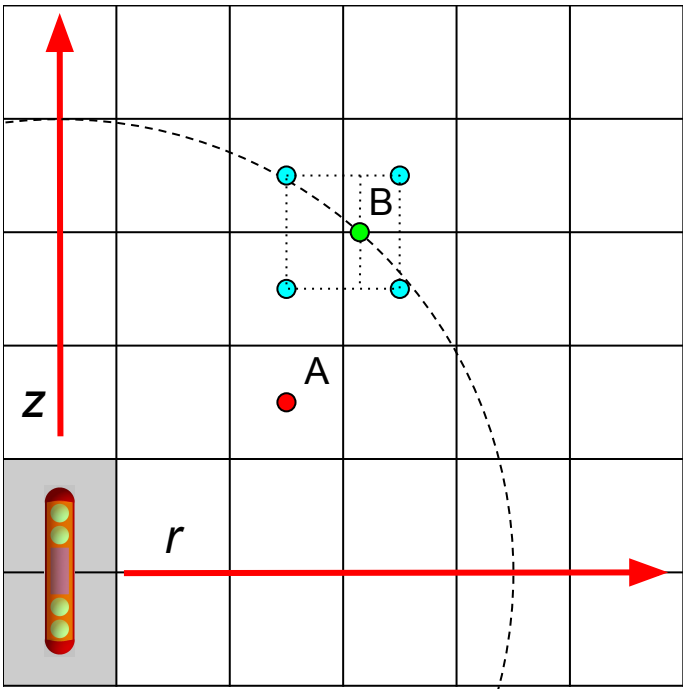

Figure 2.1: Division of phantom geometry into voxels for TG-43 validation simulations in homogeneous water medium. The IAPd-103A source is located with its centre at the origin of the rz coordinate system and its axis aligned with the z-axis. The horizontal and vertical lines forming the grid correspond to the boundaries of scoring voxels in the phantom geometry. r coordinates are measured horizontally and z coordinates are measured vertically with respect to the centre of the seed. This figure is not to scale and is only meant to illustrate general features of the phantom geometry.

Figure 2.1 illustrates how a typical rz coordinate system is defined in egs_brachy within a voxelized phantom geometry. Doses are calculated for each voxel separately and the position associated with each voxel was chosen to be at its centre. For example, the voxel containing the red dot labelled "A" would be assigned the position of this dot as a representative point of measurement. To score dose for points given by polar coordinates such as the green dot labelled "B", a bilinear interpolation was performed using the doses from the four nearest voxels shown as aqua coloured dots in this diagram. The two grey voxels surrounding the seed indicate the regions where a volume correction would be performed by egs_brachy. The volume occupied by the seed would not be included in the dose calculation in these voxels.

TG-43 parameters were obtained from three homogeneous water phantom geometries

that were included in the egs_brachy distribution which differed only in the resolution of their scoring voxels. A $30\,\mathrm{cm}^3$ cube of water was used for the simulation geometry in all three cases and the IAPd-103A source geometry was modelled in the centre, aligned along the z-axis of the coordinate system (Figure 2.1). Each simulation used a cylindrical phantom geometry with voxels defined as rings with constant r encircling the source on a grid of rz coordinates, taking advantage of the seed's cylindrical symmetry (note: r is measured from the source axis and is different from the r in Figure 1.2). The first phantom geometry used $0.1\,\mathrm{mm} \times 0.1\,\mathrm{mm}$ voxels for the region where $r \leq 1\,\mathrm{cm}$ and $z \leq 1\,\mathrm{cm}$, the second used $0.5\,\mathrm{mm} \times 0.5\,\mathrm{mm}$ voxels for the region where $r \leq 5\,\mathrm{cm}$ and $z \leq 5\,\mathrm{cm}$, and the third used $1.0\,\mathrm{mm} \times 1.0\,\mathrm{mm}$ voxels for the region where $r \leq 10\,\mathrm{cm}$ and $z \leq 10\,\mathrm{cm}$. These voxels sizes were chosen to minimize the effects of volume averaging in the regions closest to the source where the dose gradient is the greatest while allowing dose rates to be calculated farther from the source in a reasonable amount of time.

All TG-43 style dose calculations in water simulated 1×10^9 histories with a photon cut-off energy of 1 keV and an electron cut-off energy of 1.512 MeV (including electron rest energy of 0.511 MeV) so electrons were not transported. It should be noted that this electron cut-off energy is restrictive enough to prevent all electron transport because the maximum photon energy for Pd-103 (and therefore the maximum possible secondary electron energy) is 497.08 keV. 3DDOSE files from these simulations along with the results from Section 2.2.1 for the air kerma strength calculation were analysed using MATLAB. Functions were created to store data from 3DDOSE files in .mat files with rz coordinates calculated as the centre of the voxel boundaries defined in the 3DDOSE output. Doses and their statistical uncertainties were also stored in these .mat files and special functions were designed to extract doses at any specific position in the phantom geometries as needed.

The dose rate constant, radial dose function, and anisotropy function for the IAPd-103A seed were calculated using Equations (1.4), (1.6), and (1.7), respectively, on the same grids as the most recent TG-43 supplement [77] for comparison. The geometry function (Equation

Table 2.1: IAPd-103A dose rate constant in water generated using egs_brachy along with values from literature. Source indicates the study that produced the value.

Source	Calculation Method	Algorithm or Technique	Λ(cGy h^{-1} U^{-1})
This study	Monte Carlo	egs_brachy	0.659 ± 0.001
TG-43U1S2 [78]	Consensus	50 % MC and 50 % TLD	0.693 ± 0.031
Meigooni et al. [53]	Monte Carlo	PTRAN [104, 105]	0.69 ± 0.02
	Measurement	TLD	0.70 ± 0.06
Sowards [91]	Monte Carlo	PTRAN	0.709 ± 0.014
Taylor and Rogers [93]	Monte Carlo	BrachyDose (EGS) [96]	0.687 ± 0.001[a]
Rodriguez and Rogers [81]	Monte Carlo	BrachyDose (EGS)	0.661 ± 0.002

[a]The authors later corrected this value, replacing it with the value by Rodriguez and Rogers due to an error found in the original calculation. The former is not included in the consensus value used for TG-43U1S2.

Table 2.2: egs_brachy dose rates for IAPd-103A brachytherapy seed normalized to air kerma strength (cGy h^{-1} U^{-1}) in polar coordinates. Note that data is formatted in the same style as TG-43U1S2 [78] to aid in comparisons.

	r(cm)									
Polar angle θ (°)	0.1	0.25	0.5	0.75	1	2	3	5	7.5	10
0		6.35	0.825	0.324	0.1756	0.0264	0.00744	0.000762	0.0001080	0.00001467
2		6.50	0.845	0.328	0.1689	0.0272	0.00707	0.000814	0.0000938	0.00001689
5		7.15	0.879	0.340	0.1734	0.0278	0.00718	0.000832	0.0000929	0.00001668
7		7.92	0.918	0.351	0.1787	0.0284	0.00744	0.000853	0.0000942	0.00001746
10		10.01	1.019	0.381	0.193	0.0303	0.00790	0.000910	0.0000999	0.00001757
15		15.20	1.297	0.468	0.232	0.0357	0.00914	0.001030	0.0001100	0.0000196
20		19.5	1.711	0.603	0.293	0.0433	0.01095	0.001201	0.0001240	0.0000208
25		21.0	2.13	0.747	0.360	0.0517	0.01282	0.001384	0.0001410	0.0000234
30	146.3	20.6	2.47	0.873	0.420	0.0594	0.01460	0.001554	0.0001558	0.0000249
40	83.4	17.69	2.94	1.065	0.513	0.0718	0.01749	0.001842	0.0001808	0.0000270
50	56.3	15.17	3.18	1.201	0.584	0.0818	0.0199	0.00207	0.000202	0.0000297
60	42.9	13.47	3.25	1.279	0.630	0.0889	0.0216	0.00225	0.000220	0.0000320
70	35.9	12.43	3.24	1.308	0.652	0.0932	0.0227	0.00237	0.000228	0.0000332
80	32.3	11.86	3.21	1.314	0.658	0.0947	0.0231	0.00241	0.000234	0.0000333
90	31.2	11.66	3.19	1.313	0.659	0.0951	0.0232	0.00242	0.000234	0.0000333

(1.5)) was calculated using an adapted form of Equation 7 from Raisali et al. [72] to determine β from rz coordinates:

$$\beta = \theta_2 - \theta_1 = \tan^{-1}\left(\frac{|z| + L/2}{r}\right) - \tan^{-1}\left(\frac{|z| - L/2}{r}\right) \tag{2.3}$$

Published TG-43 consensus data for dose rates normalized to air kerma strength and the

Table 2.3: egs_brachy dose rates for IAPd-103A brachytherapy seed normalized to air kerma strength ($cGy\,h^{-1}\,U^{-1}$) in along-away coordinates. Note that data is formatted in the same style as TG-43U1S2 [78] to aid in comparisons.

	Away (cm)									
Along (cm)	0	0.5	1	1.5	2	3	4	5	6	7
0.0		3.19	0.659	0.225	0.0951	0.0232	0.00705	0.00242	0.000903	0.000359
0.5	0.825	1.318	0.480	0.1905	0.0857	0.0219	0.00680	0.00235	0.000889	0.000355
1.0	0.1756	0.285	0.217	0.1198	0.0630	0.01852	0.00607	0.00217	0.000836	0.000338
1.5	0.0611	0.0812	0.0885	0.0636	0.0400	0.01416	0.00508	0.00191	0.000751	0.000311
2.0	0.0264	0.0314	0.0379	0.0324	0.0234	0.01002	0.00398	0.001592	0.000653	0.000278
2.5	0.01384	0.01442	0.01725	0.01658	0.01333	0.00672	0.00298	0.001276	0.000547	0.000241
3.0	0.00744	0.00743	0.00848	0.00868	0.00756	0.00434	0.00213	0.000983	0.000448	0.000206
3.5	0.00383	0.00408	0.00444	0.00467	0.00430	0.00277	0.001483	0.000734	0.000354	0.0001689
4.0	0.00232	0.00228	0.00244	0.00259	0.00249	0.001759	0.001023	0.000544	0.000273	0.0001371
4.5	0.001344	0.001368	0.001419	0.001484	0.001456	0.001106	0.000686	0.000390	0.000208	0.0001087
5.0	0.000762	0.000808	0.000861	0.000872	0.000867	0.000704	0.000464	0.000279	0.0001563	0.0000857
5.5	0.000488	0.000508	0.000518	0.000530	0.000528	0.000446	0.000314	0.000198	0.0001155	0.0000658
6.0	0.000311	0.000317	0.000324	0.000324	0.000329	0.000290	0.000214	0.0001394	0.0000861	0.0000522
6.5	0.000182	0.000209	0.000208	0.000210	0.000209	0.0001887	0.0001464	0.0000989	0.0000632	0.0000393
7.0	0.0001210	0.0001358	0.0001352	0.0001345	0.0001328	0.0001206	0.0000976	0.0000721	0.0000469	0.0000310

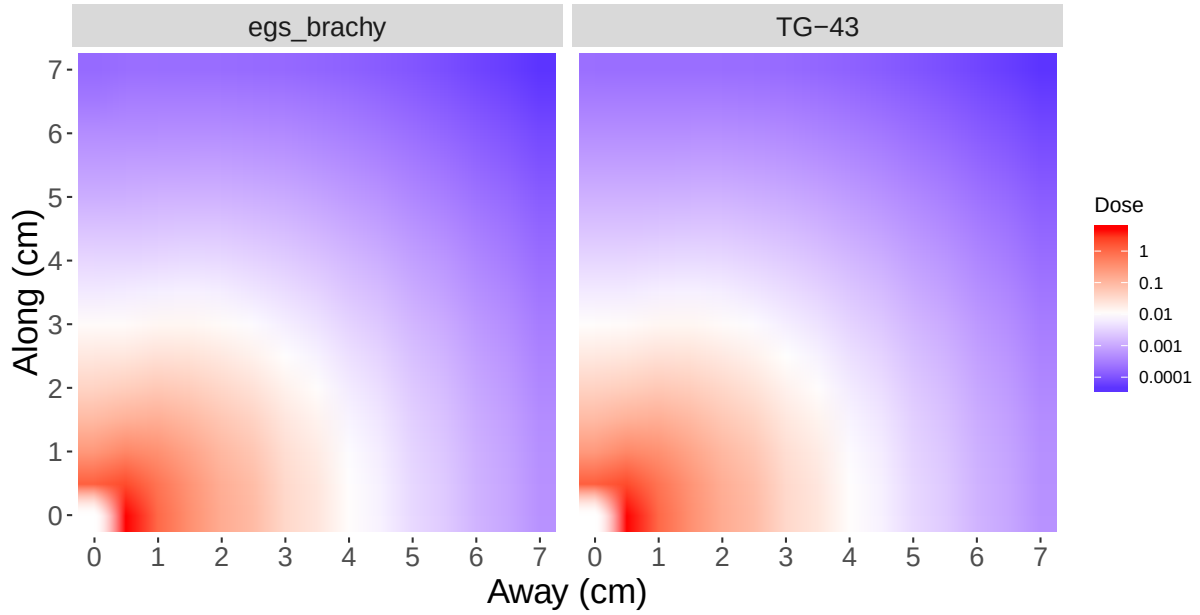

Figure 2.2: Dose distributions generated from egs_brachy simulations and published TG-43 dose rate parameters in along-away coordinates. Doses in each plot are normalized to their respective reference doses at $r = 1\,\text{cm}$ on the seed's transverse plane.

anisotropy function are tabulated in "along-away" format (corresponding to z and r coordinates from the simulations in this section, respectively) as well a polar coordinates with the r coordinate representing the radial distance from the centre of the source and the θ coordinate measured relative to the source's axis (see Figure 1.2). In the latter case, bilinear

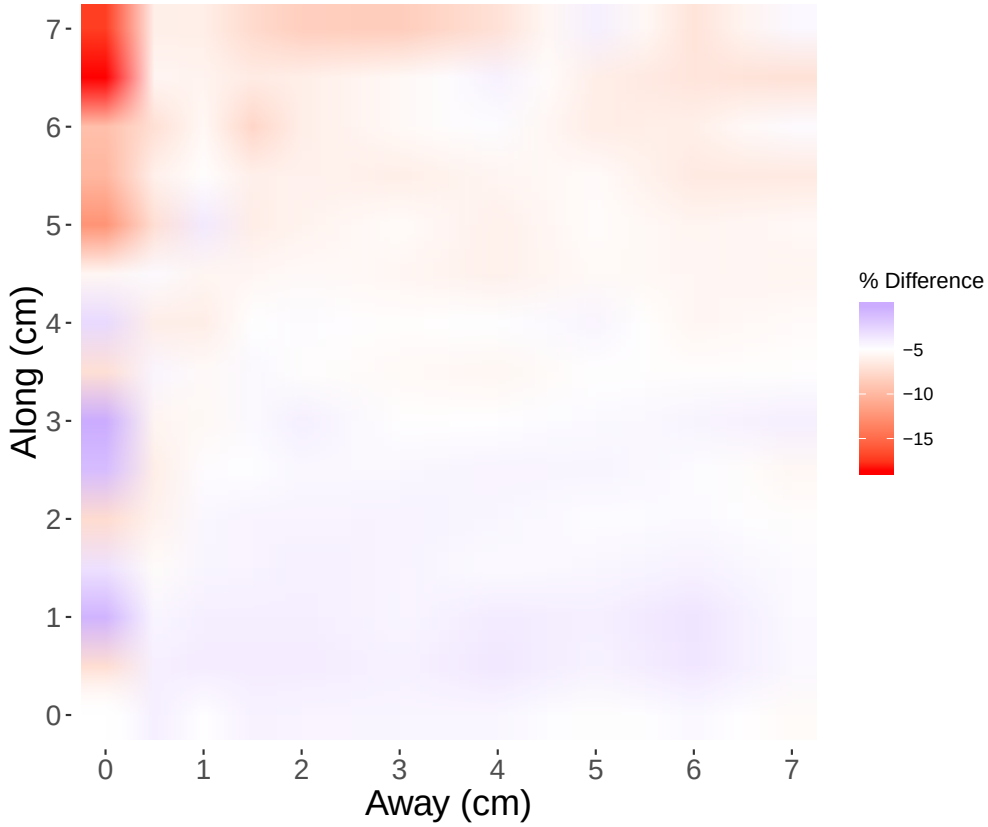

Figure 2.3: Heatmap showing the % difference in local dose calculated using egs_brachy (Table 2.3) relative to published TG-43 dose distribution for IAPd-103A seed in along-away format. White regions indicate a difference of $-5\,\%$ Note that egs_brachy consistently calculates lower dose rates than the TG-43 values.

interpolation was used to calculate doses at points represented by polar coordinates that did not coincide with the rectilinear rz coordinates in the phantom geometries used here. Additional MATLAB functions were defined so that dose rates and the TG-43 parameters based on them could be calculated in either coordinate system to produce the desired tabular data.

TG-43 parameters for the IAPd-103A seed generated using egs_brachy are tabulated in Tables 2.1–2.5 and plots comparing these parameters to published TG-43 values are shown in Figures 2.2–2.5. The dose rate constant of $(0.659 \pm 0.001)\,\mathrm{cGy\,h^{-1}\,U^{-1}}$ was just less than $5\,\%$ below than the consensus value of $(0.693 \pm 0.031)\,\mathrm{cGy\,h^{-1}\,U^{-1}}$ [78] and agreed within uncertainty with Rodriguez and Rogers ($(0.661 \pm 0.002)\,\mathrm{cGy\,h^{-1}\,U^{-1}}$) [81] who used

Table 2.4: egs_brachy radial dose function ($g_L(r)$) using line source approximation ($L = 0.362\,\text{cm}$) for IAPd-103A brachytherapy seed. Note that data is formatted in the same style as TG-43U1S2 [78] to aid in comparisons.

r(cm)	$g_L(r)$
0.10	0.795
0.15	1.091
0.25	1.265
0.50	1.250
0.75	1.130
1.00	1.000
1.50	0.764
2.00	0.573
3.00	0.314
4.00	0.169
5.00	0.0909
6.00	0.0488
7.00	0.0264
8.00	0.0146
9.00	0.00837
10.00	0.00499

Table 2.5: egs_brachy anisotropy function ($F(r,\theta)$) for IAPd-103A brachytherapy seed in polar coordinates. Note that data is formatted in the same style as TG-43U1S2 [78] to aid in comparisons.

	r(cm)									
Polar angle θ (°)	0.1	0.25	0.5	0.75	1	2	3	5	7.5	10
0		0.224	0.215	0.228	0.255	0.274	0.319	0.314	0.462	0.221
2		0.230	0.221	0.231	0.245	0.283	0.303	0.336	0.401	0.508
5		0.258	0.230	0.239	0.252	0.289	0.308	0.343	0.397	0.501
7		0.292	0.241	0.248	0.260	0.296	0.319	0.352	0.403	0.525
10		0.384	0.268	0.269	0.280	0.315	0.339	0.375	0.427	0.528
15		0.634	0.344	0.332	0.338	0.372	0.392	0.425	0.471	0.589
20		0.890	0.458	0.429	0.428	0.451	0.470	0.495	0.530	0.626
25		1.050	0.578	0.534	0.527	0.539	0.550	0.571	0.603	0.705
30	2.026	1.118	0.679	0.628	0.617	0.620	0.627	0.641	0.667	0.749
40	1.564	1.113	0.835	0.776	0.759	0.750	0.751	0.760	0.773	0.812
50	1.306	1.071	0.932	0.887	0.870	0.856	0.855	0.856	0.865	0.893
60	1.155	1.038	0.978	0.957	0.946	0.933	0.929	0.928	0.942	0.961
70	1.068	1.017	0.996	0.988	0.984	0.979	0.977	0.979	0.976	1.000
80	1.018	1.005	1.000	0.999	0.998	0.996	0.996	0.996	1.000	1.003

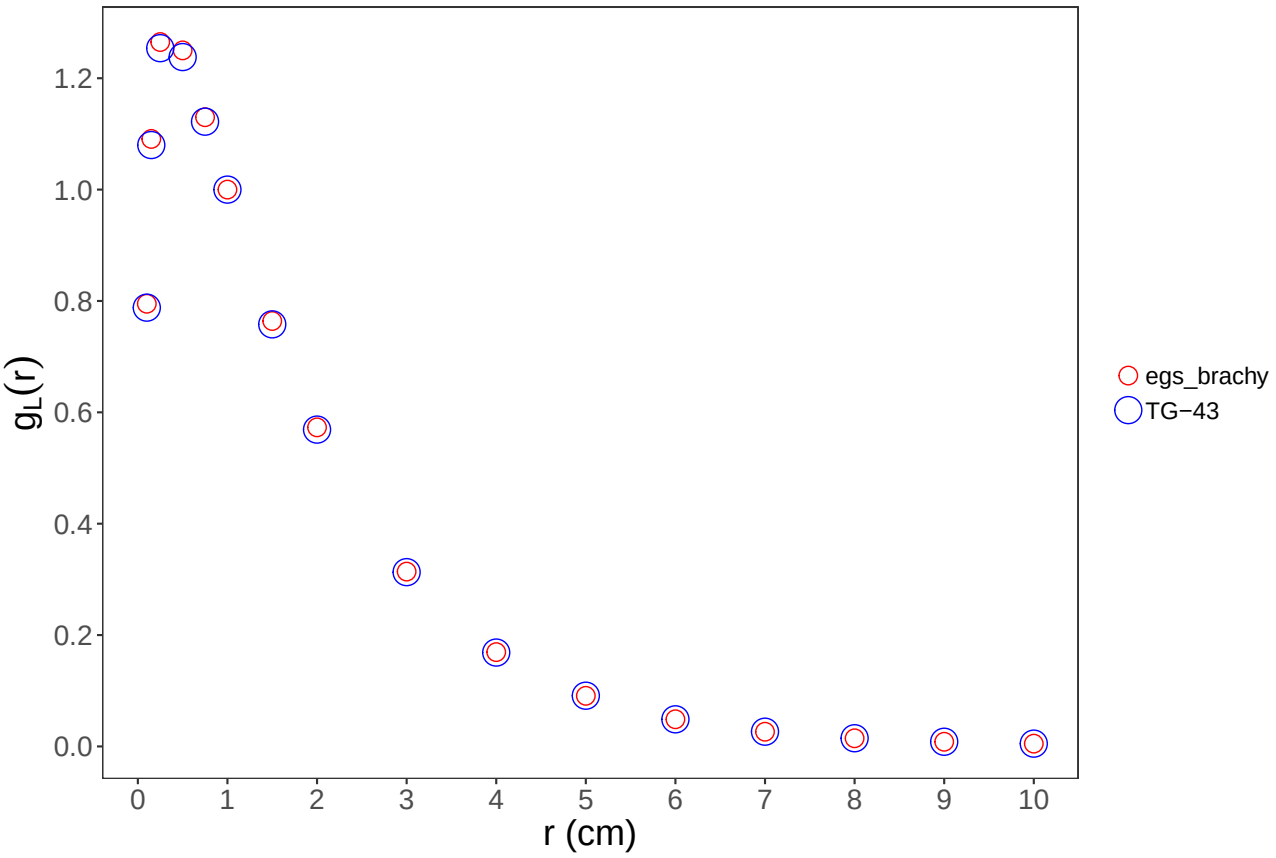

Figure 2.4: Radial dose function ($g_L(r)$) as a function of r for IAPd-103A seed. egs_brachy and TG-43 values are both shown for comparison.

BrachyDose, an EGSnrc user code and a precursor to egs_brachy, for their study. This difference is fairly consistent ($-5.2\,\%$ on average) across the dose distribution as shown in Figure 2.3 with the exception being along the seed's axis at distances of 5 cm or greater. The maximum difference of $-18.7\,\%$ occurs at 6.5 cm along and 0 cm away coordinates where the dose rate is less than $0.04\,\%$ of its value at the reference position (0 cm along and 1 cm away). The same trend is present when dose rates are mapped to polar coordinates where egs_brachy reproduces the TG-43 consensus dose rates within $5\,\%$ on average at all radial distances for polar angles of at least 2°, and at 0° up to 3 cm radial distance.

egs_brachy data for the radial dose function is tabulated in Table 2.4 and plotted along with TG-43 consensus date in Figure 2.4. The results agree quite well with a maximum difference of $1.02\,\%$ at 0.15 cm and less than $1\,\%$ for all other values of r. The egs_brachy

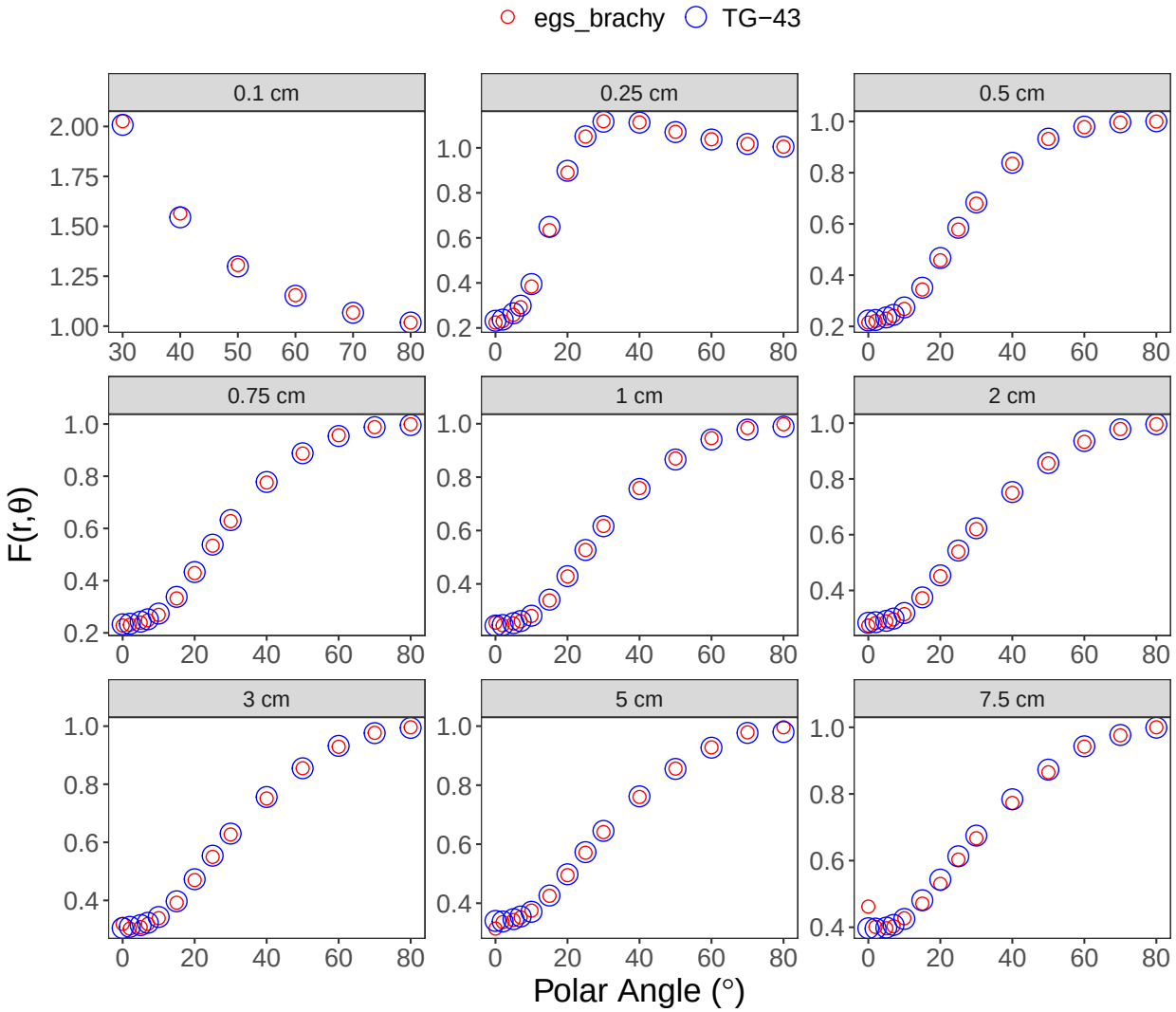

Figure 2.5: Anisotropy function ($F(r,\theta)$) for IAPd-103A seed calculated using egs_brachy (Table 2.5) and compared with TG-43 values. Each plot corresponds to a different radial distance from the centre of the seed as indicated.

anisotropy function data in Table 2.5 also agrees well with the TG-43 at 3 % or less for radial distances of up to 7.5 cm and polar angles of 2° or greater. As with the dose rate distribution, the most significant differences occur along the seed's axis at large distances. Figure 2.5 illustrates how the value of $F(r,\theta)$ varies with polar angle for a variety of radial distances. In general, egs_brachy is able to reproduce the desired TG-43 parameters for the IAPd-103A seed in the clinically relevant regions where the dose rate is highest, close to the seed.

The consensus TG-43 dose rate constant for IAPd-103A was obtained by averaging the MC calculation results of Meigooni et al., [53] Sowards, [91] and Rodriguez and Rogers [81] and the lone TLD measurement performed by Meigooni et al. [53] with a $50 - 50$ split between MC and TLD. Consensus values for the radial dose function and anisotropy function were taken exclusively from Taylor and Rogers [93] as their work utilized a grid with finer resolution than other studies. It is important to note that the details of previous MC studies are generally limited, making it difficult to pinpoint the exact source of discrepancies between published values. Differences in geometries (voxelization, coordinate systems, etc.), source parameters (photon spectra, cut-off energies, etc.), materials definitions (densities, elemental compositions, etc.), and MC algorithm used are among the many variables that can influence a MC dose calculation and the TG-43U1S2 report acknowledges that discrepancies between tabulated data, particularly along the seed's axis, are somewhat common even among the studies used to calculate the consensus values [78].

Overall, the results obtained in this work are reassuring as a validation of the egs_brachy user code and the IAPd-103A source model developed herein. The dose rate constant calculated with egs_brachy agreed within statistical uncertainty with the consensus value and the dose distributions were nearly identical (Figure 2.2). The radial dose function agreed within 1.02 % and the anisotropy function agreed within 3 % except along the source axis at radial distances of 5 cm or more. Considering the reported uncertainties, added complexity of the egs_brachy model, consistency with other detailed MC models in the literature [93], this work establishes that the IAPd-103A source model implemented in this thesis produces results accordant with the consensus standard.

2.3 egs_brachy Material Data File Generation

egs_brachy requires tabulated mass-energy absorption coefficients (μ_{en}/ρ) in order to score dose in voxels using a tracklength estimator (see Equation (1.8)). Many common tissues

as well as certain non-tissue materials are listed with pre-calculated coefficients in the "brachy_xcom_1.5MeV.muendat" data file that comes with egs_brachy. These coefficients are calculated using data from the NIST XCOM photon cross-section database [6] and the EGSnrc user code g which outputs a μ_{en}/ρ for a given photon energy and material as a by-product of calculating the average fraction of secondary electron energy that is lost to bremsstrahlung radiation (hence the name g). Any materials which are intended to be used as dose scoring media but are not included in the default egs_brachy distribution must have mass-energy absorption coefficients calculated over a range of energies, typically 2000 distinct energies from a minimum of 1 keV up to a maximum of 1.5 MeV. Unfortunately, this task would be extremely time-consuming using the "out-of-the-box" g code as each individual photon energy requires a separate simulation. It is however possible to modify the code to streamline the process.

Through correspondence with the EGSnrc developers via their Google+ page [97], instructions on how to generate μ_{en}/ρ data by modifying the g user code were obtained. First, the compositions of new dose scoring materials were added to the material.dat file if they were not already defined. The g source code was modified to increase the maximum number of photon energies to 2000 and PEGS4 material data was generated using egs_gui as required input for g. An egsinp template was provided by the developers that allowed a range of 2000 logarithmically increasing photon energies between 1 keV and 1.5 MeV to be simulated (including electron transport down to 1 keV) in the material until either a statistical uncertainty of 0.01 % was reached or 1×10^6 histories were simulated. A MATLAB function was created to extract the μ_{en}/ρ values from the simulation output files and format the results properly for use with egs_brachy.

Mass-energy absorption coefficients were calculated for four different materials: WATER_0.998, PMMA, Al2O3, and Al2O3_OSL. The first three material compositions were pre-defined in the egs_brachy material.dat file but Al2O3_OSL (corresponding to a mixture of 78.4 % Al_2O_3 and 21.6 % polyester from Lehmann et al. [43]) needed to be added. WA-

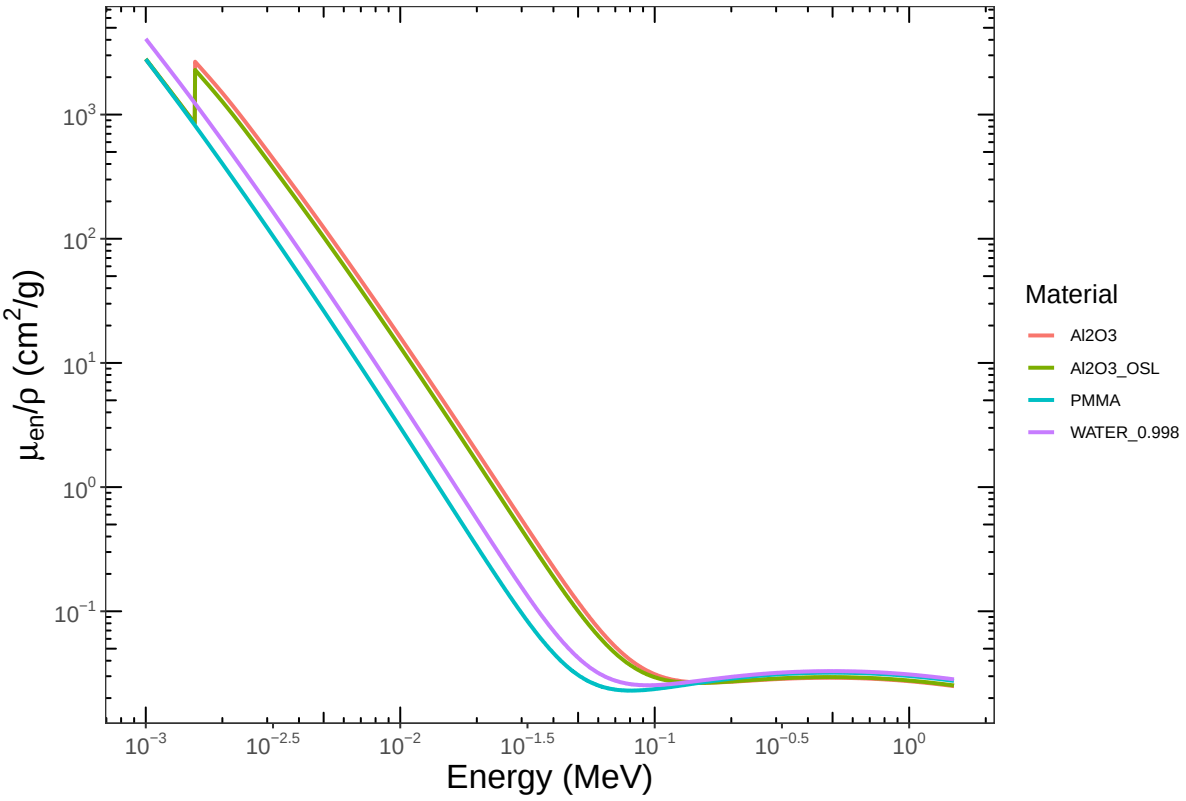

Figure 2.6: Mass-energy absorption coefficient for several materials generated using modified g user code in EGSnrc. The material names listed correspond to their names as defined in the egs_brachy material.dat file. WATER_0.998 was included to test the modified code before generating coefficients for other materials.

TER_0.998 is the standard TG-43 recommended water material and it was included here to compare with μ_{en}/ρ data included with egs_brachy and to verify that the modified g code was working as expected. PMMA was required to calculate dose in solid phantoms which is relevant for experimental measurements. Al2O3 and Al2O3_OSL were used to produce a model of the nanoDot™OSLD, specifically to score dose in the sensitive volume containing Al_2O_3 mixed with polyester.

The mass-energy absorption coefficients generated in this work are shown in Figure 2.6. These values were normalized to the pre-existing values for WATER_0.998 that came included with egs_brachy (Figure 2.7) to examine their energy dependence, particularly at low energies similar to Pd-103. The μ_{en}/ρ data calculated for WATER_0.998 was essentially identical to the pre-existing data (as evidenced by a horizontal line in Figure 2.7), indicating that the

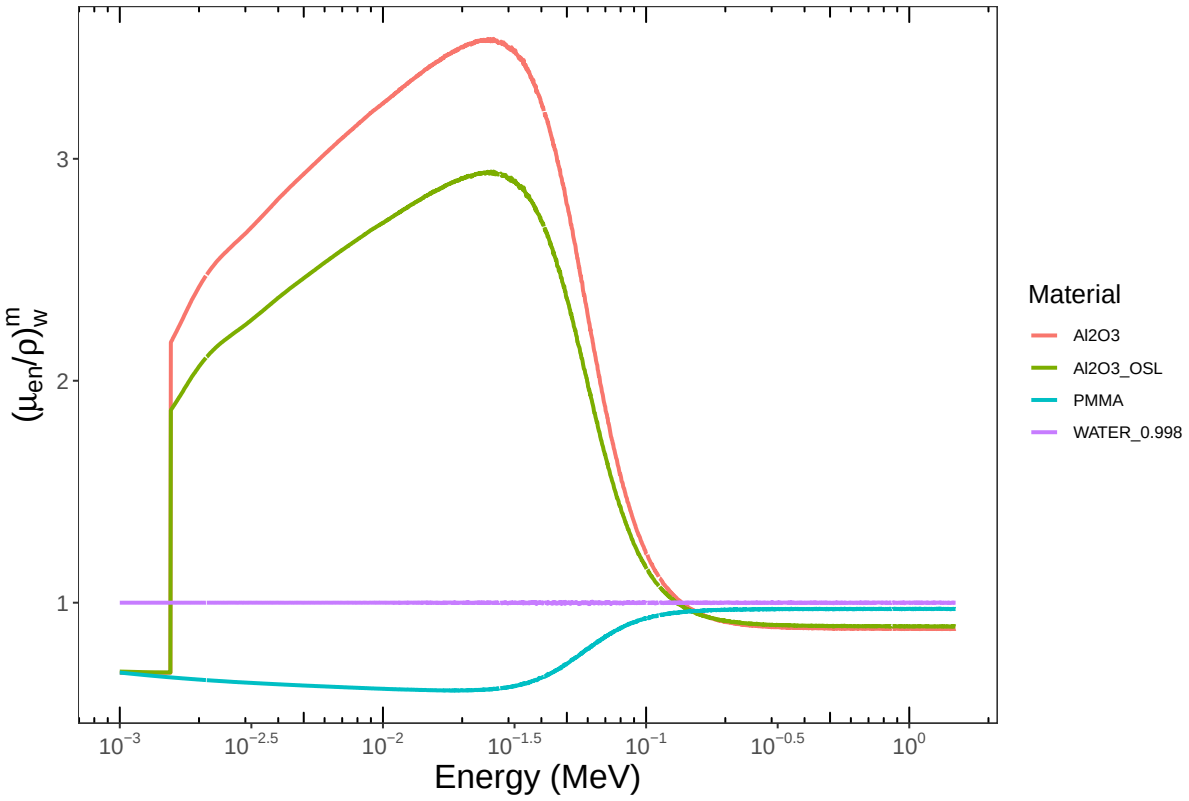

Figure 2.7: Mass-energy absorption coefficients normalized to WATER_0.998 from the default egs_brachy .muendat file. Note that the WATER_0.998 material shown in the plot corresponds to coefficients generated in the current study for comparison with those supplied with egs_brachy.

modified g code was functioning as desired. A qualitative comparison between the observed behaviour for Al2O3 and PMMA with data available on the NIST XCOM database [6] also provided additional reassurance that the results could be trusted. With essential material data calculated, it was then possible to move forward with developing more complex models of interest for this thesis.

2.4 Luxton 1994 Paper Validation

In addition to validations against consensus TG-43 parameters, egs_brachy was used to reproduce simulations performed by Luxton in 1994 [44] to determine correction factors for calculating dose in solid phantoms from low energy brachytherapy sources. The original

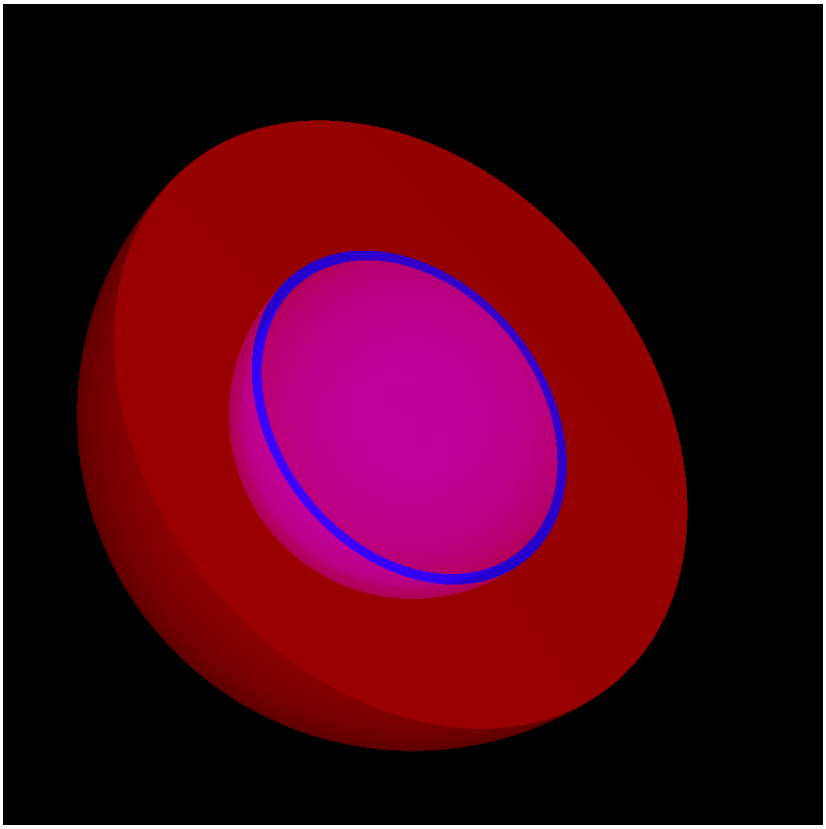

Figure 2.8: Example of a heterogeneous phantom geometry used to replicate Luxton's work using egs_brachy. The phantom is cut in half to show the distinct layers. The phantom consists of a 15 cm radius sphere of PMMA (red) containing a thin shell of water (blue) where dose is scored. The spherical shell was modelled with various radii and thicknesses (Table 2.6) to determine the dose to water in PMMA as a function of r. In homogeneous cases, the shell is replaced by the surrounding material but the dose scoring volume is identical to the heterogeneous cases.

work was motivated by the desire to use solid phantoms to perform dosimetric measurements around brachytherapy sources and being able to relate the dose in the phantom to a dose to water at the same location. Accurate positioning of sources and dosimeters in a liquid water phantom is difficult and dose measurements can be strongly affected by small errors in position due to steep dose gradients present around the sources. To address this, Luxton used the EGS4 MC code to model dose distributions in solid and liquid phantoms from which he derived dose conversion factors between the materials for Pd-103 and I-125 sources. In this thesis, radiation dosimetry in a PMMA phantom was modelled using egs_brachy and performed experimentally so replicating Luxton's earlier results was viewed as a prerequisite

to the current work.

Luxton's work simulated dose distributions in PMMA, water and two other solid water substitute materials (RW-1 and WT1) for a Pd-103 point source and two commercially available I-125 seeds. Sources were modelled as point sources at the centre of spherical phantoms using photon spectra available at the time. Two distinct groups of phantoms with radii of 15 cm were modelled: (1) homogeneous spheres of water or water substitute material and (2) heterogeneous spheres composed of otherwise homogeneous water substitute material with a spherical shell of water with a range of radii and thicknesses (Figure 2.8). These spherical shells were used as scoring voxels for both homogeneous and heterogeneous phantoms using identical dimensions in both cases (Table 2.6). Using this arrangement, dose to water in medium ($D^{w}_{med}(r)$) and dose to medium ($D_{med,point}(r)$) were calculated for heterogeneous and homogeneous phantoms, respectively.

Table 2.6: Dimensions of scoring voxels used in work by Luxton. All voxels are spherical shells centred on the source with equal thickness at either side of the effective point of measurement r.

r(cm)	Shell Thickness (mm)
0.2	0.5
0.3	0.5
0.5	0.5
1.0	0.5
2.0	1.0
3.0	1.0
5.0	1.0
8.0	5.0

Luxton determined a number of useful parameters that were derived from the dose calculations described above. The most important parameter in the context of this thesis is a distance dependent conversion factor that relates the dose to water in medium to the dose to water in water defined by the ratio of these values. This parameter is relevant to the current work because it allows a dose calculation in water (such as TG-43) to be compared to a measurement in a solid PMMA phantom which was designed and built for the OSLD calibration

procedure as detailed in Chapter 4. Luxton also calculated the dose rate constants for water substitute media relative to water, the radial dose functions for these media, and the ratio of dose to water in medium to dose to medium (averaged for $r = 1\,\text{cm}$ and $r = 5\,\text{cm}$, and denoted by F^w_{med}). These parameters are not essential for the current work, but they were calculated using egs_brachy for the purpose of further validation.

Table 2.7: Photon spectra used for simulations reproducing work by Luxton. The Luxton spectrum refers to the one used in the original work while the NNDC spectrum is the most recent Pd-103 spectrum from the Nudat database [59].

Luxton		NNDC	
Energy (keV)	Intensity (%)	Energy (keV)	Intensity (%)
20.1	83.1	2.7	10.2
22.7	16.8	20.074	26.1
		20.216	49.6
		22.699	4.13
		22.724	7.99
		23.172	1.91
		39.748	0.080
		53.29	3.50E-05
		62.41	0.0012
		241.88	5.83E-07
		294.98	0.0033
		317.72	1.75E-05
		357.45	0.026
		443.79	1.75E-05
		497.08	0.0046

Table 2.8: Summary of parameters generated using egs_brachy to compare with Luxton. The second column lists the dose rate constant for PMMA relative to water for each source used. The third column is a value for average of the ratio of the dose to water in PMMA to the dose to PMMA in PMMA calculated at $r = 1\,\text{cm}$ and $r = 5\,\text{cm}$. These values correspond to Tables III and IV from Luxton's paper, respectively.

Source	Λ_{PMMA}/Λ_w	F^w_{PMMA}
egs_brachy (Point)	0.738 ± 0.001	1.627 ± 0.001
egs_brachy (IAPd-103A)	0.730 ± 0.001	1.624 ± 0.001
Luxton (Point)	0.737 ± 0.002	1.629 ± 0.008

egs_brachy simulations were performed using the same geometries as Luxton for a Pd-

103 point source with PMMA as a water substitute medium to reproduce his MC model as accurately as possible. These simulations were repeated using the detailed IAPd-103A seed model defined earlier as a source to obtain more realistic results and to determine the effect this increased complexity has on the outcomes. The point source model utilized the same spectrum as Luxton while the detailed model incorporated the NNDC source spectrum used for the TG-43 validation (Table 2.7). The results of these simulations are show in Table 2.8 and Figures 2.9–2.10. Luxton's original results are included as well for comparison.

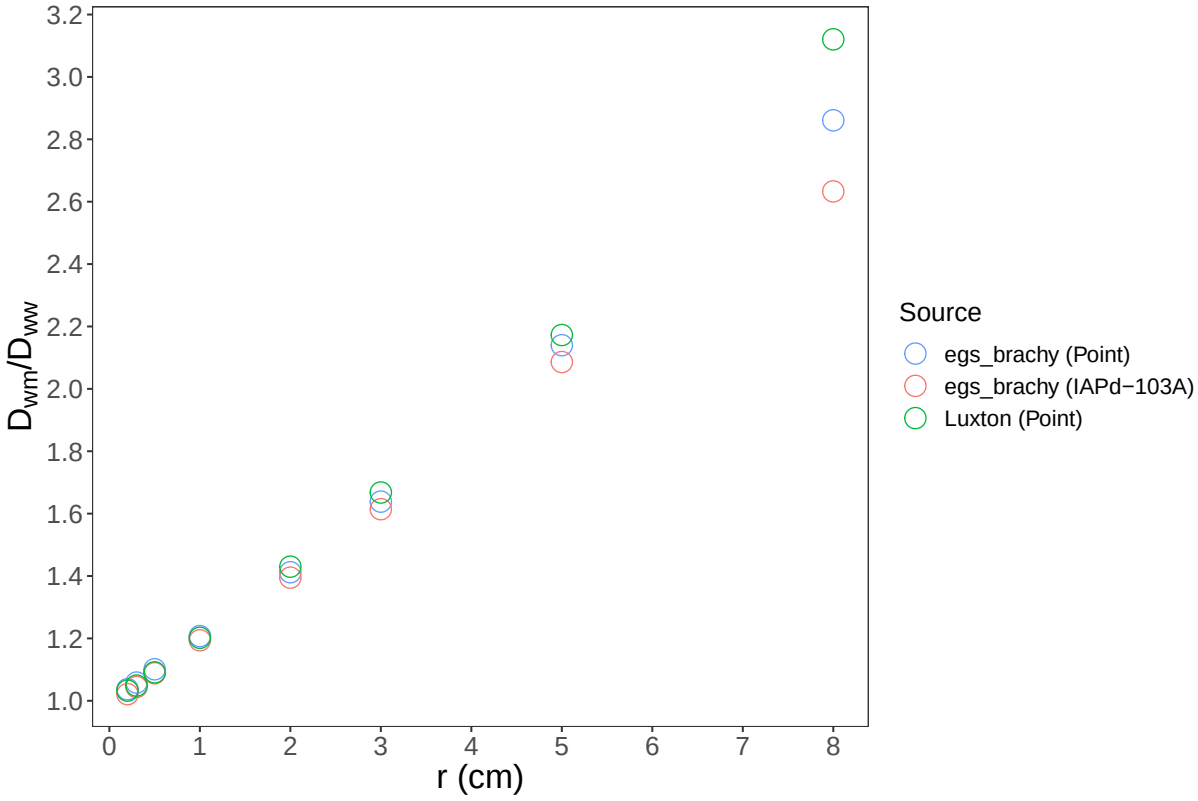

Figure 2.9: Ratio of dose to water in medium (PMMA) to dose to water in water for Pd-103 as a function of radial distance for egs_brachy Pd-103 point source and IAPd-103A source compared to Luxton's results [44]. This value serves as a conversion factor between these two dose specification metrics.

In general, egs_brachy was able to replicate Luxton's results quite well using the point source model, and the IAPd-103A model generated results that were similar despite significant differences between the source models. The main result of interest for this thesis is the ratio $D_{w,m}/D_{w,w}$ (note the notation is different from Luxton's for clarity) which serves

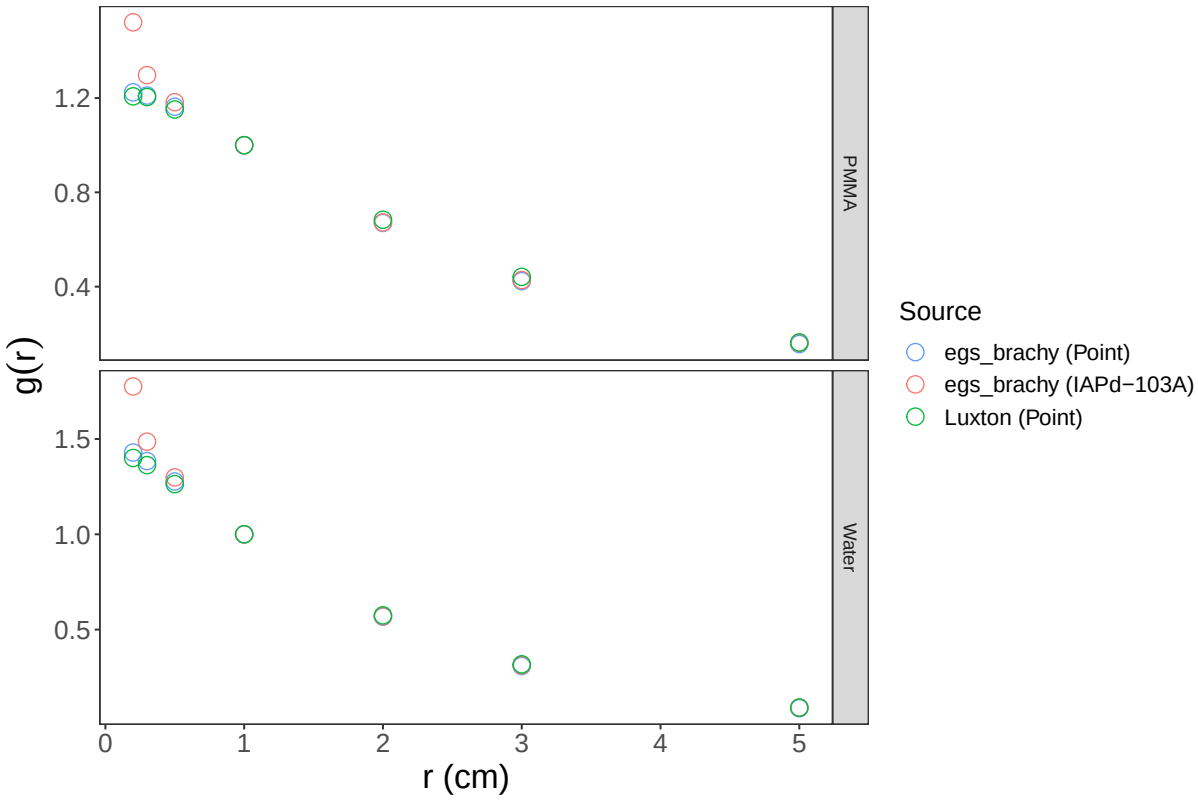

Figure 2.10: Radial dose function (point source approximation) in PMMA and water for egs_brachy Pd-103 point source and IAPd-103A source compared to Luxton's results [44].

as a conversion factor between dose to water in water and PMMA (see Figure 2.9). The egs_brachy point model agreed with the Luxton model within 2 % up to 5 cm while the IAPd-103A model differed by less than 4 % up to 5 cm. Both models differed substantially (8.4 % for the point source and 15.7 % for the IAPd-103A source) from Luxton's work at a distance of 8 cm. This is not particularly concerning considering that the dose rate is very low at this distance (less than 0.05 % of the dose rate at 1 cm) and is not relevant to the work in this thesis or in typical clinical scenarios.

The dose rate constant for PMMA relative to water was calculated for both source models and agreed within uncertainty with Luxton's result for the point source, and was lower for the IAPd-103A model. The parameter F^w_{PMMA} that is meant to convert from doses in homogeneous PMMA to doses to water in PMMA was found to agree for both models within uncertainty (Table 2.8). The calculated radial dose functions for PMMA and water

was within 5 % of Luxton's results up to 5 cm for the point source. The IAPd-103A source was within 4 % from 0.5 cm up to 5 cm but large differences (up to 27 %) were observed closer to the source, which can most likely be attributed to the source's finite dimensions.

2.5 Summary

The goal of the work outlined in this chapter was to establish consistency between MC dose calculations using the IAPd-103A source model developed for egs_brachy, and published results for this source. Validations against TG-43 consensus values for the dose rate constant, radial dose function, and anisotropy function agreed within statistical uncertainty except for points 5 cm or farther on the source's axis where dose rates are comparatively small. Mass-energy absorption coefficients generated for water were identical to values included with egs_brachy allowing calculations of μ_{en}/ρ values for materials required to score dose in PMMA and an OSLD model. Work by Luxton [44] was reproduced with egs_brachy for a point source and the detailed IAPd-103A source model which produced conversion factors (from $D_{w,w}$ to $D_{w,m}$) that agreed within 2 % and 4 % up to 5 cm from the sources, respectively, along with other comparable results. Given that the egs_brachy code was generally validated for the IAPd-103A source model, the project was able to confidently proceed with more detailed and complex simulations described later in this thesis.

Chapter 3

Determining the relationship between skin dose and OSLD dose in PBSI

Chapter Overview

Skin is a major organ at risk (OAR) for patients undergoing permanent breast seed implant (PBSI) brachytherapy treatment for early stage breast cancer and skin reactions due to radiation exposure are some of the most commonly observed side effects. *In vivo* dosimetry (IVD) measurements during radiation therapy treatments provide valuable information regarding doses received by the patient and can be used to monitor OAR dose. This work was motivated by the desire to develop a simple method to approximate skin dose for PBSI patients using optically stimulated luminescence dosimeters (OSLD) placed on the skin based on appropriate conversion factors derived from Monte Carlo dose calculations. In doing so, this addresses the lack of studies pertaining to IVD for breast brachytherapy with low energy sources such as Pd-103 [92] commonly used for PBSI. The results described in this chapter are intended to improve skin dosimetry in PBSI using OSLDs by establishing the relationship between OSLD dose and skin dose.

The work in this chapter has been published in the peer-reviewed journal *Brachytherapy*

[62] in 2019. I was the primary author and it was co-authored by Dr. Charles Kirkby and Dr. Jose Eduardo Villarreal-Barajas. I developed the egs_brachy models, performed the simulations, analysed the data, and wrote the first draft of the manuscript. Dr. Kirkby and Dr. Villarreal-Barajas provided valuable guidance needed to develop models and carry out simulations relevant for the task at hand and to interpret the results in a meaningful way. All authors contributed to subsequent drafts of the manuscript prior to submission and revisions requested by the publisher thereafter.

For permission to reproduce this work see Appendix A.1 and Appendix A.2.

Monte Carlo study of the relationship between skin dose and optically stimulated luminescence dosimeter dose in Pd-103 permanent breast seed implant brachytherapy

Steven Nich, Charles Kirkby, J. Eduardo Villarreal-Barajas

Abstract

PURPOSE: To establish a method for estimating skin dose for PBSI patients based on *in vivo* OSLD measurements.

METHODS AND MATERIALS: Monte Carlo simulations were performed in a simple breast phantom using the EGSnrc user code egs_brachy. Realistic models of the IsoAid Advantage Pd-103 brachytherapy source and Landauer nanoDot™OSLD were created to model *in vivo* skin dose measurements where an OSLD would be placed on the skin of a PBSI patient following implantation. Doses to a $0.2\,\mathrm{cm}^3$ volume of skin beneath the OSLD and to the sensitive volume within the OSLD were calculated and the ratio of these values was found for various seed positions inside the breast phantom. The maximum value of this ratio may be used as a conversion factor that would allow skin dose to be estimated from *in vivo* OSLD measurements.

RESULTS: Conversion factors of 0.5 and 1.44 are recommended for OSLDs calibrated to dose to Al_2O_3 and water, respectively, at the point of measurement in the OSLD. These factors were not significantly affected by the addition of extra seeds in the dose calculations.

CONCLUSIONS: A method for estimating skin dose from OSLD measurements was proposed. Individual institutions should calibrate OSLDs to Pd-103 seeds to apply the results of this work clinically.

3.1 Introduction

Permanent breast seed implant (PBSI) brachytherapy is a type of accelerated partial breast irradiation (APBI) prescribed as an alternative to whole breast irradiation following surgical lumpectomy. This form of radiation therapy involves the implantation of small radioactive seeds in a planning target volume containing the post-lumpectomy cavity and a margin to account for microscopic spread of disease and uncertainties in the patient's position. Because the vast majority of recurrences take place in the region immediately surrounding the seroma following surgery [63], PBSI is a reasonable alternative to whole breast irradiation. PBSI also offers the advantage of a single treatment over daily treatments for up to six weeks making it a desirable option for many women.

Skin is an important organ at risk for PBSI brachytherapy patients. Radiation exposure to the skin can lead to toxicities such as moist desquamation, erythema and indurations. These toxicities have been reported in 10.4 %, 42 % and 27 % of patients receiving PBSI, respectively, according to a study by Pignol et al. with the peak occurrence of these effects observed some six weeks after the implant is performed [69]. Delayed toxicities were seen up to two years following the implant including telangiectasia which occurred at a rate of 7 % after one year [69]. There is evidence that using more accurate dosimetry techniques increases the probability of correctly predicting the occurrence of these skin toxicities [47]. Being able to predict these toxicities would potentially allow for preventative measures to be implemented prior to their onset and potentially reduce the severity of these toxicities when they occur [47]. Therefore, a method to accurately assess skin dose post-implant would be beneficial to PBSI programs.

Clinical dose calculations in brachytherapy are commonly performed using the AAPM's TG-43 protocol which assumes that all tissue is radiologically equivalent to water in a medium with infinite backscatter [80]. These assumptions are not valid for low dose rate (LDR) brachytherapy in PBSI, which is typically administered using Pd-103 seeds, because dose deposition is highly dependent on factors such as tissue composition and mass density and

seeds can be implanted within a centimeter of the surface where the assumed backscatter media is not present [110]. Model-based dose calculation algorithms (MBDCAs) such as Monte Carlo methods have demonstrated increases in skin D10 and D50 of up to 28.2 % and 56 % relative to TG-43 dose calculations, respectively [1]. This arises due to a significant decrease in the mass energy absorption coefficients of breast tissue relative to water at the mean photon energy of Pd-103 (approximately 64 % for a mixture of 75 % adipose and 25 % gland relative to water) which reduces the attenuation of photons before they reach skin, leading to a net increase in skin dose even in the absence of backscatter. This has led to a proposal to use these techniques clinically to address this problem [5]. These algorithms can account for variations in material composition and patient geometries and provide much more accurate dose calculations than those based on the TG-43 protocol.

This study aims to examine the use of nanoDot™(Landauer Inc. Glenwood, IL) optically stimulated luminescence dosimeters (OSLDs) to assess skin dose to PBSI patients by using Monte Carlo methods to relate the dose measured (associated with the detector response) in an OSLD to the dose to the skin. OSLDs are small dosimeters containing aluminum oxide doped with carbon (Al_2O_3:C) that can be placed on a patient's skin after the seeds have been implanted. Afterwards, dose can be derived by converting the optically stimulated light signal from the OSLD into a calibrated dose reading. Monte Carlo methods are appropriate for this task because they can accurately model the dose within OSLDs relative to the dose to water or soft tissue while accounting for the strong photon energy dependence of these materials in the Pd-103 kilovoltage x-ray spectrum [70, 74]. Further, detailed source models and phantom geometries can be modelled using virtually any material and so the shortcomings of the TG-43 protocol are addressed directly.

In this work, conversion factors between OSLD dose and skin dose are determined by generating dose distributions from a Pd-103 brachytherapy source using the Monte Carlo code egs_brachy [12]. These factors may be applied to *in vivo* dosimetry measurements from PBSI patients to convert from the OSLD reported dose to a value for the dose to the skin

under the dosimeter. OSLDs have increased in popularity in recent years due their ease of use and have been applied at energies in the diagnostic x-ray range [83] so it is natural to consider them for brachytherapy applications. This study aims to facilitate accurate skin dose estimates from OSLD measurements, which will enable informed decisions as to whether skin toxicities are likely to occur following an implant. This will enable early interventions when necessary, potentially decreasing the pain and discomfort associated with the procedure.

3.2 Methods and Materials

Monte Carlo simulations in this work have been performed using the egsnrc (version 4) user code egs_brachy [12] and a modified version of the user code g. Three geometries were created: a breast phantom, a detailed model of the IsoAid Advantage Pd-103 (IAPd-103A, IsoAid, LLC, Port Richey, FL) brachytherapy seed and a Landauer nanoDot™OSLD. The mass energy absorption coefficients required to calculate dose were generated for the custom materials generated for this study using g. In the egs_brachy simulations, the seed was placed inside the breast phantom and the OSLD was modelled on a layer of skin on top of the breast phantom and the entire geometry was surrounded by a large box of either air or water.

3.2.1 Geometry Description

The IAPd-103A source was modelled according the dimensions and material compositions (Table 3.1) provided by the Carleton brachytherapy seed database [95], which are based on measurements from studies by Meigooni et al. [53] and Sowards [91] (Figure 3.1). The model contains a 1.25 mm long and 0.5 mm wide cylindrical silver marker centred in a 4.5 mm long and 0.8 mm wide titanium encapsulation that is 0.05 mm thick along its length with 0.35 mm thick hemispherical end welds. Two 0.5 mm diameter polystyrene beads containing 1 % Pd-103 are modelled on each side of the silver marker with a uniform distribution of radiation emitted isotropically from each of the beads. The remaining space within the source was

Table 3.1: Properties of materials used in egs_brachy simulations as they appear in the material data file. Elemental compositions are listed as percent by mass of the compounds. Note: ABS plastic is acrylonitrile butadiene styrene with mass density provided by Landauer (Landauer Inc. Glenwood, IL)

Material	Mass density (g/cm^3)	H	C	N	O	Trace elements
WATER_0.998	0.998	11.19			88.81	
AIR_TG43	0.0012	0.0732	0.0123	73.0325	23.6077	Ar: 1.2743
25GLAND-75ADIPOSE	0.9675	11.2	52.15	1.275	34.025	Na: 0.1, P: 0.025, S: 0.125, Cl: 0.1
SKIN2_WW86 [106]	1.09	10	20.4	4.2	64.5	Na: 0.2, P: 0.1, S: 0.2, Cl: 0.3, K: 0.1
ABS_plastic	1.03	8.1095	85.2618	6.6287		
Polyester	1.18	4.1959	62.5017		33.025	
Al2O3_OSL [43] (Al_2O_3/polyester mixture)	1.41	0.86	12.88		44.24	Al: 42.02
Ti	4.54					Ti: 100
Ag	10.5					Ag: 100
ADV_PD_POLY [53]	1.2	8	90	0.3		Cl: 0.7, Pd: 1

filled with air. All the material compositions were taken as the defaults included in the egs_brachy distribution except for minor corrections which were made to the composition of the polystyrene and Pd-103 mixture to agree with the study by Meigooni [53]. The Pd-103 photon spectrum was taken from the nuclear data sheets produced by the National Nuclear Data Center (NNDC) at Brookhaven National Laboratory, which was included with egs_brachy, but required slight modifications [19] (Table 3.2).

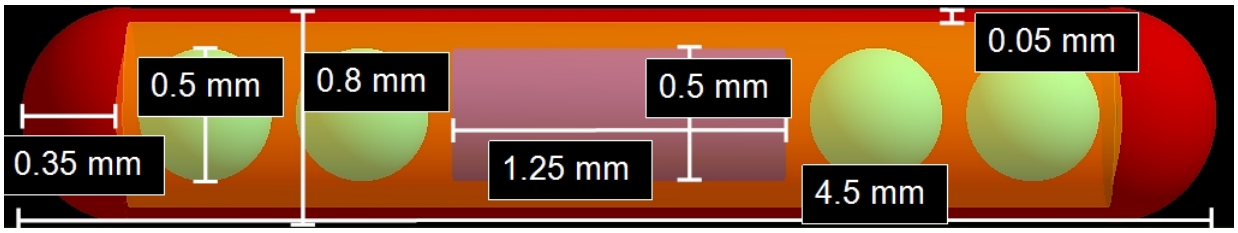

Figure 3.1: egs_brachy model of IAPd-103 brachytherapy source with radioactive polystyrene pellets (light green), silver marker (light purple), titanium encapsulation (red), and air (orange) shown.

The OSLD model was based on work by Lehmann et al. [43] where the dimensions were measured using micro-CT images and the material compositions were obtained from Landauer. The sensitive detector volume was modelled as a 5 mm diameter, 0.2 mm thick cylinder composed of a mixture of Al_2O_3 (note: the small amount of carbon doping was not modelled as there is an insignificant amount; between 0.01 % and 0.5 % [43], producing

Table 3.2: Photon spectrum used in egs_brachy simulations from nuclear data sheets provided by NNDC [19]

Energy (keV)	Intensity (%)
2.70	10.2
20.07	26.1
20.27	49.6
22.70	4.13
22.72	7.99
23.17	1.91
39.75	0.0796
53.29	0.000035
62.41	0.00121
241.88	0.000000583
294.98	0.00326
317.72	0.0000175
357.45	0.0258
443.79	0.0000175
497.08	0.00462

less than 1 % change in OSLD response with as much as 1 % dopant [55]) and polyester sandwiched between two 0.05 mm thick polyester cylinders and 0.49 mm of air on either side. The OSLD case was modelled as a 1 cm × 1 cm × 2 mm rectangular prism of ABS plastic with the sensitive volume located at its centre (Figure 3.2). Note that the sensitive material in Landauer's nanoDot™OSLDs is offset by 1 mm horizontally and vertically from the centre, but this detail was not included in this study for the sake of simplicity and the effect of this offset was found to be negligible in a set of simulations where the plastic case was shifted relative to the sensitive volume (no detectable effect on skin dose and < 0.01 % effect on OSLD dose). The ABS plastic and Al_2O_3/polyester mixture were added to the material data file included with egs_brachy, and mass energy absorption coefficients were generated using g for the latter to score dose in the sensitive volume.

A simple breast phantom was designed for this study that consisted of a 10 cm cube[1] of breast tissue with a 2 mm thick layer of skin covering one surface (Figure 3.3). The breast

[1]When a cube measurement is given as a single number in this work, this implies that all side lengths have the size listed.

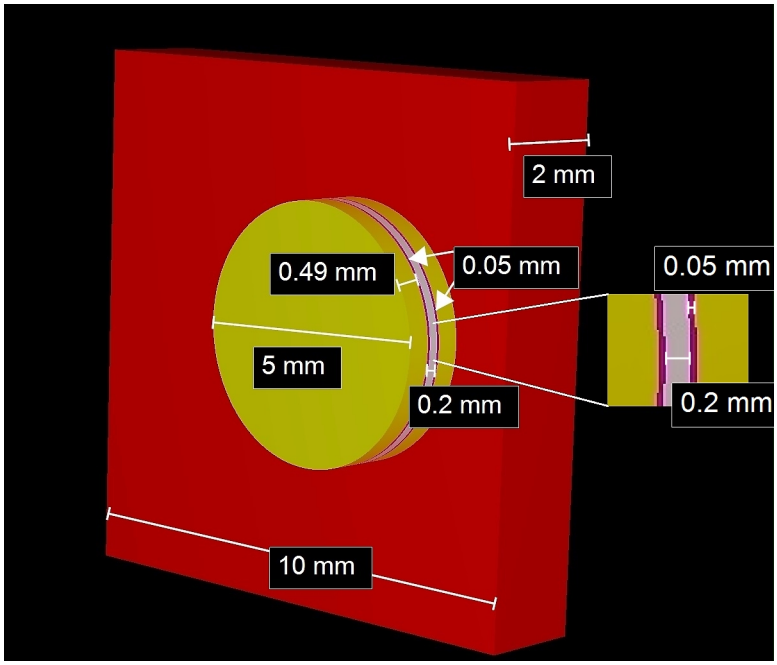

Figure 3.2: Model of OSLD used in egs_brachy simulations with plastic case (red), air (yellow), polyester (fuschia) and aluminum oxide/polyester mixture (grey) shown. A close-up of the sensitive volume and polyester layers is shown.

tissue was made up of a homogeneous mixture of 75 % adipose tissue and 25 % glandular tissue which was chosen because the material data files were readily available in egs_brachy and it has been suggested that an average breast is predominantly composed of adipose tissue [107]. Mass energy absorption coefficients for these materials were provided with egs_brachy. The SKIN2 composition from Woodard and White [106] was used for skin and the thickness was chosen to be consistent with what has been published as a robust skin dose metric by Hilts et al. [27] corresponding to a 0.2 cm^3 volume of skin . The source was modelled with its transverse axis parallel to the OSLD which was placed flat against the outside surface of the skin as this approximates the orientation of a seed in a clinical scenario and maximizes the dose to the skin. Simulations were performed with the breast phantom centred inside a 30 cm cube of air to mimic the lack of backscatter in clinical PBSI brachytherapy scenarios.

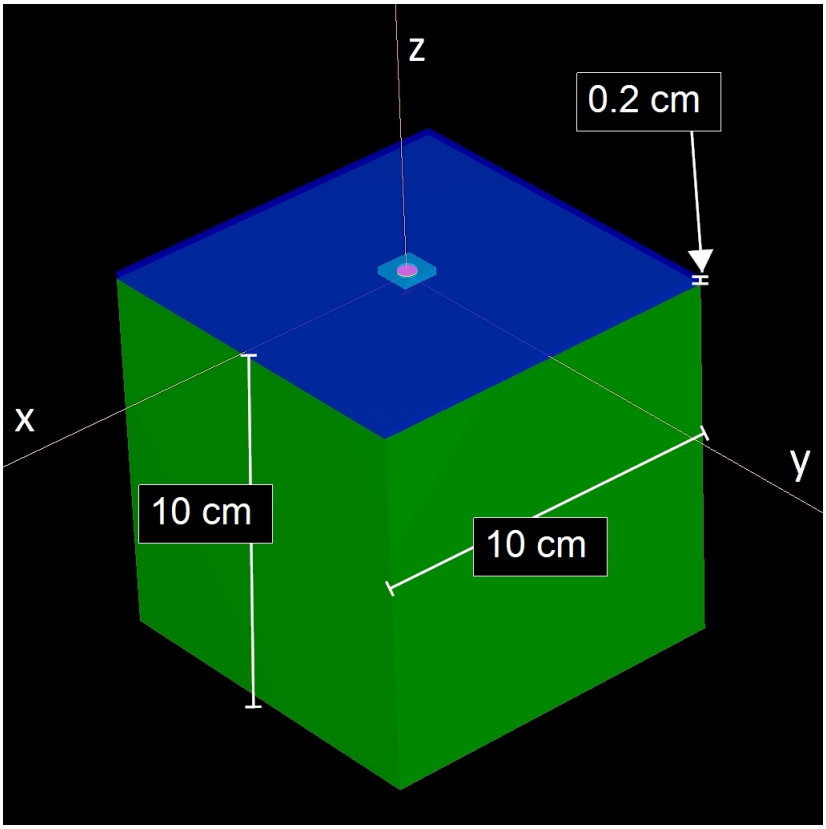

Figure 3.3: Geometry used for egs_brachy simulations. The large green cube is composed of breast tissue, the dark blue represents a 2 mm thick layer of skin and the small blue square is a model of an OSLD.

3.2.2 Monte Carlo Parameters

The low energy default transport parameters of egs_brachy were used so that electron transport was not performed (electron cut-off energy of 1.5 MeV) and photons were transported until they reached an energy of 1 keV in all simulations. Dose was scored using a tracklength estimator under the assumption of charged particle equilibrium and ignoring bremsstrahlung photons in all scoring materials to equate dose to collision kerma. NIST XCOM photon interaction cross-sections included with egs_brachy were used throughout this study both to calculate dose in the breast phantom and to generate mass energy absorption coefficients as needed. History-by-history statistical uncertainties were calculated using the default settings in egs_brachy and no variance reduction techniques were used. $1E+09$ histories were simulated in all simulations to keep statistical uncertainties below 1 %.

3.2.3 Breast Phantom Simulations

The position of the source inside the breast phantom was varied in each simulation by applying transformations that changed the seed depth relative to the skin surface (Figure 3.4) and the horizontal offset with respect to the OSLD (Figure 3.5). The seed's transverse axis remained parallel to the surface of the skin throughout each simulation. The horizontal offset was increased from 0 cm (source directly underneath OSLD) to 2 cm in 0.5 cm increments for seed depths increasing from 0.5 cm deep to 2 cm also in 0.5 cm increments. Additional simulations were performed without horizontal offset but increasing the seed depth from 0.3 cm to 1 cm in 0.1 cm increments. At seed depths of 0.5 cm and 1.0 cm, extra seeds were added at nearby positions to determine the effect that additional seeds have on the results in a more clinically relevant scenario.

Table 3.3: Material compositions used in each simulation group. OSL refers to the sensitive volume of the OSLD, backscatter is the material surrounding the breast phantom and OSLD and other media includes breast tissue and the OSLD excluding the sensitive volume. In this table, "accurate" implies that realistic material compositions were used.

Simulation group	OSL	Skin	Backscatter	Source	Other media
Al_2O_3_OSL	Al2O3_OSL	SKIN2_WW86	AIR_TG43	Accurate	Accurate
WATER_OSL	WATER_0.998	SKIN2_WW86	AIR_TG43	Accurate	Accurate
TG-43_OSL	WATER_0.998	WATER_0.998	WATER_0.998	Accurate	WATER_0.998

Skin dose was scored in a 0.2 cm^3 volume of skin directly beneath the OSLD in all simulations performed. This corresponds to a 1 cm $\times$ 1 cm $\times$ 0.2 cm voxel of skin centered on the OSLD in the region extending from the external skin surface to the interface with breast tissue. OSLD dose was determined by scoring dose in the sensitive volume of the OSLD, which was modelled as a single cylindrical volume. The ratio of the dose to the skin directly beneath the OSLD and the dose to the sensitive volume of the OSLD was calculated for each source position described above. This procedure was carried out for three distinct groups of simulations to examine the effect of material compositions on the ratio of doses: one group using accurate material compositions as in the geometry description section above, a second

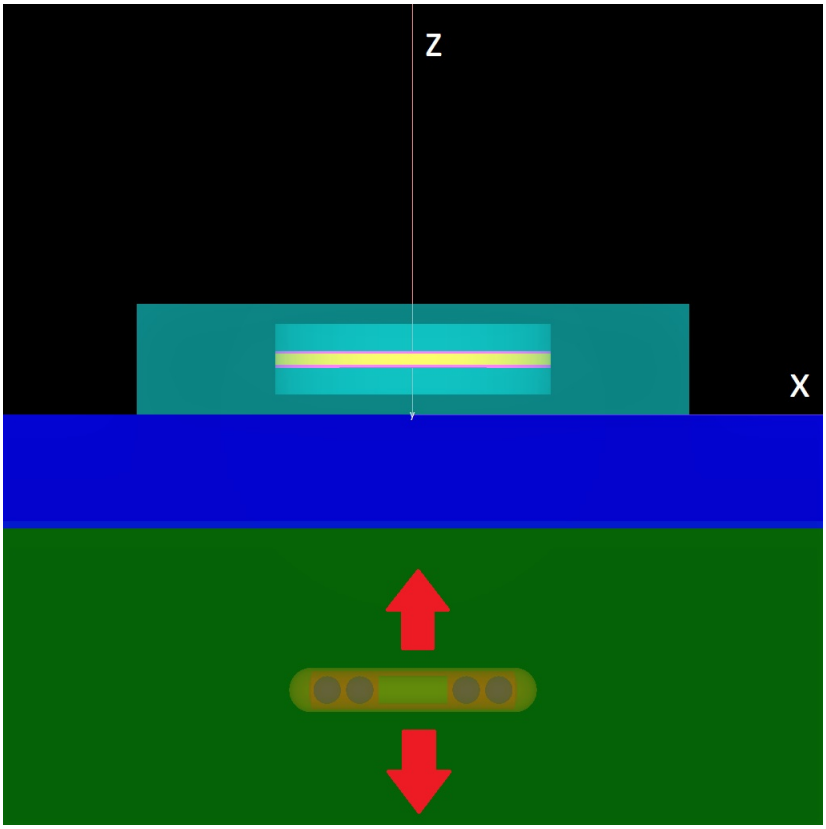

Figure 3.4: Close-up of the geometry used in egs_brachy simulations. An IsoAid Advantage Pd-103 seed is placed inside the breast tissue (dark green) parallel to an OSLD (light blue) located on top of the skin surface (dark blue). Red arrows illustrate the direction of the change in seed depth relative to the skin surface for different simulations. Yellow is the aluminium oxide/polyester mixture, fuschia is polyester. Due to the partial transparency of the OSLD case, the titanium encapsulation of the seed, and breast tissue, titanium and silver appear as light green, air appears as aqua in the OSLD and orange in the seed, and the radioactive polystyrene pellets appear as brown circles.

group using these same compositions except with water in place of the Al_2O_3/polyester mixture in the sensitive volume of the OSLD and a third group with all materials except for the source replaced with water. These groups will hereafter be referred to as Al2O3_OSL, WATER_OSL and TG-43_OSL, respectively (Table 3.3).

Skin dose may be approximated from *in vivo* OSLD measurements according to:

$$D_{skin} \approx f_{OSLD \to skin} \frac{D_{OSLD}}{1 - \exp(-\lambda t_{OSLD})} \tag{3.1}$$

where, D_{skin} is the approximate skin dose; $f_{OSLD \to skin}$ is a conversion factor between mea-

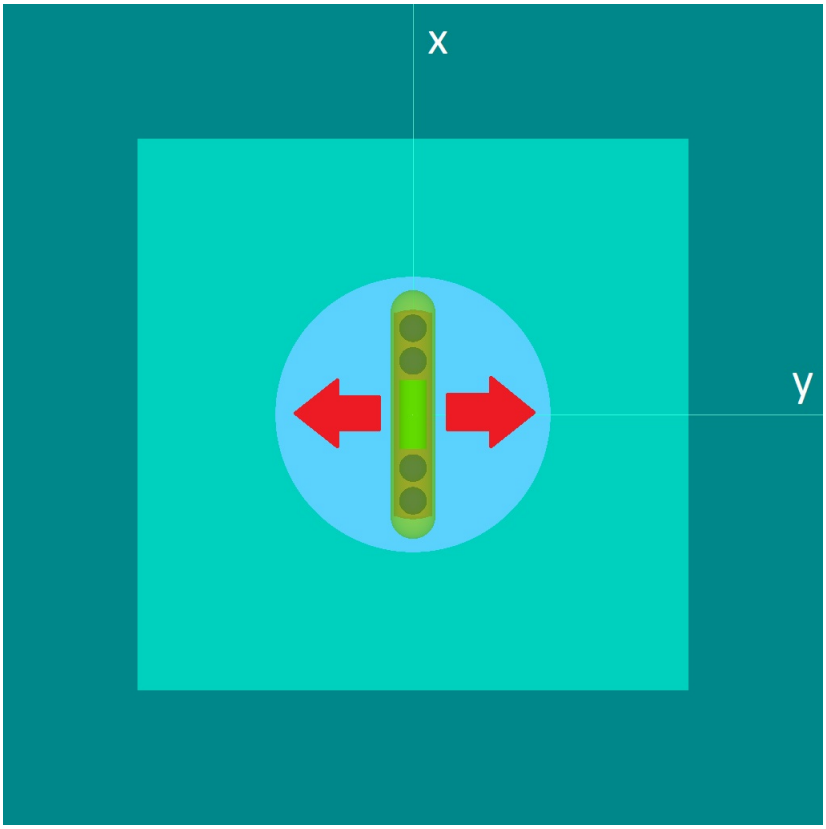

Figure 3.5: View from below source with OSLD in the background. Red arrows illustrate the direction of the horizontal seed translations examined in this study. The partial transparency of breast tissue and the OSLD case makes the OSLD case appear as aqua, polyester as light blue, breast tissue appears teal, titanium is green, silver is light green, and radioactive polystyrene pellets appear gold.

sured OSLD dose and skin dose; D_{OSLD} is the measured OSLD dose; t_{OSLD} is the total time the OSLD is placed on the patient's skin; λ is the decay constant for Pd-103.

In practice, one or more OSLDs would be placed on a patient's skin following a PBSI seed implant procedure along the main implantation axes and any other positions that are considered at risk of receiving a high dose, making sure to keep track of each OSLD's location and the total time they spend there. OSLD exposure times will be small (typically an hour) compared to the half-life of Pd-103 (16.991 days) as an integrated dose of 1 cGy could be delivered to an OSLD from a single 2 U seed at 1 cm depth in less than 20 minutes which is sufficient for accurate dose estimates to be obtained while the patient recovers post-implant. The OSLD dose would be measured and a value for $f_{OSLD \to skin}$ would be chosen based on

the results of this work and the method used to calibrate the OSLDs. The calibration should assign a dose to the point of measurement (i.e. the sensitive volume inside the OSLD) based on the OSL signal during readout in terms of the dose to water at that point or the dose to the Al_2O_3/polyester mixture contained in the sensitive volume. Both types of calibration are supported by the results of this work and it is left to each institution to determine the appropriate calibration for the Pd-103 sources used.

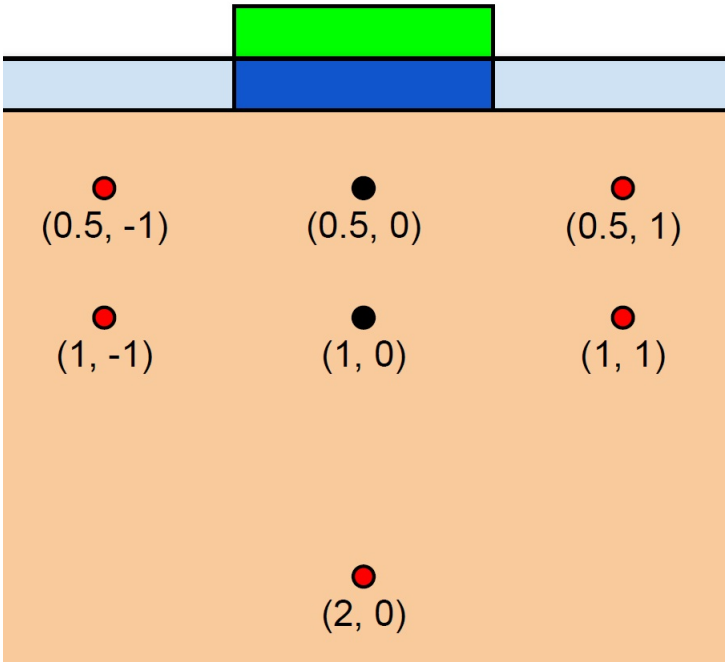

Figure 3.6: Seed positions used in simulations with multiple seeds. Coordinates indicate seed depth and horizontal offset in cm. Primary seed (black), additional seeds (red), skin dose scoring voxel (dark blue) and OSLD (green) are shown in their respective positions.

This work was extended to consider the influence of multiple seed sources on the ratio of skin dose to OSLD dose, as would more typically encountered in a clinical scenario. Simulations were performed for the Al2O3_OSL group for seed depths of 0.5 cm and 1.0 cm (referred to as primary seeds) with one or two additional seeds placed at; an offset of 1.0 cm, a depth of 1.0 cm or both positions (Figure 3.6). The 1.0 cm depth simulations had additional seeds at combinations of a 1.0 cm offset and/or a 2.0 cm depth. Two simulations with 5 seeds were performed at 0.5 cm and 1.0 cm depths with additional seeds offset by 1 cm in the

four cardinal directions relative to the primary seed but with axes oriented parallel to the primary seed.

3.3 Results

3.3.1 Impact of OSLD on Skin Dose

Relative to simulations performed with no OSLD present the maximum increase in skin dose due to the presence of the OSLD was 0.21 %. This suggests that using an OSLD to estimate the skin dose would not result in a clinically relevant increase to skin dose under the OSLD.

3.3.2 Conversion of D_{OSLD} to D_{skin}

Conversion factors ($f_{OSLD \rightarrow skin}$) were selected based on the results in Figure 3.7 illustrating how the ratio of MC calculated skin dose and OSLD dose ($D^{MC}_{skin/OSLD} = D^{MC}_{skin}/D^{MC}_{OSLD}$) varies with seed position for all three simulation groups. Each row represents a different simulation group as indicated and the graphs are organized into dose ratios without horizontal seed offsets applied (left column) and those with horizontal seed offsets (right column). The trends are nearly identical in each group except for a scaling of the ratios due to differences in the simulated materials. $D^{MC}_{skin/OSLD}$ is maximized at the same points for each group at 0.7 cm seed depth without a horizontal offset and at 0.5 cm depth with 0.5 cm horizontal offset. The recommended values for $f_{OSLD \rightarrow skin}$ (set equal to $\max(D^{MC}_{skin/OSLD})$ to err on the side of over-estimating skin dose) based on these results are 0.50 for the Al2O3_OSL group and 1.44 for the WATER_OSL group corresponding to OSLD calibrations to dose to Al_2O_3/polyester and water, respectively.

The results from the TG-43_OSL group of simulations (Figure 3.7 e and f) demonstrate the variation of $D^{MC}_{skin/OSLD}$ when differences in transport and dose scoring media were eliminated. Trends very similar to those in the Al2O3_OSL and WATER_OSL groups were observed suggesting that geometric effects such as the relative locations of the dose scoring

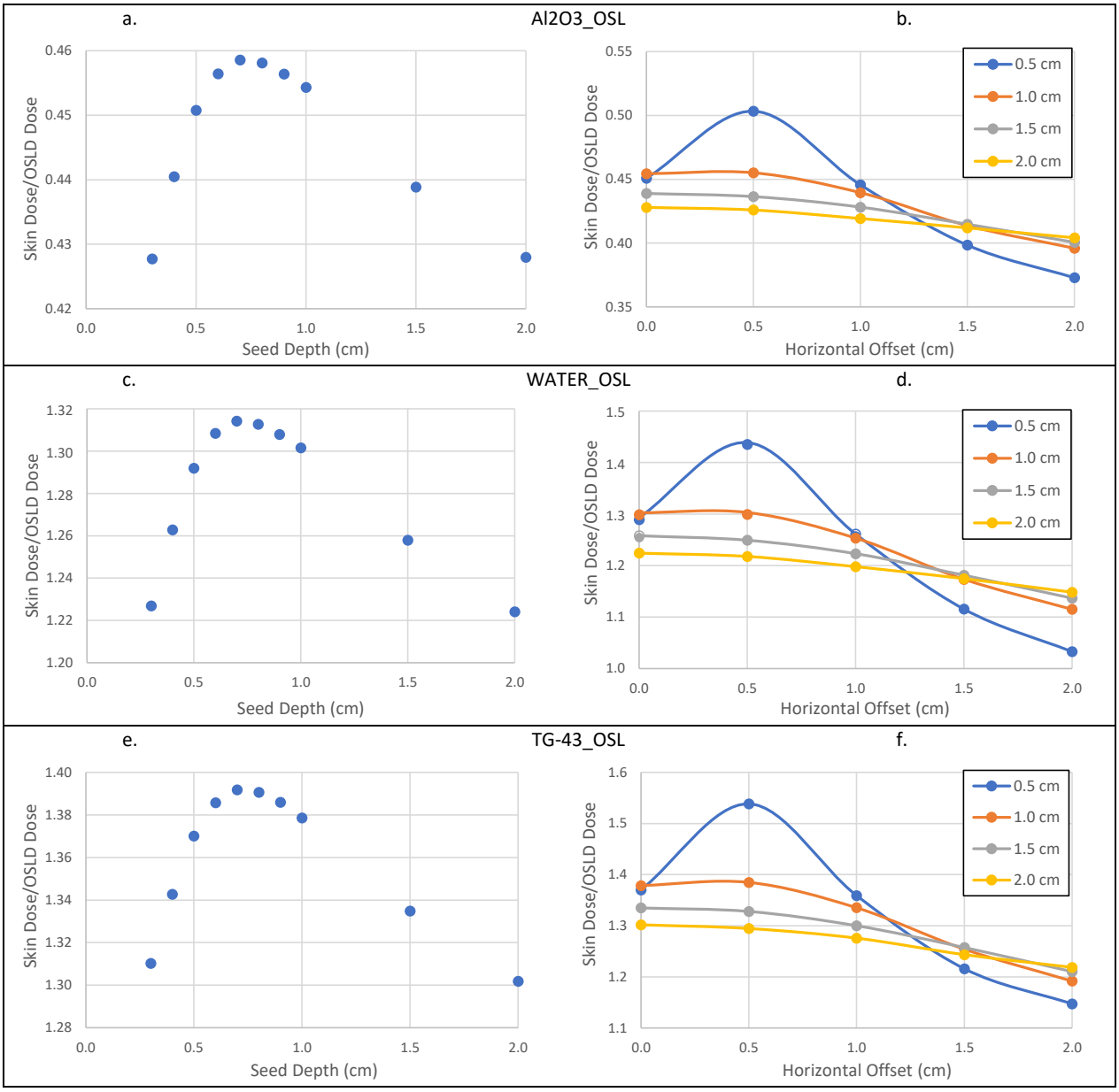

Figure 3.7: a-f: Ratios of MC calculated skin doses to OSLD doses ($D^{MC}_{skin/OSLD}$) for various seed positions and material compositions for single seed simulations. Left column: simulations with no horizontal seed offset. Right column: each line corresponds to a specific seed depth. Material compositions are indicated above each row (see Table 3.3)

regions in the skin and the OSLD as well as their volumes and shapes dictate the variation of $D^{MC}_{skin/OSLD}$ with seed position. To test this hypothesis, $D^{MC}_{skin/OSLD}$ values from the Al2O3_OSL and WATER_OSL groups for all depths without a horizontal seed offset were divided by the $D^{MC}_{skin/OSLD}$ values from the TG-43_OSL group. The resulting values

were then normalized to the ratios of mass-energy absorption coefficients for Al2O3_OSL and WATER_0.998 to SKIN2_WW86 averaged over the Pd-103 spectrum according to the respective equations below:

$$h_{\text{Al2O3\_OSL}} = \frac{(D^{MC}_{skin/OSLD})_{\text{Al2O3\_OSL}}}{(D^{MC}_{skin/OSLD})_{\text{TG-43\_OSL}}} \frac{(\overline{\mu}_{en})_{\text{Al2O3\_OSL}}}{(\overline{\mu}_{en})_{\text{SKIN2\_WW86}}} \tag{3.2}$$

$$h_{\text{WATER\_OSL}} = \frac{(D^{MC}_{skin/OSLD})_{\text{WATER\_OSL}}}{(D^{MC}_{skin/OSLD})_{\text{TG-43\_OSL}}} \frac{(\overline{\mu}_{en})_{\text{WATER\_0.998}}}{(\overline{\mu}_{en})_{\text{SKIN2\_WW86}}} \tag{3.3}$$

These values were within 0.7 % and 1.6 % of unity for the Al2O3_OSL and WATER_OSL groups, respectively (Figure 3.8).

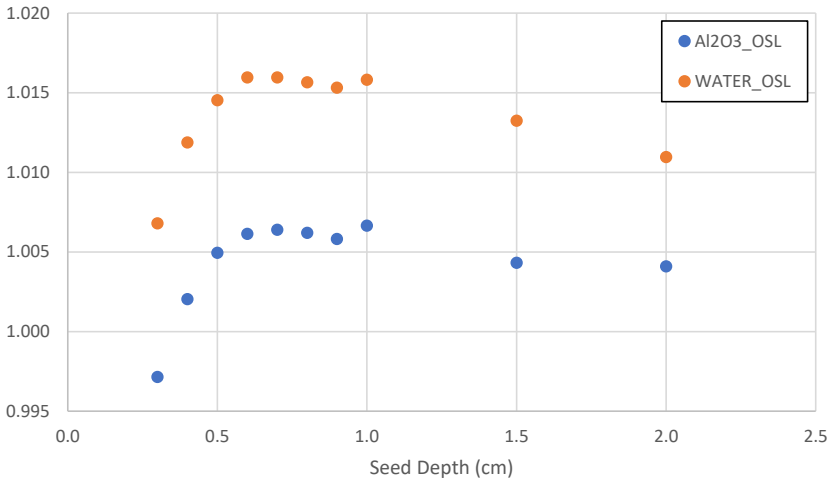

Figure 3.8: Plots of h values from Eqns. (3.2) and (3.3) as functions of seed depth.

In simulations with multiple seeds, the primary seeds were responsible for most of the dose to skin in all simulations except for five seeds at 1 cm depth. Primary seeds contributed from 68.1 % to 85.4 % (one additional seed), from 51.6 % to 67.8 % (two additional seeds), and from 36.8 % to 56.2 % (four additional seeds) of the total skin dose depending on the position of the added seeds (Table 3.4). $D^{MC}_{skin/OSLD}$ is largely unaffected by the addition of extra seeds as indicated by the results in the last column of Table 3.4 which show a slight reduction (less than 2.5 %) in the ratios compared to single seed simulations in all but one case.

Table 3.4: Results of simulations with multiple seeds. Positions of seeds, percent of skin dose due to primary seeds, $D^{MC}_{skin/OSLD}$ for primary and additional seeds is listed. The last two rows correspond to simulations with 5 seeds and the extra coordinate in the fourth and fifth columns represents the seed offset in the x-direction in cm.

Primary seed	Seed 2	Seed 3	Seed 4	Seed 5	Primary seed skin dose %	$D^{MC}_{skin/OSLD}$
(0.5, 0)					100	0.451
(0.5, 0)	(0.5, 1)				80.8	0.450
(0.5, 0)	(0.5, 1)	(0.5, -1)			67.8	0.449
(0.5, 0)	(0.5, 1)	(1, 0)			67.0	0.451
(0.5, 0)	(1, 0)				79.7	0.452
(1, 0)					100	0.454
(1, 0)	(1, 1)				68.1	0.449
(1, 0)	(1, 1)	(1, -1)			51.6	0.447
(1, 0)	(1, 1)	(2, 0)			61.0	0.447
(1, 0)	(2, 0)				85.4	0.450
(0.5, 0)	(0.5, 1)	(0.5, -1)	(0.5, 0, 1)	(0.5, 0, -1)	56.2	0.447
(1, 0)	(1, 1)	(1, -1)	(1, 0, -1)	(1, 0, -1)	36.8	0.443

3.4 Discussion

In vivo surface dosimetry using OSLDs is a convenient means of evaluating PBSI skin dose, but the dose to the sensitive volume of the OSLD and the dose delivered to the skin immediately below it is not necessarily equivalent. This difference was quantified in this work to gain a better understanding of the parameters needed to approximate skin dose based on OSLD measurements and how source positioning affects the measured doses. Conversion factors of 0.50 and 1.44 are recommended for OSLDs calibrated to dose to Al_2O_3/polyester or water at the point of measurement in the OSLD, respectively. Maximum values of $D^{MC}_{skin/OSLD}$ were chosen for conversion factors because the locations of the seeds post-implant are likely unknown, and these values represent the safer choice in terms of predicting potential skin toxicities. This approach of estimating the dose to a small volume is simpler to implement and less sensitive to the geometry than trying to approximate the maximum dose to the skin, $D_{\max}$, in addition to being arguably a more useful dose metric due to volume effects observed in irradiated skin [27, 29, 32]. It is also an intuitive metric as the volume of skin is

nearly equal in size to an OSLD.

The simulations demonstrate that variation in the ratio $D^{MC}_{skin/OSLD}$ is dominated by geometry and material composition. When these effects are explicitly accounted for (Figure 3.8) deviations are less than 2 % and may be attributed to differences in scatter doses. Simulations with multiple seeds were also performed and suggested that conclusions about $D^{MC}_{skin/OSLD}$ based on single seed simulations are robust against the addition of extra seeds. This is reassuring as it is likely that more than one seed would contribute to skin dose in clinical situations.

To apply the conversion factors found in this work, individual institutions effectively require a calibration for OSLDs for the Pd-103 spectrum. OSLDs are typically calibrated to dose to water for megavoltage x-rays (6MV or Co-60 for example) and these calibrations would not apply to Pd-103 due to the energy dependence of the OSLD response [70, 74]. This calibration would require exposing OSLDs to known doses using Pd-103 seeds and measuring the response to those doses in an OSLD reader. We recommend that the dose to water calibration be performed because this is the more clinically relevant than the dose to Al_2O_3/polyester.

The simulations performed in this study established a relationship between OSLD dose and skin dose for a simplified breast phantom geometry. These results can and should be extended to a wider variety of simulation geometries involving different material compositions (particularly modifying the ratio of adipose and glandular tissue in breast), source orientations relative to the OSLD position and for different source models. Monte Carlo investigations involving Pd-103 PBSI sources for patients undergoing this treatment have examined the effects of varying tissue composition and performing dose calculations on actual patient CT data on the outcome of the calculation (5–7). A logical progression from this work should include the incorporation of CT data into the simulations as it is likely that the conversion factor would be different for patients with significantly different tissue composition than what has been modelled here. The ultimate goal would be a comprehen-

sive procedure for assessing skin dose using OSLDs that utilizes Monte Carlo methods to simulate low energy radiation transport and patient specific data to adjust accordingly.

3.5 Conclusion

Conversion factors between measured OSLD dose and dose to the skin directly underneath it for patients receiving PBSI brachytherapy treatments were calculated using the Monte Carlo code egs_brachy. In all cases studied, the dose to skin differed from OSLD dose with conversion factors of 0.50 and 1.44 being recommended for general use when OSLDs are calibrated to dose to medium and dose to water, respectively. A combination of geometric effects and the choice of material compositions was used to explain trend in the data and the resulting ratio of doses and conversion factors. Using these conversion factors, one can perform *in vivo* dosimetry using OSLDs allowing more accurate estimates of the skin dose under the OSLD. In turn, this would enable one to act to reduce the painful effects of skin toxicities if necessary and improve patient outcomes.

Chapter 4

OSLD calibration procedure for low energy brachytherapy seeds

Chapter Overview

Optically stimulated luminescence dosimeters (OSLD) are frequently used during radiation therapy (RT) treatments to perform *in vivo* dosimetry (IVD) by placing OSLDs, in the form of small plastic chips containing Al_2O_3:C, on or near the patient. These dosimeters are typically calibrated for use with megavoltage x-ray beams (6 MV, for example) generated by clinical linear accelerators by exposing them to known doses of radiation and measuring the resulting signal produced by optical stimulation of the sensitive Al_2O_3:C layer using an OSLD reader. OSLD readings have minimal energy dependence to x-rays in the megavoltage energy range but exhibit a significant overresponse to low energy x-rays (< 100 keV) [74] such as those emitted by radioactive brachytherapy sources including Pd-103. Despite many desirable characteristics, the use of OSLDs in brachytherapy is extremely limited and there are no guidelines for how to calibrate OSLDs to measure doses from low x-ray energy brachytherapy seeds. This work details a procedure that can be used to perform this task for a Pd-103 seed and serves as a template for institutions interested in applying OSLDs to obtain IVD

measurements from their brachytherapy patients to assess the quality of the treatment.

This work in this chapter is intended to be submitted to a peer-reviewed journal. I am the primary author and it was co-authored by Dr. Charles Kirkby, Thomas Mann, Dr. Tyler Meyer, and Dr. Jose Eduardo Villarreal-Barajas. Thomas Mann performed a similar procedure using largely the same materials under the guidance of Dr. Villarreal-Barajas and Dr. Kirkby prior to the current work and was consulted frequently throughout the experiment for his insights. The phantom used in Thomas Mann's experiment, which was also used for this work, was constructed by Christian Bagg and Adam Yarschenko of the Medical Physics Design Lab at Tom Baker Cancer Centre who also contributed additional materials for the current work. I performed the measurements presented in this chapter with the assistance of Dr. Meyer who addressed radiation safety concerns associated with handling the Pd-103 seed and storage of the experimental apparatus during irradiations. I acquired and analysed data from the experiment, performed Monte Carlo dose calculations, and wrote the first draft of the manuscript in progress. Dr. Kirkby and Dr. Villarreal-Barajas were involved in designing and planning the experiment, provided their expertise to interpreting the results, and contributed to revised versions of the initial draft of the manuscript in progress.

For permission to reproduce this work see Appendix A.2.

Optically stimulated luminescence dosimeter calibration procedure for Pd-103 brachytherapy source

Steven Nich, Charles Kirkby, Thomas Mann, Tyler Meyer, J. Eduardo Villarreal-Barajas

Abstract

PURPOSE: To develop an OSLD calibration procedure that can be applied to low x-ray energy brachytherapy seeds.

METHODS AND MATERIALS: A custom PMMA phantom was constructed to simultaneously irradiate 6 Landauer nanoDot™OSLDs with a single IsoAid Advantage Pd-103 (IAPd-103A) brachytherapy seed. The egs_brachy Monte Carlo code was used to calculate OSLD doses while they were irradiated using realistic source and OSLD models and a varying amount of PMMA backscatter material. A second group of OSLDs was irradiated to a known dose from a 6 MV x-ray beam produced by a clinical linear accelerator for comparison with the Pd-103 results. These measurements were used to determine calibration factors for the IAPd-103A seed and relate the OSLD response to a standard 6 MV calibration.

RESULTS: A mean calibration factor of $(6.21 \pm 0.19) \times 10^4$ counts/cGy was found for the IAPd-103A using Monte Carlo calculated doses. The OSLD response to the IAPd-103A seed was found to be about 4 times that of the 6 MV beam. Two cm of PMMA backscatter was determined to be a reasonable approximation of full backscatter conditions for the IAPd-103A source.

CONCLUSIONS: A simple OSLD calibration procedure was implemented to determine calibration factors for IAPd-103A brachytherapy seeds. The approach used in this work is easily generalizable to other brachytherapy source models.

4.1 Introduction

Optically stimulated luminescence dosimeters (OSLDs) are a convenient tool for performing *in vivo* dosimetry for patients receiving radiation therapy. Typical OSLDs come in the form of small plastic chips containing a thin layer of carbon-doped aluminium oxide (Al_2O_3:C) where energy from ionizing radiation is stored [33,109]. These dosimeters have several desirable properties that has led to an increase in their popularity in radiation therapy applications compared with more traditional methods such as radiochromic film and thermoluminescent dosimeters (TLD). The mechanism behind the OSL phenomenon is like that of TLDs, but the output signal is stimulated by light instead of heat. OSLD readout can be performed in a matter of seconds and the signal is not destroyed in the process unlike TLDs which require longer readout times and cannot be remeasured at a later time.

Investigations into the dosimetric properties of OSLDs have been performed by numerous authors over the years. Schembri and Heijmen conducted experiments with OSL films and found no dependence on dose rate, minimal energy dependence in the 6 MV to 18 MV range and a linear response up to doses of 2 Gy [84]. Jursinic showed a minimal decrease in OSL response with each reading (0.05 %), found no angular dependence on the OSL signal and demonstrated the reusability of OSLDs following annealing with a bright light source to erase the signal [33]. However, they observed a transient signal up to 8 minutes post-irradiation which could affect the measurement if the OSLDs are not allowed enough time to stabilize before performing measurements [33]. Reft studied the energy dependence of OSLDs and while they showed results similar to Schembri and Heijmen in the megavoltage x-ray energy range, they observed a significant overresponse in OSLDs exposed to x-rays in the kilovoltage range that became more pronounced as the photon energy decreased [74].

In recent years, studies have been conducted to examine the dosimetric properties of OSLDs and potential applications in the context of brachytherapy treatments. To date these studies have been limited to high dose rate (HDR) brachytherapy sources, namely, Ir-192 [86, 99] and Co-60 [75]. Overall, these studies agreed that OSLDs are useful for *in*

vivo dosimetry in HDR brachytherapy due to their convenience and desirable dosimetric characteristics. However, OSLD response at diagnostic and orthovoltage x-ray energies has been shown to be much more complex, requiring greater care for accurate *in vivo* dosimetry due to increased variability at low energies [70, 83]. The extreme case of OSLD response to low dose rate (LDR) brachytherapy sources such as Pd-103, with an average photon energy below 20 keV, has yet to be characterized in the literature.

This work demonstrates the feasibility of an OSLD calibration procedure for *in vivo* measurements of skin or surface dose in the presence of LDR brachytherapy seeds commonly used in permanent breast and prostate seed implants. In particular, the following procedure was developed using the IsoAid Advantage Pd-103 (IAPd-103A, IsoAid, LLC, Port Richey, FL) seed. This seed is used at our institution (Tom Baker Cancer Centre (TBCC)) to perform permanent breast seed implant (PBSI) brachytherapy treatments, which are administered to low risk breast cancer patients. Given the well-established convenience and desirable dosimetric properties of OSLDs in numerous radiation therapy applications up to now, it seems only natural that they would have significant potential to measure and confirm delivered dose in LDR brachytherapy treatments. Understanding how OSLDs respond to the low energy photon spectrum produced by these sources is an essential step if they are to be applied clinically to perform *in vivo* dosimetry measurements. In this study, we employ experimental OSLD measurements and Monte Carlo methods to characterize the OSLD response to the IAPd-103A seed. Using this experimental geometry, we determine a factor that enables conversion of signal to dose as calibrated for a 6 MV beam, to the dose in response to a brachytherapy source with a mean energy < 20 keV.

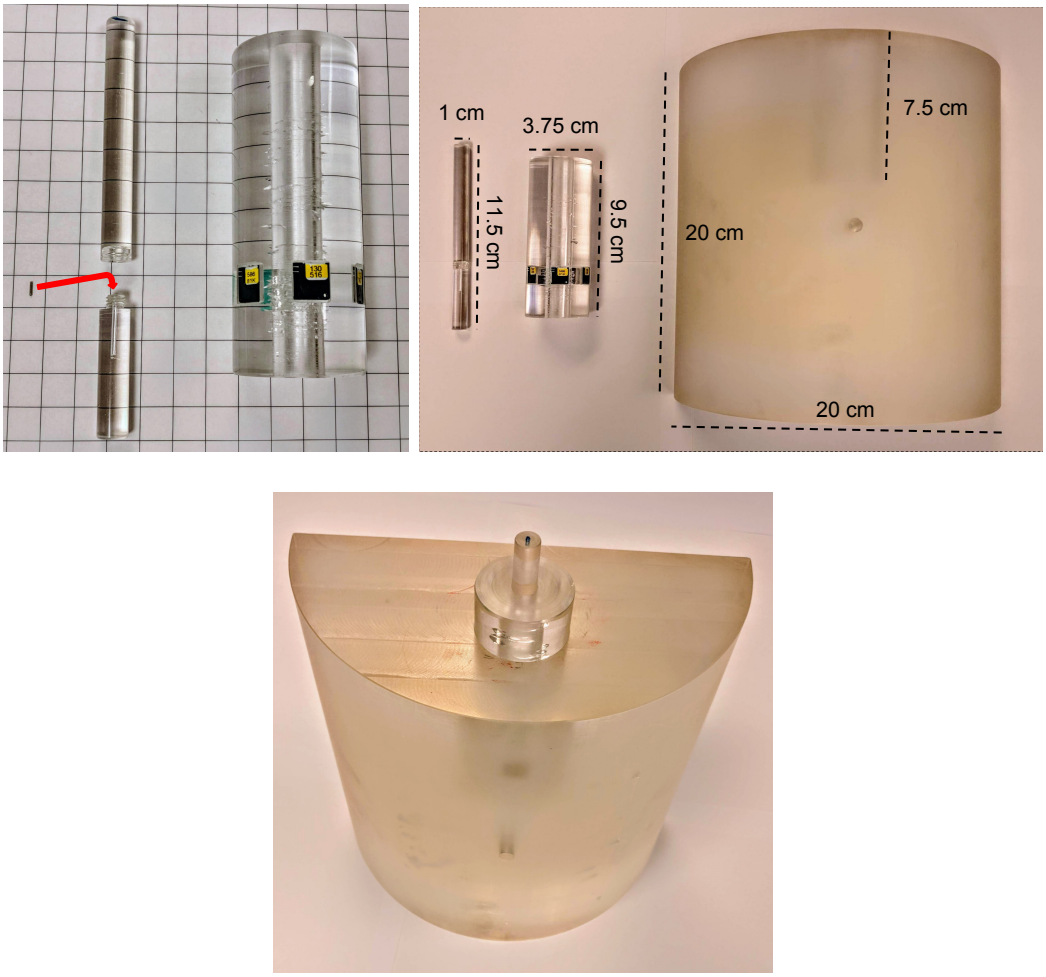

Figure 4.1: PMMA phantom used to irradiate OSLDs with IAPd-103A brachytherapy seed. (Top left) Close-up of seed holder and OSLD holder alongside an IAPd-103A seed. The red arrow indicates where the seed is inserted in the seed holder. OSLDs are shown embedded in the OSLD holder. (Top right) All components of the PMMA phantom with measurements. The measurement of 7.5 cm at the top of the backscatter block corresponds to the depth of the hole that the OSLD holder is inserted into during irradiations. (Bottom) Fully assembled phantom as it would appear during irradiations with backscatter.

4.2 Methods and Materials

4.2.1 Phantom Description

In order to derive a factor that can translate an OSLD light signal into dose, we needed to design a phantom for the simultaneous irradiation of multiple OSLDs with a single Pd-103 seed. A custom polymethyl methacrylate (PMMA) phantom, based on one used by Morrison et al. to irradiate EBT3 film [56], was made to irradiate up to six OSLDs simultaneously with a single brachytherapy seed (Figure 4.1). The primary components of this phantom were a seed holder, an OSLD holder and a large block of (PMMA) to provide backscatter. Each of these components is described below:

Seed Holder: The seed holder consisted of two separate 0.5 cm radius PMMA cylinders that could be joined by threads machined into one end of each piece. One piece had a small cavity drilled into its central axis at the threaded end so that a seed could be inserted parallel to this axis. The two pieces were then screwed together to form a single cylinder with the seed secured inside.

OSLD Holder: The OSLD holder was made from a 1.875 cm radius PMMA cylinder with a 0.5 cm radius hole drilled along its central axis where the seed holder could be inserted. Six evenly spaced, 1 cm square holes were cut out of the outside surface of the OSLD holder to accommodate OSLDs. These holes were positioned so that the centre-to-centre distance between the seed and each OSLD was 1.725 cm when the seed holder was inserted.

Backscatter Block: The backscatter block was a 10 cm radius, 20 cm tall half cylinder of PMMA. A 1.875 cm radius hole was drilled into the top of this block to fit the OSLD holder. This hole was positioned so that each OSLD would have at least 3 cm of PMMA backscatter in each direction when all three phantom components were assembled. For reference, the half-value layer of 20 keV photons in PMMA is approximately 1 cm [30].

4.2.2 Experimental Procedure

Six Landauer nanoDot™OSLDs (Landauer Inc. Glenwood, IL) were irradiated in the PMMA phantom. Each OSLD was irradiated a total of nine times. After each irradiation, PMT count measurements were obtained using a Landauer microStar® (Landauer Inc. Glenwood, IL) OSLD reader. These readout measurements were repeated three times for each OSLD to derive a mean readout value. Between subsequent irradiations, the OSLDs were annealed by exposing them to a bright white light source for approximately 24 hours to erase the OSL signal (remaining signals after annealing were less than 0.3 % and less than 0.1 % for the control group and seed group respectively). Before every set of measurements, the OSLD reader was allowed to warm-up for at least 15 minutes and a performance check was performed to ensure that the PMT was working consistently. A second set of three OSLDs (control group) was used to control for any possible systematic changes in OSLD response between subsequent irradiation and annealing events.

The control group was irradiated with 5 monitor units (MU) from a Varian Clinac 6 MV photon beam. The control group was irradiated nine times (4.86 cGy per irradiation). This procedure consisted of placing one OSLD on a $30 \times 30\,\text{cm}^2$ by 10 cm high solid water slab with a 1.5 cm bolus placed on top of the OSLD to minimize air gaps. The source-to-surface distance (SSD) was set to 100 cm at the surface of the bolus and a field size of $10 \times 10\,\text{cm}^2$ was used. The sensitive volume of the OSLDs, indicated by a cross on the outside casing, were centred on the crosshairs of the linac.

The six seed group OSLDs were irradiated using the same procedure as the control group for the first and final irradiations. The remaining irradiations were carried out using an IAPd-103A seed in the PMMA phantom with the OSLDs in place around it in the OSLD holder according to the schedule shown in Table 4.1. Four of these irradiations did not involve the backscatter block while the other three did, alternating between each irradiation. To account for any decay over the course of the experiment (which lasted several days), the time required to deliver a dose of $D = 5\,\text{cGy}$ to the centre of the sensitive volume of each

OSLD within the PMMA phantom was calculated as:

$$t = -\frac{1}{\lambda} \ln \left(1 - \frac{\lambda}{\dot{D}} \frac{D}{S_K} \right) \tag{4.1}$$

Where, t is the irradiation time, λ is the decay constant for Pd-103, $\dot{D}$ is the dose rate to water per unit air kerma strength at the point of measurement, D is the desired dose to water, usually 5 cGy, and S_K is the air kerma strength of the seed. Actual irradiation times were measured so that more accurate dose calculations could be performed afterwards.

Table 4.1: OSLD irradiation schedule for control group and seed group. 6 MV indicates that OSLDs in that group were irradiated using a linac. Seed indicates that the OSLDs were irradiated in the PMMA phantom using the Pd-103 seed. The backscatter block column applies to the seed group only and indicates whether the backscatter block was used. OSLDs were annealed following every irradiation.

Irradiation #	Control Group	Seed Group	Backscatter Block
1	6 MV	6 MV	
2	6 MV	Seed	No
3	6 MV	Seed	Yes
4	6 MV	Seed	No
5	6 MV	Seed	Yes
6	6 MV	Seed	No
7	6 MV	Seed	Yes
8	6 MV	Seed	No
9	6 MV	6 MV	

The air kerma strength of the Pd-103 seed was measured using an ADCL calibrated well chamber and electrometer. Three charge measurements were obtained over 2 minutes at a time with a 300 V bias voltage applied. The mean charge reading was corrected to account for temperature, pressure, altitude and the electrometer by applying appropriate factors. The well chamber calibration factor was then applied to determine the air kerma strength at the time of measurement. All dose calculations were based on the air kerma strength at the start of each irradiation, adjusting for the time between measurements and the exponential decay of the seed. It is worth mentioning that the air kerma strength measurements performed for this experiment are no different from the one used routinely for air kerma strength verification

for Pd-103 seeds used for clinical PBSI implants.

Raw PMT counts obtained for each OSLD following every irradiation were averaged over the three measurements performed. The mean PMT counts for each OSLD were corrected for the individual sensitivities provided by the manufacturer. OSLD calibration factors were calculated using the corrected mean PMT count measurements and the dose to water (obtained by re-arranging Equation (4.1) to determine D delivered for the actual exposure time) in the OSLDs according to the following equation:

$$\mathrm{CF(E)} = \frac{\overline{\mathrm{PMT\_COUNTS}}}{D \cdot \mathrm{SENSITIVITY}} \tag{4.2}$$

The mean calibration factors for 6 MV and Pd-103 were found by averaging over all the individual calibration factors for each modality. The OSLD response for the Pd-103 spectrum relative to the 6 MV spectrum was calculated by taking the ratio of the two mean calibration factors.

4.2.3 Monte Carlo Dose Calculations

Monte Carlo simulations were performed using the EGSnrc user code egs_brachy to model the experimental geometry previously described [12]. The IAPd-103A brachytherapy source and the Landauer nanoDot™OSLD geometries were developed for a previous study by our group [62]. The Pd-103 seed was modelled based on data from the Carleton brachytherapy seed database which came from studies by Meigooni et al. and Sowards [53,91,95]. The OSLD model was based on work by Lehmann et al. who provided details of the OSLD composition and dimensions from measurements and correspondence with Landauer [43]. Water was used in place of Al_2O_3:C in the OSLD so that dose to water could be calculated at the point of measurement in the sensitive volume of the OSLD with the following equation [98]:

$$D = \frac{(S_K)_i \dot{D}}{\lambda}(1 - \mathrm{e}^{-\lambda t}) = \frac{(S_K)_i \overline{D}^{hist}_{OSLD}}{\lambda S^{hist}_K}(1 - \mathrm{e}^{-\lambda t}) \tag{4.3}$$

Where, $(S_K)_i$ is the initial air kerma strength of the seed, $\overline{D}^{hist}_{OSLD}$ is the average dose rate per history for the OSLD scoring volume, S^{hist}_K is the air kerma strength per history. The NNDC Pd-103 photon spectrum and elemental compositions of materials simulated were included in the egs_brachy distribution.

A simplified geometry was used to model the PMMA phantom which consisted of a large box (30 cm × 30 cm×15–20 cm) of PMMA surrounded by air. The seed and the OSLD were placed 1.725 cm apart (centre-to-centre distance) with the OSLD initially on the surface of the PMMA box and the seed inside the box. Later simulations were performed with the PMMA box extending to the outside surface of the OSLD (experimental geometry without the backscatter block, see Figure 4.2) and continuing to increase the amount of backscatter up to 5 cm. This was done so that the dose enhancement to the OSLD for various amounts of backscatter could be determined relative to the scenario where no backscatter is present. This allowed theoretical doses required to compute calibration factors for Pd-103 to be calculated as well as establishing the minimum amount of backscatter needed to achieve full backscatter conditions in PMMA. Note that the egs_brachy simulations where the OSLD was embedded in the PMMA box with no PMMA beyond the surface farthest from the seed to approximate scatter conditions present in the experiment (0.2 cm PMMA minimum backscatter in Figure 4.3).

Monte Carlo calculations report dose per history and it is necessary to determine the air kerma strength per history to convert these to cumulative doses over a specific period of time. This was achieved using a geometry included in egs_brachy that approximates the NIST WAFAC geometry used as a standard to calibrate brachytherapy sources and correcting for volume averaging and inverse square law effects. This simulation used transport parameters to suppress characteristic x-rays produced in the titanium encapsulation of the seed while all other aspects of the simulation used default low energy transport parameters, both of which are distributed with egs_brachy. These settings do not simulate electron transport and correspond to photon cut off energies of 5 keV and 1 keV for air kerma strength simulations

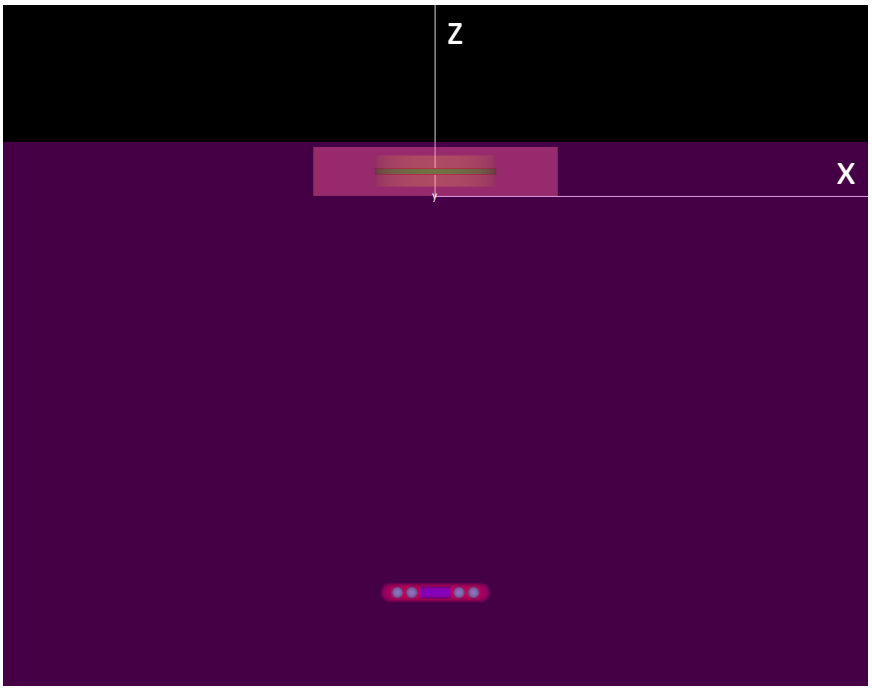

Figure 4.2: The egs_brachy simulation geometry modelling the PMMA phantom used in the experimental procedure. The IAPd-103A seed (bottom) has four polystyrene pellets containing Pd-103 (light blue), a silver CT marker (blue) and titanium encapsulation (red) visible. The OSLD is shown near the top with the sensitive volume colored green. The OSLD casing is light pink and two thin layers of polyester surround the sensitive volume. PMMA is shown in pink and completely surrounds the seed and all but one face of the OSLD. The no backscatter calibration factor (Table 4.2) condition is shown. Additional simulations were performed with varying amounts of PMMA surrounding the OSLD (Figure 4.3).

and all other simulations, respectively. 4×10^9 histories were simulated for air kerma strength simulations and 1×10^9 histories were simulated for the PMMA phantom to keep statistical uncertainties below 1 %.

We were also interested in determining the difference between the predictions of the detailed Monte Carlo simulations and those more commonly employed as per the TG-43 formalism [77, 80]. We used this formalism to determine the dose to water at the position of the point of measurement in the OSLD, 1.725 cm from the source. This dose was corrected for the PMMA transport media by scaling the result by a factor of 1.37. This correction factor was derived from work by Luxton [44] and corresponds to the ratio of the dose to water in PMMA to the dose to water in water at 1.725 cm. The ratio of this corrected TG-43 dose

to the egs_brachy calculated dose with full backscatter then provided a means to scale the calibration factor determined with egs_brachy to generate a TG-43 based calibration factor.

4.3 Results

Summary statistics for the OSLD calibration factors obtained for Pd-103 and 6 MV photon spectra are listed in Table 4.2. The most important results in this table are mean calibration factors given by $(6.21 \pm 0.19) \times 10^4$ counts/cGy and $(1.556 \pm 0.023) \times 10^4$ counts/cGy for Pd-103 and 6 MV, respectively. From these results, a relative OSLD response of 3.99 for Pd-103 compared to 6 MV photons was calculated. The no backscatter results in Table 4.2 correspond to egs_brachy simulations where the OSLD was embedded in the PMMA box with no PMMA beyond the surface farthest from the seed to approximate scatter conditions present in the experiment (0.2 cm PMMA backscatter in Figure 4.3). In general, seed irradiations without the backscatter block exhibited more variation in the calibration factors than those with backscatter and all seed irradiations were more variable than 6 MV irradiations.

Table 4.2: Summary statistics for OSLD calibration factors. The 6 MV column includes all irradiations performed on a linac, the seed column refers to all Pd-103 seed irradiations and the fourth and fifth columns represent subsets of the seed irradiations with and without the backscatter block. The final column corresponds to the calibration factor for Pd-103 with the dose calculated using the TG-43 formalism.

Statistic	6 MV	Seed			
		Total	No Backscatter	Backscatter	TG-43
N	38	42	24	18	42
$\langle CF \rangle$ (1×10^4 counts/cGy)	1.556	6.21	6.17	6.25	5.94
σ_{CF} (1×10^4 counts/cGy)	0.023	0.19	0.21	0.15	0.18
$\sigma_{CF}/\langle CF \rangle$ (%)	1.4	3.0	3.4	2.4	2.9
Relative Response	1.00	3.99	3.96	4.01	3.81

The amount of PMMA backscatter required to attain full backscatter conditions was investigated in Figure 4.3 using egs_brachy simulations. In this figure, 0 cm backscatter implies that the OSLD is in contact with the PMMA box on one surface while the other sides

are surrounded by air. A backscatter thickness of 0.2 cm corresponds to the experimental geometry with the OSLD embedded in the OSLD holder without the backscatter block. All the other values beyond 0.2 cm involve simulations where the OSLD is fully surrounded by PMMA. As the amount of backscatter increases, the dose relative to the 0 cm backscatter scenario increases up to 10 %, where it saturates at a thickness of roughly 2 cm. After this point, the calculated dose is relatively constant regardless of how much PMMA is added beyond the OSLD indicating that full backscatter conditions have been effectively achieved.

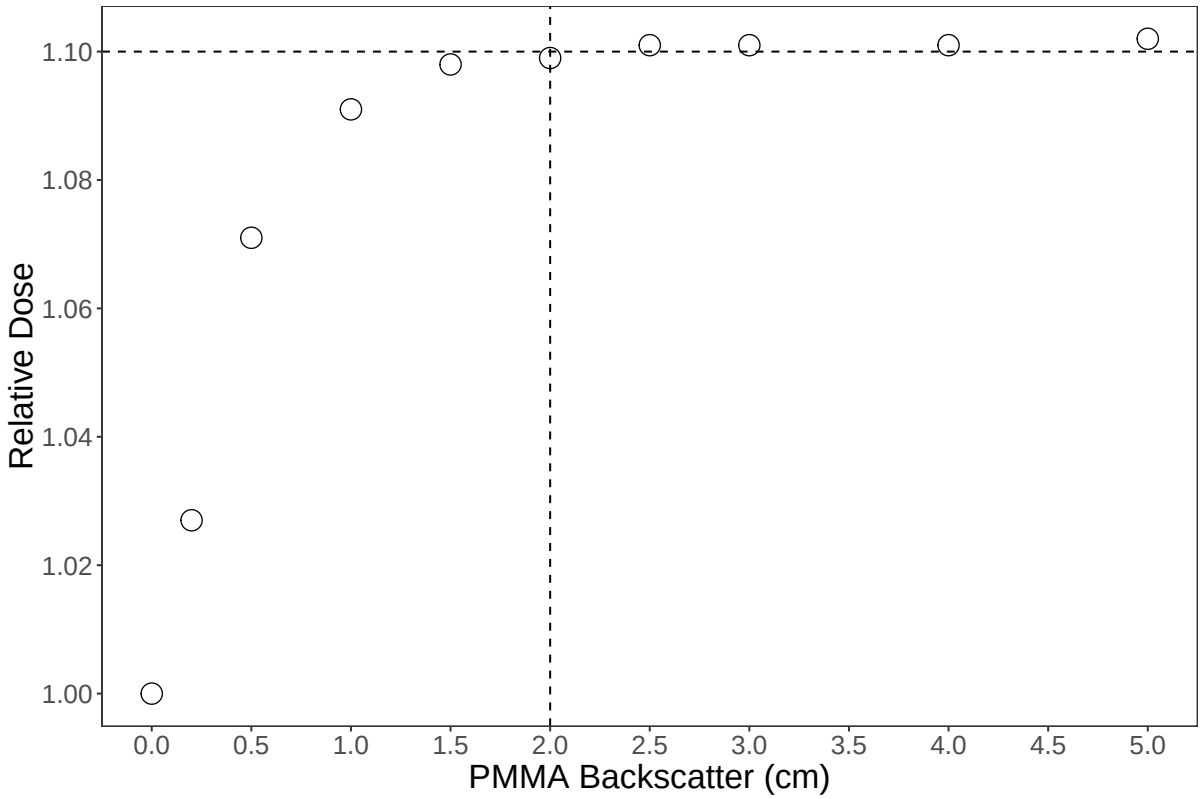

Figure 4.3: OSLD dose with increasing thickness of PMMA backscatter relative to OSLD dose without backscatter.

Figure 4.4 shows the response of control group OSLDs relative to the signal from the initial irradiation. There is approximately 2 % difference between the largest and smallest responses of the control group and no clear trend on the relative OSLD response with each increasing irradiation and annealing cycle. To within experimental uncertainty, this eliminates any concerns that the OSLD response changed with subsequent measurements.

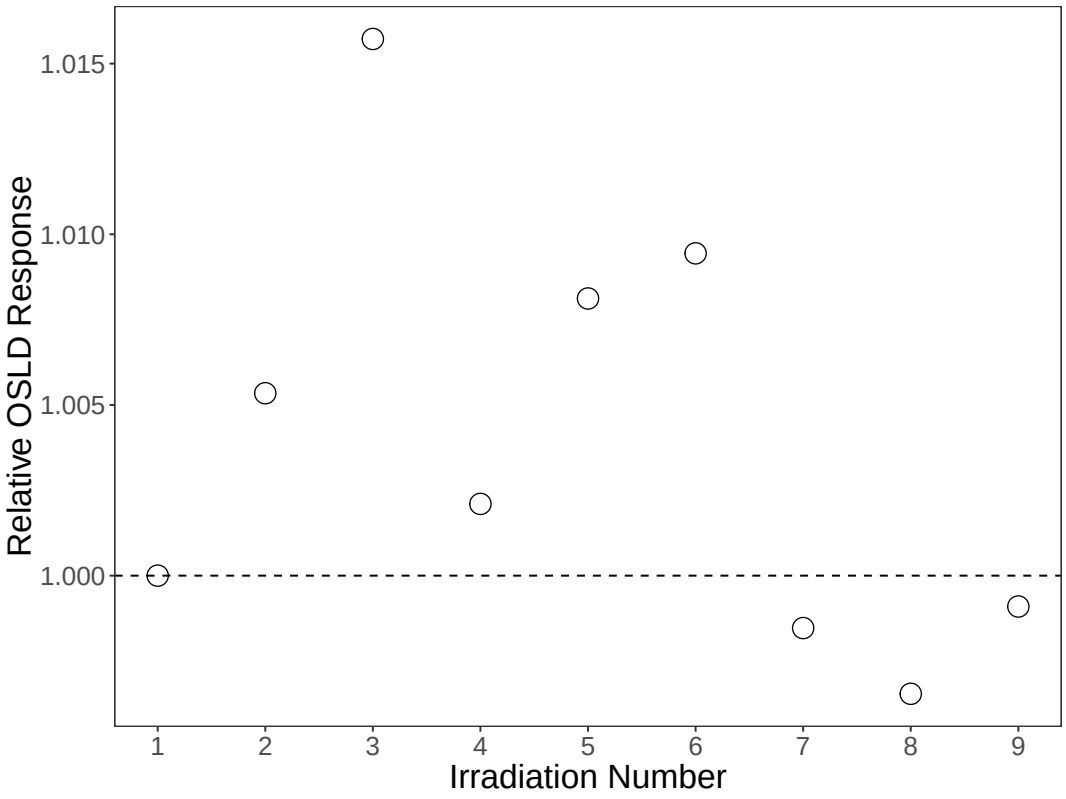

Figure 4.4: Control group mean OSLD response as a function of irradiation/annealing cycle. The response has been normalized to measurements from the first irradiation (all irradiations performed using a clinical 6 MV beam).

4.4 Discussion

This work aimed to demonstrate the viability of an OSLD calibration procedure for LDR brachytherapy seeds. The primary results were a calibration factor for the IAPd-103A model brachytherapy seed as well as the relative response of nanoDot™OSLDs to this source compared to a clinical 6 MV photon beam from a linear accelerator (Table 4.2). In general, this calibration factor would be expected to vary from institution to institution so it is recommended that individuals interested in applying these results perform their own calibrations. An alternative to this would be to use an institution specific 6 MV calibration factor and correct for the relative response between Pd-103 and 6 MV photon spectra. It is important to note that the beam strength used in the OSLD readout process to stimulate the luminescence signal (strong beam or weak beam) needs to be consistent between Pd-103 and 6 MV

calibrations (strong beam was used for all OSLD readouts in this experiment).

Our measurements show that for a system calibrated at 6 MV, absolute dose measurements made with OSLDs in the presence of Pd-103 seeds will over-report dose by a factor of four. Or, more appropriately a correction factor of 1/3.99 will yield the correct dose at the point of measurement. This factor varied by only about 1 % in the presence/absence of backscatter, which was less than experimental uncertainty (about 3 %). One concern of course is that changes in distance from the Pd-103 seed (i.e. experimental setup) would result in changes to the energy spectrum and this would in turn alter the derived correction factor. However, the fact that the presence/absence of backscatter media does not significantly alter the correction factor suggests that the measured result is relatively robust against experimental conditions.

Details of the effect of backscatter on the dose to the OSLDs was examined using egs_brachy. Simulations determined the amount of backscatter needed to achieve full backscatter conditions (Figure 4.3). Overall, there was an increase in dose of approximately 10 % as the amount of backscatter increased from 0 cm to 2 cm before leveling off, implying that 2 cm of PMMA is sufficient to establish full backscatter conditions. This result justifies the assumption that the PMMA phantom used in the calibration procedure was large enough to account for all potential contributions to OSLD dose from scatter. Although the results in Table 4.2 (without backscatter) correspond to simlations of 0.2 cm backscatter, it should be noted that the most clinically relevant scenarios for *in vivo* surface dosimetry would correspond to the simulated 0 cm backscatter condition since the OSLDs would be outside the patient's skin unlike the phantom where they were embedded in the PMMA.

Although this procedure only examined the IAPd-103A seed, it could easily be adapted to other source models by adjusting the seed holder to accommodate different source geometries. This would also require Monte Carlo simulations to be performed to determine the dose at the point of measurement in the OSLD. A calibration factor was found using a TG-43 based dose calculation which was roughly 5 % lower than the factors determined using egs_brachy. If

one wished to forego modelling their particular source model and calibration geometry using Monte Carlo they could apply a TG-43 based calibration factor bearing in mind that model-based dose calculations are generally preferred over this approach. Extending this work to other sources would be highly desirable in order to determine how sensitive the calibration factors and relative responses are to source geometries as well as different radionuclides.

The OSLDs used in this experiment showed a very minor decrease in response with cumulative dose (Figure 4.4) which can essentially be ignored given the much more significant, albeit still small, random variations between each irradiation. The OSLDs were exposed to doses of less than 10 cGy in each irradiation, far less than the threshold of 2 Gy where their response is expected to become supralinear [84]. In clinical situations, it would be ideal to limit the dose that each OSLD receives particularly because of the significant over-response at low energies as they may cross the threshold at lower doses than when exposed to high energy photons. For example, a dose of 1 cGy can be deposited in an OSLD in under 20 minutes by a 2 U Pd-103 seed at 1 cm depth in breast tissue so useful measurements could be obtained quite quickly. Overall, the calibration procedure used in this experiment was relatively straightforward to carry out with easy to acquire materials at a low cost. Given the benefits of using OSLDs for *in vivo* dosimetry in RT, being able to apply them in the context of LDR brachytherapy is a desirable goal, and this work represents a step towards achieving that goal.

4.4.1 Clinical Considerations and Error Analysis

The OSLD calibration procedure applied in this work was partly motivated by the desire to use OSLDs to measure skin doses following PBSI treatment with Pd-103 sources. The work presented in this Chapter along with the published results in Chapter 3 combine to form a procedure for obtaining a skin dose measurement for PBSI patients. OSLDs would be placed on a patient's skin for a short period of time (approximately 20 minutes) following implantation with Pd-103 seeds. These OSLDs would then be stimulated using an OSLD reader to

generate a measurement of PMT counts which would be converted to a skin dose measurement using a OSLD calibration factor for Pd-103 and a conversion factor from Chapter 3. In order to interpret this type of measurement in a clinical setting it is important to examine the potential sources of error in this procedure along with practical clinical considerations which inevitably influence the dose deposited in the patient's skin.

To estimate the error in a skin dose obtained using an OSLD for PBSI, the procedure above was broken down into four distinct parts: the use of a skin dose measurement obtained over a small time interval as an estimate for the total dose to the skin over the entire course of the treatment, the conversion from an OSLD dose to a skin dose, the OSLD calibration, and the inherent uncertainty of any OSLD measurement. The first of these addresses changes to the dose rate over time at the location on the patient's skin where the OSLD is applied which occur due to seed migration and differences in scattering conditions. The second accounts for uncertainties in the MC simulations used to determine a conversion factor relating skin dose to OSLD dose and differences between simulated geometries and actual patient geometries. The third deals with uncertainties in the calibration factor arising from deviations in the experimental phantom from simulated conditions, uncertainties in the activity of the seed used for calibration, and the variability of the raw OSLD measurements. The final factor is dependent on the choice of general purpose OSLDs vs. screened OSLD which have errors supplied by the manufacturer. These factors were treated independently and summed in quadrature to arrive at a final estimated error (Table 4.3).

The estimation of dose to a point in the skin where about 94 % of the dose is delivered over 68 days when that estimation is based on measurement made over approximately twenty minutes to an hour will be subject to uncertainty if the seed positions change (seed migration) relative to the measurement point of interest over that 68 day period. In fact, due to the high dose falloff with distance from a given Pd-103 seed, the impact of seed migration on the total dose to the skin over the course of treatment could potentially be the greatest source of error in the procedure described above. A study by Watt et al. found that most seed

Table 4.3: Estimated errors associated with skin dose measurements using results of Chapter 3 and the current Chapter.

Error Source	Estimate Error (%)
Seed Migration	25
Patient Backscatter	2
MC Calculations (TG-43)	5
$f_{OSLD \rightarrow skin}$	20
Skin Thickness	4
Breast Composition	5
Seed Activity	2.6
OSLD Calibration Position	15
OSLD Standard Deviation	3.4
OSLD Backscatter	1.3
Pd-103 Spectrum Changes	3
nanoDot™	
Screened	5
General Purpose	10
Total Combined	37 (Screened) 38 (General Purpose)

migration occurs in the first 15 days post-implant with a median migration of 3.6 mm with additional migrations of 2.1 mm over the following 15 days and 2.5 mm over the 30 days following that [101]. MC calculated skin doses for a single seed at 1 cm depth performed in the current work show between a change of between 20 % and 50 % for a differences in seed position of 5 mm and 10 mm, respectively, assuming the seeds do not change in activity. Given these observations along with the fact that the seed activity decreases exponentially over time and Pd-103 has a short half-life (16.991 days), a reasonable estimate for the error due to seed migration on the proposed OSLD measurements is 25 %. That of course may be mitigated and reduced using subsequent measurements or by the fact that while some seeds may migrate away from the point of interest, others may migrate toward it.

The error due to changing backscatter conditions is presumed to be much smaller than the effects of seed migration. MC calculations performed during the course of this work found that the maximum dose enhancement due to full backscatter (vs. conditions without any backscatter) was approximately 10 %. This only applies for the duration in which backscatter

such as clothing, water, or another body tissue such as an arm are in the vicinity of the implant. Watt et al. conducted a study to determine the impact of patient arm position on dosimetry which found that the arm position (up or down) did not lead to a significant difference in the patient's skin dose [102]. Based on these considerations, a conservative estimate for the error resulting from backscatter conditions would be 2 %.

The conversion factor relating skin dose to OSLD dose ($f_{OSLD \rightarrow skin}$) derived in Chapter 3 is based solely on MC calculations which are intended to approximate typical patient geometries. The uncertainty associated with MC calculations for LDR brachytherapy sources due to factors such as variability in the source geometry, statistical uncertainties associated with Poisson processes, and the accuracy of tabulated photon cross-section data and source spectra have been provided in the TG-43 protocol with at most 5 % ($k = 1$) uncertainty expected at 5 cm from the source on the transverse plane [80]. The simulations used to calculate $f_{OSLD \rightarrow skin}$ were primarily performed with the seed much closer to the dose scoring voxels, which were also much larger than the voxels used to generate TG-43 parameters, so an uncertainty of 5 % seems to be more than reasonable in this instance.

The variation in the ratios of skin dose to OSLD with respect to seed position makes up a large portion of the error in the recommended value for $f_{OSLD \rightarrow skin}$. Since only the maximum value of this ratio is used and the seed positions are unknown, an error of approximately 20 % can be associated with this value based on the greatest amount of variation in the dose ratio with position, which occurs for very shallow implants. Note that a value closer to the average of the dose ratios could be used as a conversion factor in order to reduce this uncertainty but the maximum was chosen purposefully to minimize false negatives in the interest of patient safety. Other factors contributing to errors in $f_{OSLD \rightarrow skin}$ include how well the MC geometry approximates an actual breast. Variations in skin thickness are expected to contribute errors of at most 4 % to the value of 0.2 cm^3 for skin up to 4 mm thick based on the results of Hilts et al. [27]. The recommended conversion factors should only be applied to breasts with 75 % adipose tissue and 25 % glandular tissue, however this is likely not realistic

so an error of 5 % may be associated with a 10 % change in the ratio of adipose to glandular tissue based on the sensitivity of skin dose to variations in breast composition [1].

Errors in the OSLD calibration factor for Pd-103 primarily stem from uncertainty in the source activity, the positions of the OSLDs relative to the seed, variations of the spectrum with distance, and the variations in the OSLD measurements. The TG-138 report provides an estimate for uncertainties in measurements of source activity (or air kerma strength) for LDR sources based on measurements with ADCL calibrated well chambers [20]. This type of chamber was used to measure the activity of the source used in this work and the total combined uncertainty associated with this measurement is estimated to be 2.6 % ($k = 1$) [20]. Based on MC calculations performed during the course of this work, the effect of source positioning is approximately 15 % for differences in distance of up to 1 mm which can be reasonably obtained with careful construction of the PMMA phantom. This uncertainty is associated with a single calibration and a centre performing this calibration procedure could likely reduce this uncertainty significantly by repeating the calibration with the OSLDs at different positions relative to the source. The OSLD measurements themselves were observed to have a standard deviation of at most 3.4 % and approximately 1.3 % difference based on backscatter conditions.

The effect of changes in the Pd-103 spectrum on the OSLD calibration factor are important to consider these changes may occur for different calibration phantoms. Pd-103 has a spectrum dominated by two photon energies of approximately 20 keV. The remaining energies are concentrated around 22 keV and 2.7 keV. These photons interact primarily via the photoelectric effect in which all of the photon's energy is absorbed. Additional MC simulations were performed using monoenergetic pencil beam sources with energies around the mean energy of Pd-103 to determine the change in the spectrum with distance and the resulting effect on dose scored in Al_2O_3 surrounded by water. Over a distance of 5 cm the spectrum changed by roughly 2.3 % with the resultant dose to Al_2O_3 differing by approximately 3 % between a distance of 1 cm and 5 cm from the source. Thus an uncertainty of 3 %

due to changes in photon spectrum energy seems reasonable. The remaining source of error in this procedure is due to the inherent uncertainties in the OSLDs provided by Landauer of 5 % and 10 % for screened and general purpose nanoDots™, respectively.

The combined uncertainty for an skin dose measurement based on all of the above factors is 37 % and 38 % for screened and general purpose nanoDots™, respectively. Although these values are quite large, many of the larger contributions could be reduced with adjustments to the procedure. The largest single error source arises due to the effects of seed migration. Performing a second measurement at an appropriate time after the implant such as at 30 days [100] would not only be useful for verifying the validity of the previous measurement, but it could also be used to evaluate the extent to which the dose distribution may have changed following the implant. The estimated error of 25 % assumes that only a single measurement immediately following the implant is obtained after which it is difficult to predict how the skin dose will evolve over time without more information.

The error associated with $f_{OSLD \rightarrow skin}$ accounts for the situation where an OSLD is placed at least 2 cm from the seeds at the edge of the implant. This may be done in practice to ensure a large area of skin is measured, but the primary region that should be measured with this technique is the skin directly above the implant which should be relatively simple to locate intuitively. Knowledge of the position of the OSLD during calibration could potentially be improved with precise machining of the phantom, but as an alternative the calibration could be performed with a larger separation between the seed and the OSLDs. The effect of the distance becomes smaller as the distance is increased and so this error could potentially be minimized with a modest increase in the separation.

Further refinements of the work conducted in this thesis would surely help to reduce the estimated errors associated with the results. The primary focus of this research has been to examine the physical aspects of performing OSLD measurements in the vicinity of Pd-103 sources, which are novel in their own right. This research provides a stepping stone towards improving *in vivo* dosimetry in PBSI brachytherapy which is necessary before

clinical applications can occur and large uncertainties should not be seen as a deterrent to achieving this goal at the current stage.

4.5 Conclusion

An OSLD calibration procedure for LDR brachytherapy was developed and tested using a custom PMMA phantom and a Pd-103 source. Monte Carlo simulations were performed to determine OSLD dose and experimental measurements were taken to compare OSLD response between Pd-103 and commonly used 6 MV photons. Using this procedure, calibration factors were found for the IAPd-103A brachytherapy seed ($(6.21 \pm 0.19) \times 10^4$ counts/cGy) as well as the relative response at this energy (3.99 for Pd-103 relative to 6 MV photons). The effects of backscatter on OSLD dose was also quantified and recommendations were made to adapt the procedures used for implementation at other institutions. OSLDs show promise for *in vivo* dosimetry applications in LDR brachytherapy and given the simplicity of the calibration procedure described in this work, further studies can and should be carried out with other sources used clinically.

Acknowledgements

The authors would like to thank Adam Yarschenko and Christian Bagg from the Medical Physics Design Lab at the Tom Baker Cancer Centre for their contribution to this work in designing and constructing the PMMA phantom used to perform experimental measurements.

Chapter 5

Conclusions and future work

Permanent breast seed implant (PBSI) is a one day brachytherapy procedure that offers a desirable treatment option for many low risk breast cancer patients. While treatment objectives include limiting dose to the skin, skin toxicities are among the most common adverse reactions to this type of treatment [47, 69]. The standard approach to determining skin dose is to calculate it using the TG-43 formalism, which relies on assumptions about the treatment geometry that are often not satisfied for low energy brachytherapy treatments such as the presence of backscatter material and a medium that is radiologically equivalent to water [5]. The TG-43 approach has been shown to underestimate skin dose by more than 50 % [1] and so more advanced model-based dose calculation algorithms (MBDCAs) such as Monte Carlo (MC) have been recommended to address this issue [5]. This thesis explored the use of optically stimulated luminescence dosimeters (OSLDs) as a means of *in vivo* dose measurement for the estimation of skin dose and ultimately treatment delivery verification, following implantation with Pd-103 brachytherapy seeds.

5.1 Summary

The primary objective of this thesis was to facilitate the use of OSLDs to assess skin dose for PBSI patients based on conversion factors derived using the MC radiation transport code,

egs_brachy [12]. This broad objective was effectively divided into three smaller tasks that are detailed in Chapters 2-4 of this thesis. The first task was to design and test models of the IsoAid Advantage™Pd-103 (IAPd-103A) brachytherapy seed and the Landauer nanoDot™OSLD using egs_brachy (Chapter 2). The second task involved simulations in a simple breast phantom using the previously tested models to determine appropriate conversion factors between skin dose and OSLD dose (Chapter 3). The final task was to establish an OSLD calibration procedure for the IAPd-103A source based on a combination of experimental measurements and MC dose calculations in egs_brachy (Chapter 4).

egs_brachy is a relatively new MC code and, although it utilizes the well-established EGSnrc radiation transport algorithm, it was necessary to test the models developed for this thesis against published work before proceeding to more novel simulations. A detailed model of the IAPd-103A seed was created based on descriptions from previous MC studies [53,91,95] using realistic material compositions and a photon spectrum obtained from the extensive National Nuclear Data Center (NNDC) database of radionuclides [19, 59]. Validation of the IAPd-103A source model was performed by calculating dose distributions in an all water geometry and a geometry designed to approximate the National Institute of Standards and Technology's (NIST) Wide-Angle Free-Air Chamber (WAFAC) to derive TG-43 parameters for comparison with published consensus data. The dose rate constant, radial dose function, and anisotropy function calculated using egs_brachy agreed reasonably well with TG-43 consensus values (within 5 % in general) in clinically relevant positions around the IAPd-103A source. Minor disagreements were observed along the source axis at distances beyond 5 cm from the source, which is common in studies of this nature and usually not a cause for concern due to the rapid drop in dose rate with distance from the source [78].

Material data not included in the egs_brachy distribution needed to be generated for simulations involving the nanoDot™OSLD and PMMA. Mass-energy absorption coefficients (μ_{en}/ρ) were calculated using a modified version of the EGSnrc user code g for PMMA and a mixture of Al_2O_3 and polyester found in nanoDots™. Additional calculations were performed

using water as the transport medium to compare with published μ_{en}/ρ data. Secondary validations were carried out to replicate work by Luxton relating dose calculations in water to dose calculations in solid PMMA phantoms [44]. Like the TG-43 validations, the results of these simulations also agreed well in clinically relevant regions surrounding the source for a point source consistent with the original work and the detailed IAPd-103A source model. Successful validations of the egs_brachy code enabled the more novel investigations that motivated it at the outset.

A breast phantom was modelled in egs_brachy to calculate skin doses from an IAPd-103A seed at various positions inside the breast tissue, simulating a simplified PBSI implant. In this model, a nanoDot™OSLD was placed at a fixed location on the skin surface while the seed was shifted vertically (away from the surface) and horizontally (parallel to the surface). Doses were scored in a small sensitive volume inside the OSLD (D_{OSL}) and a $0.2\,\text{cm}^3$ volume of skin underneath the OSLD ($D_{0.2cc}$). The ratio of these doses was calculated as the seed's position changed. These ratios were used to define conversion factors to estimate skin dose from OSLD dose. Conversion factors of 0.50 and 1.44 were determined for scenarios where the OSLDs are calibrated to dose to water, or dose to Al_2O_3, respectively. The recommended conversion factors were found to be largely unaffected by the addition of extra seeds, which is a desirable property for potential clinical applications of these results.

The final major task of this thesis was to calibrate a set of OSLDs to the Pd-103 spectrum. This step was necessary because of a known over-response of these detectors at low energies with respect to megavoltage x-rays typically used for OSLDs calibrations [74]. PMT count measurements were obtained from a set of OSLDs that were repeatedly irradiated with an IAPd-103A seed in a PMMA phantom, which was modelled in egs_brachy to determine the corresponding OSLD doses. Through this approach, a mean calibration factor of 6.21×10^4 counts/cGy was found for the seed which was found to between approximately 4 times higher than the value for a 6 MV beam from a clinical linear accelerator. These calibration factors make it possible to properly interpret OSLD dose measurements in the

context of *in vivo* dosimetry in PBSI and enable the results from Chapter 3 to be clinically implemented.

5.2 Future Work

This thesis aimed to fill part of a void that exists in the currently available literature regarding the topics of *in vivo* dosimetry in PBSI brachytherapy, MC dose calculations in brachytherapy, and the use of OSLDs for dose measurements from low energy x-rays ($E < 25\,\text{keV}$). This work also represents an early example of the use of the egs_brachy MC code, which was released shortly after commencement of the project. Much of the work performed in this thesis could be easily reproduced using the same materials and software, but it could just as easily be adapted to conduct similar research that has yet to be explored. As such, the procedures developed in this work can and should be extended to improve understanding of complexities associated with brachytherapy and ultimately to achieve better outcomes for patients.

This work examined a single brachytherapy source model (IAPd-103A) and was predominantly focused on *in vivo* dosimetry for PBSI patients using a particular mixture of adipose and glandular tissues to model breast tissue. One obvious direction for future work would be to model other brachytherapy sources and breast compositions to determine the robustness of the results to changes in these factors. The breast composition chosen for this work was meant to be a representative mixture of tissues, but there is a large variation in breast composition between patients and it has been shown that this can dramatically affect dosimetry [1]. It is also possible to import patient CT data as a phantom geometry in egs_brachy, so it would be useful to repeat aspects of this work with actual patient data. In such cases the sensitivity of low energy photon transport to medium composition (effective atomic number and density), suggests that one major challenge will be accurate translation from CT number to voxel composition parameters. This will be a likely avenue for further

exploration if model-based dose calculation algorithms as to be effectively employed for the planned of brachytherapy treatments with low energy sources. Further, this work does not need to be limited to breast patients specifically. It could reasonably be adapted to other treatment sites such as prostate, which could benefit from the insights gained in the process.

The work performed in this thesis has not been applied in an actual clinical scenario and it would be useful to carry out measurements on patients with OSLDs to test the results and possibly improve upon them. This would involve measuring skin doses for PBSI patients by attaching OSLDs to their skin following implantation and removing them before they are released to assess their skin dose. In order to use these measurements, a calibration procedure such as the one described in this thesis would need to be completed to properly convert from the raw OSLD measurement to an approximation of the expected skin dose as the seeds decay over time. Initially, these measurements should be repeated for multiple patients to gain experience performing them and to accumulate data before any decisions can be made regarding the risk of a patient developing skin toxicities and its relationship with the skin dose derived from the proposed procedure. Any institution interested in applying the results of this thesis in their brachytherapy treatment programs should perform similar dose calculations to those in this work to ensure that their measurements are reliable, particularly if they use a different source model for their implants.

More work should be done to validate the egs_brachy code for other brachytherapy sources as it is fairly new and there are very few studies that use egs_brachy for dose calculations apart from those performed by its developers. Additional independent validations of the code would be useful to assess its performance with other brachytherapy sources and to strengthen the argument for model-based dose calculation algorithms as a viable alternative to the TG-43 formalism. The egs_brachy code includes a number of novel features to improve the efficiency of dose calculations, which were not used in this thesis for the sake of simplicity, but should be tested as this could potentially address one of the key disadvantages of MC algorithms which is the resources required to perform these calculations. It should be noted

that patient-specific dose calculations are not required to apply the results of this thesis clinically, so it is not essential that an MC algorithm such as egs_brachy replaces the TG-43 formalism. In fact, a means of accurately measured treatment delivery verification via OSLD measurements of skin dose may provide useful insights for programs that continue to plan brachytherapy treatments using the TG-43 formalism.

5.2.1 Overall Conclusions

This thesis demonstrated a relatively simple approach to determining skin dose in PBSI patients by performing measurements with OSLDs calibrated to a Pd-103 brachytherapy seed. These measurements are a means to estimate the dose that is actually delivered to the patient providing valuable information with comparatively little effort and resources required in contrast to direct calculation with MBDCAs. Through improved skin dose monitoring in PBSI from *in vivo* dosimetry measurements, a better understanding of the risk of commonly encountered skin toxicities as a function skin dose can be attained. Not only can this potentially lead to more desirable outcomes for patients, but it also illustrates a useful and easily generalizable application of model based dose calculation algorithms to improve upon the TG-43 formalism without the need for time consuming, patient specific calculations.

Bibliography

[1] H. Afsharpour, J. P. Pignol, B. Keller, J. F. Carrier, B. Reniers, F. Verhaegen, and L. Beaulieu. Influence of breast composition and interseed attenuation in dose calculations for post-implant assessment of permanent breast103Pd seed implant. *Phys. Med. Biol.*, 55(16):4547–4561, 2010.

[2] M. Akselrod, F. Rice, M. Ennis, S. Khanng, and D. Chendra. microSTAR ii and nanoDots Frequently Asked Question. Technical report, 2019.

[3] P. Andreo, D. T. Burns, A. E. Nahum, J. P. Seuntjens, and F. H. Attix. The Monte Carlo Simulation of the Transport of Radiation Through Matter. In *Fundamentals of Ionizing Radiation Dosimetry*, number 2017, pages 349–396. Wiley, 2017.

[4] F. H. Attix. *Introduction to Radiological Physics and Radiation Domisetry*. 1986.

[5] L. Beaulieu, Å. Carlsson Tedgren, J. F. Carrier, S. D. Davis, F. Mourtada, M. J. Rivard, R. M. Thomson, F. Verhaegen, T. A. Wareing, and J. F. Williamson. Report of the Task Group 186 on model-based dose calculation methods in brachytherapy beyond the TG-43 formalism: Current status and recommendations for clinical implementation. *Med. Phys.*, 39(10):6208–6236, 2012.

[6] M.J. Berger, J.H. Hubbell, S.M. Seltzer, J. Chang, J.S. Coursey, R. Sukumar, D.S. Zucker, and K. Olsen. XCOM: Photon Cross Section Database (version 1.5), 2010.

[7] Z. Brownlee, R. Garg, M. Listo, P. Zavitsanos, D. E. Wazer, and K. E. Huber. Late complications of radiation therapy for breast cancer: Evolution in techniques and risk over time. *Gland Surg.*, 7(4):371–378, 2018.

[8] W. M. Butler, G. S. Merrick, J. H. Lief, and A. T. Dorsey. Comparison of seed loading approaches in prostate brachytherapy. *Med. Phys.*, 27(2):381–392, 2000.

[9] Å. K. Carlsson and A. Ahnesjö. The collapsed cone superposition algorithm applied to scatter dose calculations in brachytherapy. *Med. Phys.*, 27(10):2320–2332, 2000.

[10] G. A. Carlsson. Theoretical Basis for Dosimetry. In Kenneth R. Kase, Bengt E. Bjarngard, and Frank H. Attix, editors, *The Dosimetry of Ionizing Radiation*, volume 1, chapter 1, pages 1–75. Academic Press, 1985.

[11] A. Challapalli, E. Jones, C. Harvey, G. O. Hellawell, and S. A. Mangar. High dose rate prostate brachytherapy: An overview of the rationale, experience and emerging applications in the treatment of prostate cancer, 2012.

[12] M. J. P. Chamberland, R. E. P. Taylor, D. W. O. Rogers, and R. M. Thomson. Egsbrachy: A versatile and fast Monte Carlo code for brachytherapy. *Phys. Med. Biol.*, 61(23):8214–8231, 2016.

[13] W. Z. Chen. Impact of dose calculation algorithm on radiation therapy. *World J. Radiol.*, 6(11):874, 2014.

[14] Z. Chen and R. Nath. Dose rate constant and energy spectrum of interstitial brachytherapy sources. *Med. Phys.*, 28(1):86–96, 2001.

[15] I. J. Chetty, B. Curran, C. M. C. Ma, J. J. DeMarco, J. Seuntjens, J. E. Cygler, B. A. Faddegon, H. Liu, G. Ezzell, I. Kawrakow, P. J. Keall, J. V. Siebers, D. W. O. Rogers, and D. Sheikh-Bagheri. Report of the AAPM Task Group No. 105: Issues associated

with clinical implementation of Monte Carlo-based photon and electron external beam treatment planning. *Med. Phys.*, 34(12):4818–4853, 2007.

[16] O. Chibani and J. F. Williamson. MCPI©: A sub-minute Monte Carlo dose calculation engine for prostate implants. *Med. Phys.*, 32(12):3688–3698, 2005.

[17] J. D. Cox and J. Stetz. Toxicity Criteria of the Radiation Therapy Oncology Group Rtog 1995. *Int. J. Radiat. Oncol. Biol. Phys.*, 31(5):1341–1346, 1995.

[18] S. C. Darby, P. McGale, C. W. Taylor, and R. Peto. Long-term mortality from heart disease and lung cancer after radiotherapy for early breast cancer: Prospective cohort study of about 300 000 women in US SEER cancer registries. *Lancet Oncol.*, 6(8):557–565, 2005.

[19] D. De Frenne and E. Jacobs. Nuclear Data Sheets for A = 103. *Nuclear Data Sheets*, 110(9):2081–2256, sep 2009.

[20] L. A. DeWerd, G. S. Ibbott, A. S. Meigooni, M. G. Mitch, M. J. Rivard, K. E. Stump, B. R. Thomadsen, and J. L. M. Venselaar. A dosimetric uncertainty analysis for photon-emitting brachytherapy sources: Report of AAPM Task Group No. 138 and GEC-ESTRO. *Med. Phys.*, 38(2):782–801, 2011.

[21] G. K. Edmundson, F. A. Vicini, P. Y. Chen, C. Mitchell, and A. A. Martinez. Dosimetric characteristics of the MammoSite RTS, a new breast brachytherapy applicator. *Int. J. Radiat. Oncol. Biol. Phys.*, 52(4):1132–9, 2002.

[22] B. Fisher, S. Anderson, J. Bryant, R. G. Margolese, M. Deutsch, E. R. Fisher, J. H. Jeong, and N. Wolmark. Twenty-year follow-up of a randomized trial comparing total mastectomy, lumpectomy, and lumpectomy plus irradiation for the treatment of invasive breast cancer. *N. Engl. J. Med.*, 347(16):1233–1241, 2002.

[23] A. Frederick, T. Meyer, and M. Roumeliotis. Treatment planning considerations for permanent breast seed implant. *Brachytherapy*, 17(2):456–464, 2018.

[24] K. A. Gifford, O. Pacha, A. A. Hebert, C. L. Nelson, S. M. Kirsner, M. T. Ballo, and E. S. Bloom. A new paradigm for calculating skin dose. *Brachytherapy*, 12(2):114–119, 2013.

[25] J. Godinez and E. C. Gombos. A permanent breast seed implant as partial-breast radiation therapy for early-stage patients: In regards to Keller et al. *Int. J. Radiat. Oncol. Biol. Phys.*, 64(5):1611, 2006.

[26] P. Grégoire, P. Grégoire, T. Ronan, R. Julien, A. Ruffion, and O. Chapet. The difference in implantation quality between loose seed and variable spacing strand seeds in the field of prostate brachytherapy. *J. Clin. Oncol.*, 32(4):252–252, 2014.

[27] M. Hilts, H. Halperin, D. Morton, D. Batchelar, F. Bachand, R. Chowdhury, and J. Crook. Skin dose in breast brachytherapy: Defining a robust metric. *Brachytherapy*, 14(6):970–978, 2015.

[28] N. Hoekstra, E. Fleury, T. R. Merino Lara, P. van der Baan, A. Bahnerth, G. Struik, M. Hoogeman, and J. P. Pignol. Long-term risks of secondary cancer for various whole and partial breast irradiation techniques. *Radiother. Oncol.*, 128(3):428–433, 2018.

[29] J. W. Hopewell and K. R. Trott. Volume effects in radiobiology as applied to radiotherapy. *Radiother. Oncol.*, 56(3):283–288, 2000.

[30] J. H. Hubbell and S. M. Seltzer. X-Ray Mass Attenuation Coefficients — NIST, 2004.

[31] N. Jansen, J. M. Deneufbourg, and P. Nickers. Adjuvant stereotactic permanent seed breast implant: A boost series in view of partial breast irradiation. *Int. J. Radiat. Oncol. Biol. Phys.*, 67(4):1052–1058, 2007.

[32] M. Joiner and A. J. van der Kogel. *Basic Clinical Radiobiology*. CRC Press, 2009.

[33] P. A. Jursinic. Characterization of optically stimulated luminescent dosimeters, OSLDs, for clinical dosimetric measurements. *Med. Phys.s*, 34(12):4594–4604, 2007.

[34] I. Kawrakow, E. Mainegra-Hing, D. W. O. Rogers, F. Tessier, and B. R. B. Walters. The EGSnrc code system: Monte Carlo simulation of electron and photon transport NCR Report PIRS-701. Technical report, National Research Council Canada, Ottawa, 2017.

[35] I. Kawrakow, E. Mainegra-Hing, F. Tessier, R. Townson, and B. Walters. EGSnrc C++ class library, 2006.

[36] B. M. Keller, A. Ravi, R. Sankreacha, and J. P. Pignol. Permanent breast seed implant dosimetry quality assurance. *Int. J. Radiat. Oncol. Biol. Phys.*, 83(1):84–92, 2012.

[37] T. A. King, J. S. Bolton, R. R. Kuske, G. M. Fuhrman, T. G. Scroggins, and X. Z. Jiang. Long-term results of wide-field brachytherapy as the sole method of radiation therapy after segmental mastectomy for T(is,1,2) breast cancer. *Am. J. Surg.*, 180(4):299–304, 2000.

[38] C. Kirkby, M. Balderson, I. Nygren, and J. E. Villarreal-Barajas. Optically-stimulated luminescent dosimetry: an alternative to TLD for in vivo measurements? *C.O.M.P. InterACTIONS*, 58(4):107–112, 2012.

[39] LANDAUER Inc. microStar User Manual. Technical report, 2012.

[40] LANDAUER Inc. microSTARii medical dosimetry system USER MANUAL. Technical report, Glenwood, IL, 2016.

[41] G. Landry, B. Reniers, L. Murrer, L. Lutgens, E. B. V. Gurp, J. P. Pignol, B. Keller, L. Beaulieu, and F. Verhaegen. Sensitivity of low energy brachytherapy Monte Carlo dose calculations to uncertainties in human tissue composition. *Med. Phys.*, 37(10):5188–5198, 2010.

[42] G. Landry, B. Reniers, J. P. Pignol, L. Beaulieu, and F. Verhaegen. The difference of scoring dose to water or tissues in Monte Carlo dose calculations for low energy brachytherapy photon sources. *Med. Phys.*, 38(3):1526–1533, 2011.

[43] J. Lehmann, L. Dunn, J. E. Lye, J. W. Kenny, A. D. C. Alves, A. Cole, A. Asena, T. Kron, and I. M. Williams. Angular dependence of the response of the nanoDot OSLD system for measurements at depth in clinical megavoltage beams. *Med. Phys.*, 41(6), 2014.

[44] G. Luxton. Comparison of radiation dosimetry in water and in solid phantom materials for I-125 and Pd-103 brachytherapy sources: EGS4 Monte Carlo study. *Med. Phys.*, 1994.

[45] D. Mann-Krzisnik, F. Verhaegen, and S. A. Enger. The influence of tissue composition uncertainty on dose distributions in brachytherapy. *Radiot. Oncol.*, 126(3):394–410, 2018.

[46] D. M. Marcus, A. B. Jani, K. Godette, and P. J. Rossi. A review of low-dose-rate prostate brachytherapy - Techniques and outcomes. *J. Natl. Med. Assoc.*, 102(6):500–510, 2010.

[47] S. Mashouf, E. Fleury, P. Lai, T. Merino, E. Lechtman, A. Kiss, C. McCann, and J. P. Pignol. Clinical significance of accounting for tissue heterogeneity in permanent breast seed implant brachytherapy planning. *Int. J. Radiat. Oncol. Biol. Phys.*, 94(4):816–823, 2016.

[48] J. Mason, B. Al-Qaisieh, P. Bownes, A. Henry, and D. Thwaites. Investigation of interseed attenuation and tissue composition effects in 125I seed implant prostate brachytherapy. *Brachytherapy*, 13(6):603–610, 2014.

[49] J. J. Mazeron, P. Scalliet, E. V. Limbergen, and E. Lartigau. Radiobiology of brachytherapy and the dose-rate effect. *GEC-ESTRO handbook*, pages 1–10, 2003.

[50] M. McGuffin, J. P. Pignol, and B. Keller. The cost of convenience: A cost-comparison analysis comparing external beam radiation therapy, high-dose rate brachytherapy and permanent seed implants for early stage breast cancer. *Brachytherapy*, 45(2):163, 2014.

[51] S. W. S. McKeever. Optically stimulated luminescence: A brief overview. *Radiation Measurements*, 46(12):1336–1341, 2011.

[52] S. W. S. McKeever and M. Moscovitch. On the advantages and disadvantage of optically stimulated luminescence dosimetry and thermoluminescence dosimetry. *Radiat. Prot. Dosimetry*, 104(3):263–270, 2003.

[53] A. S. Meigooni, S. A. Dini, S.B. Awan, K. Dou, and R. A. Koona. Theoretical and experimental determination of dosimetric characteristics for ADVANTAGE™ Pd-103 brachytherapy source. *Appl. Radiat. Isot.*, 64(8):881–887, 2006.

[54] N. Miksys, J. E. Cygler, J. M. Caudrelier, and R. M. Thomson. Patient-specific Monte Carlo dose calculations for 103 Pd breast brachytherapy. *Phys. Med. Biol.*, 61(7):2705–2729, 2016.

[55] P. Mobit, E. Agyingi, and G. Sandison. Comparison of the energy-response factor of LiF and Al2O3 in radiotherapy beams. *Radiat. Prot. Dosimetry*, 119(1-4):497–499, 2006.

[56] H. Morrison, G. Menon, and R. S. Sloboda. Radiochromic film calibration for low-energy seed brachytherapy dose measurement. *Med. Phys.*, 41(7), 2014.

[57] D. Morton, M. Hilts, D. Batchelar, and J. Crook. Seed Placement in Permanent Breast Seed Implant Brachytherapy: Are Concerns Over Accuracy Valid? *Int. J. Radiat. Oncol. Biol. Phys.*, 95(3):1050–1057, 2016.

[58] R. Nath, L. L. Anderson, G. Luxton, K. A. Weaver, J. F. Williamson, and A. S. Meigooni. AAPM TG 43. Dosimetry of interstitial brachytherapy sources. *Med. Phys.*, 22(2):209–234, 1995.

[59] National Nuclear Data Center Brookhaven National Laboratory. NuDat 2.7, 2009.

[60] National Research Council Canada. EGSnrc: software tool to model radiation transport - National Research Council Canada, 2018.

[61] NHS Quality Improvement Scotland. Skincare of patients receiving radiotherapy - best practice statement. Technical Report March, 2010.

[62] S. Nich, C. Kirkby, and J. E. Villarreal-Barajas. Monte Carlo study of the relationship between skin dose and optically stimulated luminescence dosimeter dose in Pd-103 permanent breast seed implant brachytherapy. *Brachytherapy*, 18(3):387–395, 2019.

[63] C. F. Njeh, M. W. Saunders, and C. M. Langton. Accelerated Partial Breast Irradiation (APBI): A review of available techniques. *Radiat. Oncol.*, 5(1):90, 2010.

[64] M. Oldham, J. F. Dempsey, D. A. Low, J. M. Moran, and L. Dong. Dosimetry tools and techniques for IMRT. *Med. Phys.*, 38(3):1313–1338, 2011.

[65] J. P. Pignol, J. M. Caudrelier, J. Crook, C. McCann, P. Truong, and H. A. Verkooijen. Report on the clinical outcomes of permanent breast seed implant for early-stage breast cancers. *Int. J. Radiat. Oncol. Biol. Phys.*, 93(3):614–621, 2015.

[66] J. P. Pignol, B. Keller, E. Rakovitch, R. Sankreacha, H. Easton, and W. Que. First report of a permanent breast 103Pd seed implant as adjuvant radiation treatment for early-stage breast cancer. In *Int. J. Radiat. Oncol. Biol. Phys.*, volume 64, pages 176–181, 2006.

[67] J. P. Pignol, B. M. Keller, and A. Ravi. Doses to internal organs for various breast radiation techniques - implications on the risk of secondary cancers and cardiomyopathy. *Radiat. Oncol.*, 6(1):5, 2011.

[68] J. P. Pignol, I. Olivotto, E. Rakovitch, S. Gardner, K. Sixel, W. Beckham, T. T. T. Vu, P. Truong, I. Ackerman, and L. Paszat. A multicenter randomized trial of breast intensity-modulated radiation therapy to reduce acute radiation dermatitis. *J. Clin. Oncol.*, 26(13):2085–2092, 2008.

[69] J. P. Pignol, E. Rakovitch, Brian M. Keller, Raxa Sankreacha, and Carole Chartier. Tolerance and acceptance results of a palladium-103 permanent breast seed implant phase I/II study. *Int. J. Radiat. Oncol. Biol. Phys.*, 73(5):1482–1488, 2009.

[70] Y. Poirier, S. Kuznetsova, and J. E. Villarreal-Barajas. Characterization of nanoDot optically stimulated luminescence detectors and high-sensitivity MCP-N thermoluminescent detectors in the 40-300 kVp energy range. *Med. Phys.*, 45(1):402–413, 2018.

[71] Princess Royal Radiotherapy Review Clinic. Managing Radiotherapy Induced Skin Reactions: A Toolkit for Healthcare Professionals. Technical report, St James's Institute of Oncology, The Leeds Teaching Hospitals NHS Trust, 2011.

[72] G. Raisali, M. G. Ghonchehnazi, P. Shokrani, and M. Sadeghi. Determination of the geometry function for a brachytherapy seed, comparing MCNP results with TG-43U1 analytical approximations. *Nukleonika*, 53(2):45–49, 2008.

[73] N. T. Ranger. The microStar Reader Quality Assurance Program for Medical Dosimetry Users. Technical report, 2014.

[74] C. S. Reft. The energy dependence and dose response of a commercial optically stimulated luminescent detector for kilovoltage photon, megavoltage photon, and electron, proton, and carbon beams. *Med. Phys.*, 36(5):1690–1699, 2009.

[75] M. Rejab, J. H. D. Wong, Z. Jamalludin, W. L. Jong, R. A. Malik, W. Z. Wan Ishak, and N. M. Ung. Dosimetric characterisation of the optically-stimulated luminescence dosimeter in cobalt-60 high dose rate brachytherapy system. *Australas. Phys. Eng. Sci. Med.*, 41(2):475–485, 2018.

[76] G. M. Richards, A. M. Berson, J. Rescigno, S. Sanghavi, B. Siegel, D. Axelrod, S. Bernik, V. Scarpinato, and C. Mills. Acute toxicity of high-dose-rate intracavitary brachytherapy with the MammoSite applicator in patients with early-stage breast cancer. *Ann. Surg. Oncol.*, 11(8):739–746, 2004.

[77] M. J. Rivard, F. Ballester, W. M. Butler, L. A. Dewerd, G. S. Ibbott, A. S. Meigooni, C. S. Melhus, M. G. Mitch, R. Nath, and P. Papagiannis. Supplement 2 for the 2004 update of the AAPM Task Group No. 43 Report: Joint recommendations by the AAPM and GEC-ESTRO: Joint. *Med. Phys.*, 44(9):e297–e338, 2017.

[78] M. J. Rivard, L. Beaulieu, and B. Thomadsen. *Clinical brachytherapy physics : American Association of Physicists in Medicine 2017 Summer School proceedings : in conjunction with the American Brachytherapy Society, Lewis & Clark College, Portland, Oregon, June 10-14, 2017*. Medical Physics Publishing Inc., 2017.

[79] M. J. Rivard, W. M. Butler, L. A. DeWerd, M. S. Huq, G. S. Ibbott, Ali S. Meigooni, C. S. Melhus, M. G. Mitch, R. Nath, and J. F. Williamson. Supplement to the 2004 update of the AAPM Task Group No. 43 Report. *Med. Phys.*, 34(6):2187–2205, 2007.

[80] M. J. Rivard, B. M. Coursey, L. A. DeWerd, W. F. Hanson, M. S. Huq, G. S. Ibbott, M. G. Mitch, R. Nath, and J. F. Williamson. Update of AAPM Task Group No. 43 Report: A revised AAPM protocol for brachytherapy dose calculations. *Med. Phys.*, 31(3):633–674, 2004.

[81] M. Rodriguez and D. W. O. Rogers. Effect of improved TLD dosimetry on the determination of dose rate constants for 125 I and 103 Pd brachytherapy seeds. *Med. Phys.*, 41(11):114301, 2014.

[82] D. J. Scanderbeg, C. Yashar, R. Rice, and T. Pawlicki. Clinical implementation of a new HDR brachytherapy device for partial breast irradiation. *Radiot. Oncol.*, 90(1):36–42, jan 2009.

[83] S. B. Scarboro, D. Cody, P. Alvarez, D. Followill, L. Court, F. C. Stingo, D. Zhang, M. McNitt-Gray, and S. F. Kry. Characterization of the nanoDot OSLD dosimeter in CT. *Med. Phys.*, 42(4):1797–1807, 2015.

[84] V. Schembri and B. J. M. Heijmen. Optically stimulated luminescence (OSL) of carbon-doped aluminum oxide (Al2 O3:C) for film dosimetry in radiotherapy. *Med. Phys.*, 34(6):2113–2118, 2007.

[85] C. Shah, F. Vicini, D.E. Wazer, D. Arthur, and R. R. Patel. The American Brachytherapy Society consensus statement for accelerated partial breast irradiation. *Brachytherapy*, 12(4):267–277, 2013.

[86] R. Sharma and P. A. Jursinic. In vivo measurements for high dose rate brachytherapy with optically stimulated luminescent dosimeters. *Med. Phys.*, 40(7), 2013.

[87] L. Sharp. Radiotherapy-related skin reactions. *Cancer World*, (July):39–43, 2016.

[88] J. Skowronek. Current status of brachytherapy in cancer treatment - short overview. *J. Contemp. Brachytherapy*, 9(6):581–589, 2017.

[89] Canadian Cancer Society. Canadian Cancer Society's Advisory Committee on Cancer Statistics. Technical report, Toronto, ON, 2017.

[90] Canadian Cancer Society. Canadian Cancer Statistics. Technical report, 2018.

[91] K. T. Sowards. Monte Carlo dosimetric characterization of the IsoAid ADVANTAGE 103Pd brachytherapy source. *J. Appl. Clin. Med. Phys.*, 8(2):18–25, 2007.

[92] K. Tanderup, S. Beddar, C. E. Andersen, G. Kertzscher, J. E. Cygler, and S. Beddar. In vivo dosimetry in brachytherapy. *Med. Phys.*, 40(7):070902, 2014.

[93] R. E. P. Taylor and D. W. O. Rogers. An EGSnrc Monte Carlo-calculated database of TG-43 parameters. *Med. Phys.*, 35(9):4228–4241, 2008.

[94] R. E. P. Taylor and D. W. O. Rogers. EGSnrc Monte Carlo calculated dosimetry parameters for 192Ir and 169Yb brachytherapy sources. *Med. Phys.*, 35(11):4933–4944, 2008.

[95] R. E. P. Taylor and D. W. O. Rogers. The CLRP TG-43 Parameter Database for Brachytherapy — Department of Physics, 2013.

[96] R. E. P. Taylor, G. Yegin, and D. W. O. Rogers. Benchmarking BrachyDose: Voxel based EGSnrc Monte Carlo calculations of TG-43 dosimetry parameters. *Med. Phys.*, 34(2):445–457, 2007.

[97] F. Tessier. EGSnrc - Google+.

[98] R. M. Thomson, R. E. P. Taylor, M. J. P. Chamberland, and D. W. O. Rogers. *User manual for egs _ brachy A versatile and fast EGSnrc application for brachytherapy.* 2017.

[99] C. J. Tien, R. Ebeling, J. R. Hiatt, B. Curran, and E. Sternick. Optically stimulated luminescent dosimetry for high dose rate brachytherapy. *Front. Oncol.*, 2(91):1–7, 2012.

[100] E. Watt, L. Conroy, M. Peacock, M. Roumeliotis, A. Frederick, S. Husain, and T. Meyer. Appropriate timing for postimplant imaging in permanent breast seed implant: Results from a serial CT study. *Brachytherapy*, 17(3):609–614, 2018.

[101] E. Watt, A. Guebert, S. Quirk, M. Skarsgard, M. Roumeliotis, and T. Meyer. Tracking post-implant seed migration in permanent breast seed implant. *Brachytherapy*, 17(4):S50, 2018.

[102] E. Watt, S. Husain, M. Sia, D. Brown, K. Long, and T. Meyer. Dosimetric variations in permanent breast seed implant due to patient arm position. *Brachytherapy*, 14(6):979–985, 2015.

[103] S. A. White, G. Landry, G. P. Fonseca, R. Holt, T. Rusch, L. Beaulieu, F. Verhaegen, and B. Reniers. Comparison of TG-43 and TG-186 in breast irradiation using a low energy electronic brachytherapy source. *Med. Phys.*, 41(6), 2014.

[104] J. F. Williamson. Monte Carlo evaluation of kerma at a point for photon transport problems. *Med. Phys.*, 14(4):567–576, 1987.

[105] J. F. Williamson. Comparison of measured and calculated dose rates in water near I-125 and Ir-192 seeds. *Med. Phys.*, 18(4):776–786, 1991.

[106] H. Q. Woodard and D. R. White. The composition of body tissues. *Brit. J. Radiol.*, 59(708):149–159, 1986.

[107] M. J. Yaffe, J. M. Boone, N. Packard, O. Alonzo-Proulx, S. Y. Huang, C. L. Peressotti, A. Al-Mayah, and K. Brock. The myth of the 50-50 breast. *Med. Phys.*, 36(12):5437–5443, 2009.

[108] K. Yoshida, T. Ohashi, A. Yorozu, K. Toya, T. Nishiyama, S. Saito, T. Hanada, Y. Shiraishi, and N. Shigematsu. Comparison of preplanning and intraoperative planning for I-125 prostate brachytherapy. *Jpn. J. Clin. Oncol.*, 43(4):383–389, 2013.

[109] E. G. Yukihara and S. W. S. McKeever. *Optically Stimulated Luminescence: Fundamentals and Applications*. John Wiley & Sons, Ltd, Chichester, UK, feb 2011.

[110] M. Zehtabian, R. Faghihi, and S. Si. A review on main defects of TG-43. In Kazushi Kishi, editor, *Brachytherapy*, chapter 1, pages 3–16. InTech, 2012.

[111] C. Zhou and F. Inanc. Integral-transport-based deterministic brachytherapy dose calculations. *Phys. Med. Biol.*, 48(1):73–93, 2003.

Appendix A

Copyright permissions

A.1 Article permissions

The article presented in Chapter 3 is reproduced under Elsevier's Copyright policy. As the author of this article, I retain the right to reproduce it in a thesis according to the terms described below:

Copyright Clearance Center RightsLink®

Home | Account Info | Help | LIVE CHAT

Title: Monte Carlo study of the relationship between skin dose and optically stimulated luminescence dosimeter dose in Pd-103 permanent breast seed implant brachytherapy

Author: Steven Nich,Charles Kirkby,J. Eduardo Villarreal-Barajas

Publication: Brachytherapy

Publisher: Elsevier

Date: May–June 2019

Logged in as:
Steven Nich
[redacted]
LOGOUT

Please note that, as the author of this Elsevier article, you retain the right to include it in a thesis or dissertation, provided it is not published commercially. Permission is not required, but please ensure that you reference the journal as the original source. For more information on this and on your other retained rights, please visit: https://www.elsevier.com/about/our-business/policies/copyright#Author-rights

BACK | CLOSE WINDOW

A.2 Co-author permissions

Chapter 3

Co-author permission has been obtained to reproduce the article presented in Chapter 3:

Alberta Health Services
Cancer Control

Jack Ady Cancer Centre
Department of Medical Physics

Charles Kirkby PhD, FCCPM
Senior Medical Physicist
Jack Ady Cancer Centre, Lethbridge
Adjunct Associate Professor
Dept. of Oncology and
Dept. of Physics and Astronomy
University of Calgary
[redacted]

August 14, 2019

To whom it may concern,

I grant Steven Nich permission to use our co-authored work in his MSc thesis at the University of Calgary. This work is:

Steven Nich, Charles Kirkby, and J Eduardo Villarreal-Barajas. "Monte Carlo study of the relationship between skin dose and optically stimulated luminescence dosimeter dose in Pd-103 permanent breast seed implant brachytherapy." Brachytherapy, 18(3), 387-395 (2019)

Sincerely,

[redacted]

Charles Kirkby

14 August 2019

To whom it may concern,

I grant Steven Nich permission to use our co-authored work in his MSc. thesis at the University of Calgary. This work is:

Steven Nich, Charles Kirkby, and J Eduardo Villarreal-Barajas. *Monte Carlo study of the relationship between skin dose and optically stimulated luminescence dosimeter dose in Pd-103 permanent breast seed implant brachytherapy. Brachytherapy*, 18(3), 387-395 (2019)"

Many thanks in anticipation

Dr. J Eduardo Villarreal-Barajas DABR, FCCPM
Head of Radiotherapy Physics
Royal Devon and Exeter Hospital – NHS Foundation Trust
Medical Physics Department

Chapter 4

Co-author permission has been obtained to reproduce the unpublished article presented in Chapter 4:

Jack Ady Cancer Centre
Department of Medical Physics

Charles Kirkby PhD, FCCPM
Senior Medical Physicist
Jack Ady Cancer Centre, Lethbridge
Adjunct Associate Professor
Dept. of Oncology and
Dept. of Physics and Astronomy
University of Calgary
[redacted]

August 15, 2019

To whom it may concern,

I grant Steven Nich permission to use our co-authored work in his MSc thesis at the University of Calgary. This work is:

Steven Nich, Charles Kirkby, Thomas Mann, Tyler Meyer, J Eduardo Villarreal-Barajas. Optically stimulated luminescence dosimeter calibration
procedure for Pd-103 brachytherapy source. Unpublished manuscript.

Sincerely,

[redacted]

Charles Kirkby

15 August 2019

To whom it may concern,

I grant Steven Nich permission to use our co-authored work in his MSc. thesis at the University of Calgary. This work is:

Steven Nich, Charles Kirkby, and J Eduardo Villarreal-Barajas. *Monte Carlo study of the relationship between skin dose and optically stimulated luminescence dosimeter dose in Pd-103 permanent breast seed implant brachytherapy. Brachytherapy*, 18(3), 387-395 (2019)

Steven Nich, Charles Kirkby, Thomas Mann, Tyler Meyer, J Eduardo Villarreal-Barajas. *Optically stimulated luminescence dosimeter calibration procedure for Pd-103 brachytherapy source*. Unpublished manuscript.

Many thanks in anticipation

Dr. J Eduardo Villarreal-Barajas DABR, FCCPM
Head of Radiotherapy Physics
Royal Devon and Exeter Hospital – NHS Foundation Trust
Medical Physics Department

RE: Thesis Copyright Permissions

Thomas Mann

Sent: August 15, 2019 4:18 PM

To: Steven Nich

To whom it may concern,

I grant Steven Nich permission to use our co-authored work in his MSc. thesis at the University of Calgary. This work is:

Steven Nich, Charles Kirkby, Thomas Mann, Tyler Meyer, J Eduardo Villarreal-Barajas. Optically stimulated luminescence dosimeter calibration procedure for Pd-103 brachytherapy source. Unpublished manuscript

I agree to the above statement.

-Thomas Mann

Thesis copyright permission

Tyler Meyer

Sent: August 15, 2019 8:00 AM

To: Steven Nich

To whom it may concern,

I grant Steven Nich permission to use our co-authored work in his MSc. thesis at the University of Calgary. This work is:

Steven Nich, Charles Kirkby, Thomas Mann, Tyler Meyer, J Eduardo Villarreal-Barajas. Optically stimulated luminescence dosimeter calibration procedure for Pd-103 brachytherapy source. Unpublished manuscript

Sincerely,

Tyler Meyer

Tyler Meyer, Ph.D, MCCPM
Medical Physicist, Tom Baker Cancer Centre
Adjunct Assistant Professor Dept. of Oncology, University of Calgary
Adjunct Assistant Professor Dept. of Physics and Astronomy, University of Calgary
[redacted]

A.3 Figure permissions

Figure 1.1 is reproduced with permission from Dr. Elizabeth Watt. This figure has not been published in any other work and was created specifically for this thesis. Permissiom for use of this figure is shown below:

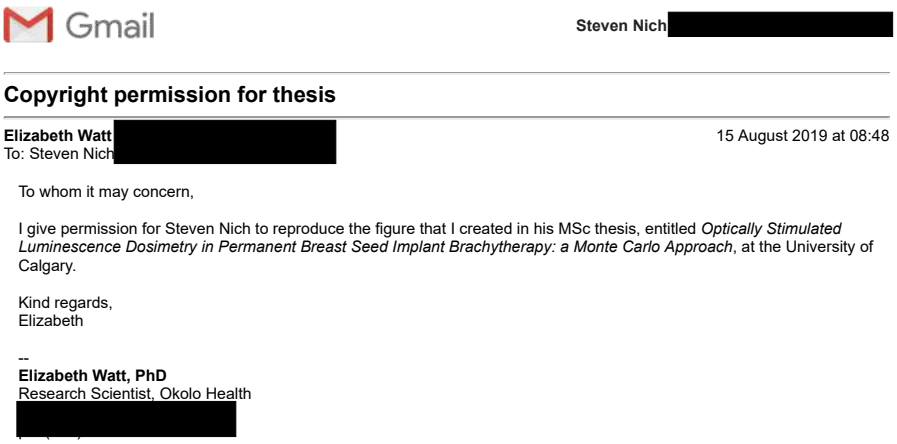

Gmail Steven Nich [redacted]

Copyright permission for thesis

Elizabeth Watt [redacted] 15 August 2019 at 08:48
To: Steven Nich

To whom it may concern,

I give permission for Steven Nich to reproduce the figure that I created in his MSc thesis, entitled *Optically Stimulated Luminescence Dosimetry in Permanent Breast Seed Implant Brachytherapy: a Monte Carlo Approach*, at the University of Calgary.

Kind regards,
Elizabeth

--
Elizabeth Watt, PhD
Research Scientist, Okolo Health
[redacted]

Figure 1.2 is reproduced with permission from the following source: Mark J. Rivard, Bert M. Coursey, Larry A. DeWerd, William F. Hanson, M. Saiful Huq, Geoffrey S. Ibbott, Michael G. Mitch, Ravinder Nath, and Jeffrey F. Williamson. Update of AAPM Task Group No. 43 Report: A revised AAPM protocol for brachytherapy dose calculations. Medical Physics, 31(3):633674, 2004. Permission for use of this figure is shown below:

Title:	Update of AAPM Task Group No. 43 Report: A revised AAPM protocol for brachytherapy dose calculations
Author:	Mark J. Rivard, Bert M. Coursey, Larry A. DeWerd, et al
Publication:	Medical Physics
Publisher:	John Wiley and Sons
Date:	Feb 27, 2004